

ASSESSMENT OF THE IMPACTS OF HYPERLIPIDEMIA ON BRAIN AND
MODULATION OF PERK PATHWAY AGAINST HYPERLIPIDEMIA-
INDUCED SYNAPTIC IMPAIRMENT ON HIPPOCAMPUS

A THESIS SUBMITTED TO
THE GRADUATE SCHOOL OF NATURAL AND APPLIED SCIENCES
OF
MIDDLE EAST TECHNICAL UNIVERSITY

BY

BILGE AŞKIN

IN PARTIAL FULFILLMENT OF THE REQUIREMENTS
FOR
THE DEGREE OF MASTER OF SCIENCE
IN
MOLECULAR BIOLOGY AND GENETICS

JULY 2019

Approval of the thesis:

**ASSESSMENT OF THE IMPACTS OF HYPERLIPIDEMIA ON BRAIN AND
MODULATION OF PERK PATHWAY AGAINST HYPERLIPIDEMIA-
INDUCED SYNAPTIC IMPAIRMENT ON HIPPOCAMPUS**

submitted by **BILGE AŞKIN** in partial fulfillment of the requirements for the degree
of **Master of Science in Molecular Biology and Genetics Department, Middle East
Technical University** by,

Prof. Dr. Halil Kalıpçılar
Dean, Graduate School of **Natural and Applied Sciences**

Prof. Dr. Ayşe Gül Gözen
Head of Department, **Molecular Biology and Genetics**

Assoc. Prof. Dr. Tülin Yanık
Supervisor, **Molecular Biology and Genetics, METU**

Prof. Dr. Michelle Adams
Co-Supervisor, **Department of Psychology, Bilkent Uni.**

Examining Committee Members:

Prof. Dr. Sreeparna Banerjee
METU, Biological Sciences

Assoc. Prof. Dr. Tülin Yanık
Molecular Biology and Genetics, METU

Assoc. Prof. Dr. Çağdaş Devrim Son
METU, Biological Sciences

Assoc. Prof. Dr. Soner Doğan
Yeditepe University, Medical Biology

Assist. Prof. Dr. Bilge Güvenç Tuna
Yeditepe University, Biophysics

Date: 11.07.2019

I hereby declare that all information in this document has been obtained and presented in accordance with academic rules and ethical conduct. I also declare that, as required by these rules and conduct, I have fully cited and referenced all material and results that are not original to this work.

Name, Surname: Bilge Aşkın

Signature:

ABSTRACT

ASSESSMENT OF THE IMPACTS OF HYPERLIPIDEMIA ON BRAIN AND MODULATION OF PERK PATHWAY AGAINST HYPERLIPIDEMIA- INDUCED SYNAPTIC IMPAIRMENT ON HIPPOCAMPUS

Aşkın, Bilge

Master of Science, Molecular Biology and Genetics

Supervisor: Assoc. Prof. Dr. Tülin Yanık

Co-Supervisor: Prof. Dr. Michelle Adams

July 2019, 96 pages

Hyperlipidemia is characterized by elevated total cholesterol levels in the circulation, and it is often associated with co-occurrence of neuronal dysfunction and subsequent neurodegeneration. Hyperlipidemia-induced inflammation, synaptic damage and neuronal loss in hippocampus as well as in other regions of the brain consequently leads to cognitive decline. Due to its role in protein translation and cell fate determination, PKR-like endoplasmic reticulum kinase (PERK) arm of the Endoplasmic Reticulum (ER) stress is likely to be involved in hyperlipidemia-induced neurodegeneration. Therefore, attenuation of PERK pathway would provide a neuroprotective effect against the negative effects of hyperlipidemia. The first half of the study was aimed to examine hyperlipidemia-induced inflammatory and synaptic changes in the cortex and hippocampus and the involvement of PERK pathway in hyperlipidemia-induced changes. The second half of the study was aimed to assess the impacts of PERK pathway modulation using Sephin1 on hyperlipidemia-induced synaptic impairment in hippocampus.

Our results showed that hyperlipidemia elevated the stress status of the cortex and potentially impaired synaptic integrity by decreasing synaptic protein levels. In the

cortex, decreased synaptic protein levels coincided with elevated astrogliosis and pro-inflammatory cytokine levels. Unlike cortex, hippocampus was not affected by the early effects of hyperlipidemia even though astrogliosis level was markedly increased. Increased astrogliosis may provide a neuroprotective activity against the early effects of hyperlipidemia in hippocampus due to its privileged involvement in neurogenesis. Sephin1 was not an effective therapeutic approach to prevent hyperlipidemia-induced synaptic protein loss seen in hippocampus since stress response was not yet triggered in hippocampus.

Keywords: Hyperlipidemia, Hippocampus, ER Stress, PERK

ÖZ

HİPERLİPİDEMİNİN BEYİN ÜZERİNE ETKİLERİNİN VE PERK YOLAĞI MODULASYONUNUN HİPOKAMPÜSTE GÖRÜLEN HİPERLİPİDEMİ KAYNAKLI SİNAPTİK BOZUKLUĞA ETKİSİNİN ARAŞTIRILMASI

Aşkın, Bilge

Yüksek Lisans, Moleküler Biyoloji ve Genetik

Tez Danışmanı: Doç. Dr. Tülin Yanık

Ortak Tez Danışmanı: Prof. Dr. Michelle Adams

Temmuz 2019, 96 sayfa

Hiperlipidemi genellikle dolaşımdaki kolesterol seviyesinin yükselmesi ile karakterize edilir ve sıklıkla nöronal fonksiyon bozukluğuna ve nörodejenerasyona neden olur. Hiperlipidemi; enflamasyona ve sinaptik hasarlara neden olarak hipokampüste ve beynin diğer bölgelerinde sinaptik proteinlerin azalmasına ve nöron kayıplarına yol açarak bilişsel azalmaya neden olmaktadır. Protein translasyonundaki ve hücre kaderinin belirlenmesindeki rolünden dolayı, Endoplazmik Retikulum (ER) stresinin PKR benzeri endoplazmik retikulum kinaz (PERK) kolunun, hiperlipidemi kaynaklı nörodejenerasyonda rol oynaması muhtemeldir. Bu nedenle, PERK yolağının inhibe edilmesi hiperlipideminin olumsuz etkilerine karşı nöroprotektif bir etki sağlayacağı düşünülmektedir. Çalışmanın ilk yarısında; korteks ve hipokampüste hiperlipideminin neden olduğu enflamasyon ve sinaptik değişiklikler ve PERK yolağının bu değişikliklerdeki rolü araştırıldı. Çalışmanın ikinci yarısında; Sephin1 kullanılarak, PERK yolağı modülasyonunun, hipokampüste hiperlipidemi kaynaklı sinaptik bozukluk üzerine etkisi değerlendirildi.

Sonuçlarımız, hiperlipideminin korteksin stres durumunu artırarak ve sinaptik protein düzeylerini azaltarak, potansiyel olarak sinaptik bozukluğa neden olduğunu

göstermektedir. Kortekste azalan sinaptik protein seviyeleri, astroglioz ve pro-enflamatuar sitokin artışı ile birlikte gözlemlenmiştir. Korteksin aksine, hipokampüste astroglioz düzeyinde belirgin bir artış gözlemlense de, hipokampus stres durumunun hiperlipideminin erken etkilerinden etkilenmediği görülmüştür. Astroglioz seviyesindeki artış, hipokampüste hiperlipidemin erken etkilerine karşı nöroprotektif bir aktivite sağlamış olabilir. Bu potansiyel koruma mekanizmasının aktive edilmesinin nedeni, hipokampusün nörojenezdeki önemli rolü olabilir. Sephin1'in hipokampüste görülen hiperlipidemi kaynaklı sinaptik protein kaybını önlemek için etkili bir terapötik yaklaşım olmadığı görülmüştür, olası sebep stres yanıtının hipokampüste henüz indüklenmemesi olabilir.

Anahtar Kelimeler: Hiperlipidemi, Hipokampus, ER Stres, PERK

To my parents

ACKNOWLEDGEMENTS

First and foremost, I would like to thank my supervisor Assoc.Prof.Dr. Tülin Yanık for her patient guidance, support and encouragement she has provided throughout my time as her student. Her positive outlook and belief in me and my research inspired me and gave me confidence. Additionally, I want to thank our lab member Didem Mimirođlu for her help and friendship.

I also want to express my sincere gratitude to my co-advisor Prof.Dr.Michelle Adams for her patience and endless support throughout this study and allowing me to be part of her lab at Bıkent University, Ankara, Turkey. She and her team were always supportive both scientifically and emotionally. In this regard, I would like to thank the members of her team: Begün Erbaba, Dilan Çelebi, Göksemin Fatma Şengül, Duygu Macarođlu, Duygu Mutlu, Elif Tuğçe Karođlu, Hande Özge Aydođan, Melek Umay Tüz Şaşıık, Narin İlgım Ardıç and Naz Şerifođlu for their valuable help, suggestions, comments and support.

I would like to thank Prof.Dr. Ebru Erbay and her team for involving me in their project, allowing me to study in their lab and supporting this project through EMBO installation grant. Special thanks to Buket Gültekin for her technical and personal helps. I want to thank Dr. Begüm Kocatürk and Dr.Umut İnci Onat for letting me take part in their animal experiments and providing the experimental animals. Additionally, I would like to thank to Aslı Ekin Dođan and Zehra Yıldırım for their helps in experimental protocols.

I also appreciate the scientific contributions of my thesis committee members: Prof.Dr.Sreeparna Banerjee and Assoc.Prof.Dr.Çađdaş Devrim Son. I want to especially thank Assoc.Prof.Dr.Soner Dođan and Assist. Prof.Dr. Bilge Güvenç Tuna for coming all the way from İstanbul to attend my jury.

I would like to thank Naz Mengi for her friendship and emotional support as well as for her help with the experiments. I cannot imagine how I would survive this rough two years without her.

I also have to mention Cennet Gül, my dear friend of 12 years. Her hilarious remarks and jokes, and the long and soothing conversations we had helped relieve the enormous stress I was under and enabled me to focus on my work.

Finally, I want to express my gratitude for my parents and older sister for their understanding and unconditional love. I would not achieve anything without them and their support. Thanks to my dear mother, Tülay Aşkın, bringing me this far. I would like to also thank my love Yiğit Kalyoncu and his family. His support and great understanding were so important for me to overcome this difficult process.

I would like to acknowledge ODTÜ-BAP for supporting this study through YLT-108-2018-3630 project.

TABLE OF CONTENTS

ABSTRACT	v
ÖZ	vii
ACKNOWLEDGEMENTS.....	x
TABLE OF CONTENTS	xii
LIST OF FIGURES	xv
CHAPTERS	
1. INTRODUCTION.....	1
1.1. Hyperlipidemia	1
1.1.1. Risk Factors.....	2
1.1.2. Associated Diseases	2
1.1.3. Animal Models	3
1.2. Hyperlipidemia and Brain.....	4
1.2.1. Hyperlipidemia Associated Neurodegeneration.....	6
1.2.1.1. Hippocampus	7
1.3. Endoplasmic Reticulum (ER) Stress.....	9
1.3.1. Unfolded Protein Response (UPR)	9
1.3.1.1. PERK - eIF2 α Regulated Stress Response	13
1.4. Hyperlipidemia-Induced ER Stress in Brain.....	14
1.5. PERK Pathway as a Potential Therapeutic Target.....	16
1.5.1. Selective Inhibition of Stress Induced Phosphatase	17
1.6. Aim of the Study	17
2. MATERIALS AND METHODS.....	19

2.1. Ethics Statement	19
2.2. Animal Studies	19
2.3. Non-Sephin1 Groups	19
2.3.1. Brain Dissection.....	21
2.3.2. Brain Tissue Homogenization	23
2.3.3. Total Protein Isolation	23
2.3.4. Protein Concentration Measurement	24
2.3.5. Western Blot	24
2.3.5.1. Sample Preparation	24
2.3.5.2. Preparation of Resolving and Stacking Gel	24
2.3.5.3. Loading and Running the Samples	25
2.3.5.4. Transfer of Proteins to PVDF Membrane	25
2.3.5.5. Blocking and Antibody Incubation	26
2.3.5.6. Chemiluminescent Detection	26
2.3.5.7. Band Intensity Quantification	27
2.3.5.8. Statistical Analysis	27
2.4. Sephin1 Groups	28
2.4.1. Whole Brain Cryopreservation	29
2.4.2. Cryosectioning	30
2.4.3. Immunostaining	34
2.4.4. Microscopy Imaging	35
2.4.5. Stereological Analysis	36
2.4.6. Statistical Analysis.....	38
3. RESULTS	39

3.1. Hyperlipidemia Status of Experimental Groups	39
3.2. Effects of Hyperlipidemia on Synaptic Protein Levels.....	39
3.3. Effects of Hyperlipidemia on Astrogliosis	44
3.4. Effects of Hyperlipidemia on Cytokine Level	47
3.5. Effects of Hyperlipidemia on PERK pathway Activation	50
3.5.1. p-PERK	50
3.5.2. p-eIF2 α	53
3.5.3. CHOP	56
3.6. Effects of Sephin1 Injection on Hippocampal Gephyrin Level.....	58
4. DISCUSSION	61
5. CONCLUSION AND FUTURE ASPECTS.....	71
REFERENCES	73
APPENDICES	
A. General Lab Materials	87
B. Homogenization Buffer Preparation	90
C. Total RNA Isolation	91
D. RIPA Buffer Preparation.....	92
E. Western Blot Solutions.....	92
F. Primary and Secondary Antibody Dilutions	95
G. Immunostaining Solutions.....	96

LIST OF FIGURES

FIGURES

- Figure 1.1. Image of Nissl-stained mouse brain section showing the principle areas of hippocampus.** Hippocampus is embedded into temporal lobe and can be distinguished by layers of densely packed neurons. Based on its histology, hippocampus is divided into four major areas, namely Dentate Gyrus, CA1, CA2 and CA3 (Lein et al., 2007).7
- Figure 1.2. Overview of UPR signaling pathways.** Association of BiP with IRE1, PERK and ATF6 blocks their activation in the absence of ER stress. Accumulation of unfolded proteins in the ER lumen releases BiP and activates the transmembrane proteins. Dimerization and autophosphorylation of IRE1 activates its endonuclease activity that splices XBP1 mRNA. Spliced mRNA encodes for a transcription factor regulating synthesis of chaperones, lipids and protein degradation. Dimerization and autophosphorylation of PERK lead to eIF2 α phosphorylation which inhibits global protein translation while enabling preferential translation of ATF4. Upon activation of ATF6, it is transported into Golgi. After phosphorylation and cleavage of the luminal domain, phosphorylated ATF6 releases and acts as a transcription factor in the nucleus contributing upregulation of ER resident chaperon transcription and lipid synthesis (Navid & Colbert, 2017).....12
- Figure 2.1. Experimental design for non-Sephin1 animal groups.** Animals were assigned into either Western diet or chow diet. There were 7 male mice in each diet group for both *ApoE*^{-/-} and WT mice at the age of 9 weeks. Mice had free access to their designated diet ad libitum for 16 weeks. At the end of 16 weeks of diet duration, animals were sacrificed.20
- Figure 2.2. Dissected hippocampi from left and right hemispheres of the mouse brain.** After removal of olfactory bulb and cerebellum, whole brain was divided into two halves through the midline. Both hemispheres were placed in a petri dish in which

the medial surfaces were facing upwards. One hemisphere was hold in position using forceps and both anterior and posterior portion of the hippocampi were cut in order to free the tissue. Hippocampi was then peeled off from the cortex by gently sliding of the microspatula from posterior to anterior. 22

Figure 2.3. Experimental design for Sefhin1 animal groups. Apoe^{-/-} male mice were assigned into either Sefhin1 injection group or DMSO control group (*n*=3 per group). Diet started at the age of 9-week and after 10 weeks of Western diet, intraperitoneal injection of Sefhin1 (5 mg/kg/day) and DMSO was started. Injections were continued for the last 4 weeks with Western diet. After 14 weeks of diet, animals were sacrificed. 28

Figure 2.4. Cryopreservation of whole brain. The brain was placed inside the labeled cryomold in a proper orientation in which midline should be vertical (Left). Orientation of the tissue should be labeled on cryomold, A stands for anterior and P stands for Posterior. After freezing step, O.C.T. was solidified. Color of O.C.T changes from transparent to white as it freezes and there shouldn't be any crack formation (Right). 29

Figure 2.5. Coronal plane within the volumetric mouse brain atlas, developed by Allen Institute for Brain Research. The coronal plane, represented by a red frame in the figure, divides the brain into an anterior (left side of the image) and posterior (right side of the image) portion parallel to the long axis. 31

Figure 2.6. Schematic illustration of serial hippocampal sectioning. Hippocampus slice collection started when the hippocampal tissue became visible. 10 μm thick sections coronally and sequentially collected onto the microscope slides until the end of the hippocampus. Estimated stereological coordinates of the sliced hippocampus were between -0.94 mm / -2.92 mm from the bregma. White structures represent hippocampus in the figure and images were acquired from Allen Mouse Brain Atlas for construction of the illustration (Lein et al., 2007). 31

Figure 2.7. Schematic illustration of serial slice collection from whole hippocampus. Rectangles represent microscope slides, which were labelled with slide number and sections numbers. Sections were collected sequentially in labelled

microscope slides. 10 μm thick hippocampal section sets, s1 to s40, s41 to s80, and s81 to s120, were serially placed onto left side, middle and right side of the microscope slides, respectively. Whole hippocampus was sectioned in 40 slides x 3 sections/slide. In total, 120 coronal sections were obtained from a single mouse. Nissl stained mouse brain images were taken from Allen Mouse Brain Atlas for construction of the illustration (Lein et al., 2007).....33

Figure 2.8. Representative fluorescence image of the entire right hippocampi stained with anti-Gephyrin. 24 tile images, which were obtained from manual and side by side scanning of the entire hippocampal section, were aligned, stitched and reconstructed by Hugin software. Images were acquired with Zeiss fluorescent microscopy, AxioVision AX10.....36

Figure 2.9. Schematic illustration of systematic stereological sampling method. After conversion of stitched image into a gray scale, threshold was adjusted in order to differentiate background fluorescence from gephyrin signal. Then, 212 μm x 212 μm sampling grids were randomly generated across whole image. CA1, CA3 and DG regions in left and right hippocampi were sampled with sampling frame at every 212 μm in *X* and *Y* level. Yellow frames were located at CA1, blue frames were located at CA3 and purple frames were located at DG. For each animal, mean fluorescence intensity was calculated by averaging values obtained from sampling frames of each subfield ($n=3$).37

Figure 3.1. Effects of hyperlipidemia on pre-synaptic protein level in cortex. After 16 weeks of diet duration, animals were sacrificed, and brain dissection was carried out. After protein isolation, relative synaptophysin protein levels were analyzed with Western blot in the cortex of WT and *ApoE*^{-/-} mice fed on either chow or Western diet, ($n=7$ per group). For the detection of protein of interest, 40 μg protein sample were loaded. (A.) Protein bands corresponding to the synaptophysin were detected at 38 kDa. Tubulin was used as a loading control (55 kDa). (B.) At least 2 technical replicates were used for synaptophysin level comparison between the animal groups. Synaptophysin level in the cortex was calculated relative to tubulin. Significance was

determined using two-way ANOVA. Each bar represents the mean \pm SEM, * $p < 0.05$.

..... 40

Figure 3.2. Effects of hyperlipidemia on pre-synaptic protein level in hippocampus. After 16 weeks of diet duration, animals were sacrificed, and brain dissection was carried out. Hippocampi was isolated from left and right hemisphere. Relative synaptophysin protein levels were analyzed with Western blot in the hippocampus of WT and *ApoE*^{-/-} mice fed on either chow or western diet, ($n=7$ per group). (A.) Representative image shows corresponding synaptophysin (38 kDa) and tubulin (55 kDa) bands (B.) 3 technical replicates were used for synaptophysin level comparison between the animal groups. Synaptophysin level in the hippocampus was calculated relative to tubulin. Statistical significance was determined using two-way ANOVA. Each bar represents the mean \pm SEM..... 41

Figure 3.3. Effects of hyperlipidemia on gephyrin protein level in cortex. Relative gephyrin protein levels were analyzed with Western blot in the cortex of WT and *ApoE*^{-/-} mice fed on either chow or Western diet, ($n=7$ per group). (A.) Protein bands corresponding to the gephyrin were detected at 83 kDa. Tubulin was used as a loading control (55 kDa). (B.) At least 2 technical replicates were used for gephyrin level comparison between the animal groups. Gephyrin level in the cortex was calculated relative to tubulin. Statistical significance was determined using two-way ANOVA. Each bar represents the mean \pm SEM, ** $p < 0.01$ 42

Figure 3.4. Effects of hyperlipidemia on gephyrin protein level in hippocampus. Relative gephyrin protein levels were analyzed with Western blot in the hippocampus of WT and *ApoE*^{-/-} mice fed a chow vs Western diet ($n=7$ per group). (A.) Protein bands corresponding to the gephyrin were detected at 83 kDa. Tubulin was used as a loading control (55 kDa). (B.) Each experiment was repeated 3 times for comparison of gephyrin levels between the animal groups. Gephyrin level in the hippocampus was calculated relative to tubulin. Statistical significance was determined using two-way ANOVA. Each bar represents the mean \pm SEM, ** $p < 0.01$ 43

Figure 3.5. Effects of hyperlipidemia on GFAP protein level in cortex. Relative GFAP protein levels were analyzed with Western blot in the cortical tissue of WT and

Apo^e-/- mice fed a chow vs Western diet (*n*=7 per group). (A.) Protein bands corresponding to the GFAP were detected at 50 kDa. Tubulin was used as a loading control (55 kDa). (B.) Each experiment was repeated at least 2 times for comparison of GFAP levels between the animal groups. GFAP level in the cortex was calculated relative to tubulin. Statistical significance was determined using two-way ANOVA. Each bar represents the mean ± SEM, **p* < 0.05.45

Figure 3.6. Effects of hyperlipidemia on GFAP protein level in hippocampus.

Relative GFAP protein levels were analyzed with Western blot in the hippocampus of WT and *Apo^e-/-* mice fed a chow vs Western diet (*n*=7 per group). (A.) Protein bands corresponding to the GFAP were detected at 50 kDa. Tubulin was used as a loading control (55 kDa). (B.) Each experiment was repeated at least 2 times for comparison of GFAP levels between the animal groups. Hippocampal GFAP level was calculated relative to tubulin. Statistical significance was determined using two-way ANOVA. Each bar represents the mean ± SEM, ***p* < 0.01.46

Figure 3.7. Effects of hyperlipidemia on IL-1β protein level in cortex.

Relative IL-1β protein levels were analyzed with Western blot in the cortical tissue of WT and *Apo^e-/-* mice fed a chow vs Western diet (*n*=7 per group). (A.) Protein bands corresponding to the IL-1β were detected at 35 kDa. Tubulin was used as a loading control (55 kDa). (B.) Each experiment was repeated at least 2 times for comparison of IL-1β levels between the animal groups. IL-1β level in cortex was calculated relative to tubulin. Statistical significance was determined using two-way ANOVA. Each bar represents the mean ± SEM.48

Figure 3.8. Effects of hyperlipidemia on IL-1β protein level in hippocampus.

Relative IL-1β protein levels were analyzed with Western blot in the hippocampal tissue of WT and *Apo^e-/-* mice fed a chow vs Western diet (*n*=7 per group). (A.) Protein bands corresponding to the IL-1β were detected at 35 kDa. Tubulin was used as a loading control (55 kDa). (B.) Each experiment was repeated at least 2 times for comparison of IL-1β levels between the animal groups. Hippocampal IL-1β level was calculated relative to tubulin. Statistical significance was determined using two-way ANOVA. Each bar represents the mean ± SEM, **p* < 0.05 and ***p* < 0.01.....49

Figure 3.9. Effects of hyperlipidemia on p-PERK level in cortex. Relative p-PERK protein levels were analyzed with Western blot in the cortical tissue of WT and *ApoE*^{-/-} mice fed a chow vs western diet (*n*=7 per group). (A.) Protein bands corresponding to the p-PERK were detected at 170 kDa. Tubulin was used as a loading control (55 kDa). (B.) Each experiment was repeated at least 2 times for comparison of p-PERK levels between the animal groups. p-PERK level in cortex was calculated relative to tubulin. Statistical significance was determined using two-way ANOVA. Each bar represents the mean ± SEM, **p* < 0.05. 51

Figure 3.10. Effects of hyperlipidemia on p-PERK level in hippocampus. Relative p-PERK protein levels were analyzed with Western blot in the hippocampal tissue of WT and *ApoE*^{-/-} mice fed a chow vs Western diet (*n*=7 per group). (A.) Protein bands corresponding to the p-PERK were detected at 170 kDa. Tubulin was used as a loading control (55 kDa). (B.) Each experiment was repeated at least 2 times for comparison of p-PERK levels between the animal groups. p-PERK level was calculated relative to tubulin. Statistical significance was determined using two-way ANOVA. Each bar represents the mean ± SEM. 52

Figure 3.11. Effects of hyperlipidemia on p-eiF2α level in cortex. Relative p-eiF2α protein levels were analyzed with Western blot in the cortical tissue of WT and *ApoE*^{-/-} mice fed a chow vs Western diet (*n*=7 per group). (A.) Protein bands corresponding to the p-eiF2α were detected at 36 kDa. Tubulin was used as a loading control (55 kDa). (B.) Each experiment was repeated at least 2 times for comparison of p-eiF2α levels between the animal groups. p-eiF2α level in cortex was calculated relative to tubulin. Statistical significance was determined using two-way ANOVA. Each bar represents the mean ± SEM, **p* < 0.05. 54

Figure 3.12. Effects of hyperlipidemia on p-eiF2α level in hippocampus. Relative p-eiF2α protein levels were analyzed with Western blot in the cortical tissue of WT and *ApoE*^{-/-} mice fed a chow vs Western diet (*n*=7 per group). (A.) Protein bands corresponding to the p-eiF2α were detected at 36 kDa. Tubulin was used as a loading control (55 kDa). (B.) Each experiment was repeated at least 2 times for comparison of p-eiF2α levels between the animal groups. p-eiF2α level in hippocampus was

normalized to tubulin and statistical significance was determined using two-way ANOVA. Each bar represents the mean \pm SEM.55

Figure 3.13. Effects of hyperlipidemia on CHOP level in cortex. Relative CHOP protein levels were analyzed with Western blot in the cortical tissue of WT and *ApoE*^{-/-} mice fed a chow vs Western diet (*n*=7 per group). (A.) Protein bands corresponding to the CHOP were detected at 27 kDa. Tubulin was used as a loading control (55 kDa). (B.) Each experiment was repeated at least 2 times for comparison of CHOP levels between the animal groups. p-eiF2 α level in cortex was normalized to tubulin and statistical significance was determined using two-way ANOVA. Each bar represents the mean \pm SEM.56

Figure 3.14. Effects of hyperlipidemia on CHOP level in hippocampus. Relative CHOP protein levels were analyzed with Western blot in the hippocampal tissue of WT and *ApoE*^{-/-} mice fed a chow vs Western diet (*n*=7 per group). (A.) Protein bands corresponding to the CHOP were detected at 27 kDa. Tubulin was used as a loading control (55 kDa). (B.) Each experiment was repeated at least 2 times for comparison of CHOP levels between the animal groups. CHOP level in hippocampus was normalized to tubulin. Statistical significance was determined using two-way ANOVA. Each bar represents the mean \pm SEM. **p* < 0.05, ****p* < 0.0005.57

Figure 3.15. Representative immunofluorescence images for gephyrin and DAPI staining in hippocampus. *ApoE*^{-/-} male mice were started to be fed Western diet at the age of 9-week. After 10 weeks of Western diet, half of the animals were intraperitoneally injected with Sephin1(5mg/kg/day) and the rest of the animals were injected with DMSO (*n*=3), injection continued for the last 4 weeks along with the diet. After 14 weeks of diet duration, animals were perfused with 10% formalin and brain tissue was dissected. After cryopreservation of the brain tissue, hippocampal tissue was serially sectioned at 10 μ m and immunofluorescence of gephyrin was performed. Images were acquired with Zeiss fluorescent microscopy, AxioVision AX10. Image A, E and I show gephyrin staining of CA1, CA3 and DG subfields of hippocampus in DMSO group, respectively. B, F and J show DAPI staining of CA1, CA3 and DG subfields of hippocampus in DMSO group, respectively. C, G and K

show Gephyrin staining of CA1, CA3 and in Sephin1 group, respectively. D, H and L show Gephyrin staining of CA1, CA3 and in Sephin1 group, respectively. Scale bars, 100 μm 58

Figure 3.16. Changes in gephyrin immunoreactivity in CA1, CA3 and DG regions between DMSO and Sephin1 groups. Mean intensity quantification of gephyrin was performed with systematic sampling method at every 212 μm through X and Y axis through left and right hippocampi. Intensity measurements were done separately in CA1, CA3 and DG regions. CA1, CA3 and DG were sampled an average of ~ 75 , ~ 60 and ~ 60 sites for each animal, respectively ($n=3$). Measurements were obtained by averaging the mean intensities of total sampling frames for each region and each animal. Statistical differences were determined with independent sample t-test between DMSO and Sephin1 group for each subfields of hippocampus. Each bar represents the mean \pm SEM. 59

CHAPTER 1

INTRODUCTION

1.1. Hyperlipidemia

Hyperlipidemia is a multifactorial disease which is usually characterized by elevated cholesterol levels in the circulation, but it may not be always associated with increased triglyceride level in the blood. Therefore, hyperlipidemia and hypercholesterolemia are often used interchangeably in order to define increased blood cholesterol levels (Nelson, 2013). Due to its lipophilic feature, cholesterol is transported through blood via lipoprotein particles such as high-density lipoprotein (HDL), low-density lipoprotein (LDL) and very low-density lipoproteins (VLDL) (Karr, 2017a). LDL is the major transporter particle facilitating cholesterol transport to the peripheral tissues and around 60% of circulating cholesterol resides in LDL in the form of LDL cholesterol (LDL-C) (Sacks et al., 2017). Lipid level standards used in clinic classifications define LDL-C level at or below 100 mg/dL as optimal while LDL-C level higher than 190 mg/dL as very high in humans (Lowden, 2002).

According to World Health Organization's (WHO) statistics from 2008, worldwide estimation of high cholesterol in adults is around 39% and it is responsible for almost 2.6 million (4.5%) deaths in the world. The income level of the country seems to be affecting the prevalence of elevated cholesterol in the population. The prevalence of raised cholesterol is noticeably high in high-income countries 48%, while it is around 25% in low-income countries (WHO, 2008). These global statistics shows the urgent need of interventions for diagnosis and treatment of hyperlipidemia.

1.1.1. Risk Factors

Studying the causes of hyperlipidemia may provide a great insight in order to elucidate the underlying mechanisms of the disease. In fact, there are several documented genetic and environmental factors that are often associated with increased risk of hyperlipidemia (Karr, 2017b). First of all, genetics play a vital role in the progression of elevated blood cholesterol in the form of Familial Hypercholesterolemia (FH). FH is primarily caused by defective genes involved in lipid metabolism pathways. Disturbance of highly regulated lipid pathways via mutations in LDL receptors and lipoproteins results in diminished uptake of cholesterol from circulation leading to severely elevated LDL-C level in blood (Manning & Oakeshott, 2009). Clinical reports show that LDL-C level in individuals with homozygous mutation is usually higher than 500 mg/dL and is categorized as very high level (Cuchel et al., 2014).

In addition to the genetic disposition, environmental factors also play a role in the development of hyperlipidemia. It has been well documented that high consumption of saturated fatty acids is correlated with increased LDL-C level in the circulation (Ooi, Watts, Ng, & Barrett, 2015). Also, being overweight puts individuals at higher risk of hyperlipidemia (DiNicolantonio & O'Keefe, 2018; Zhu et al., 2018). Additionally, physical inactivity and lifestyle choices such as smoking and alcohol consumption have been shown to effect serum lipid profile and increase LDL-C level, leading individuals to become more vulnerable to hyperlipidemia. (Neki, 2002; S. Mannu, J.S. Zaman, Gupta, U. Rehman, & K. Myint, 2013). While genetic and environmental factors are known to increase the risk of hyperlipidemia, it is very likely that hyperlipidemia itself can also be a risk factor for the progression of many other diseases (C.-J. Lin et al., 2015).

1.1.2. Associated Diseases

Hyperlipidemia is often associated with co-occurrence of many other diseases. Elevated blood lipid level contributes to the vascular endothelial dysfunction via

accumulation of fatty plaques in vascular wall lining (Papapanagiotou, Siasos, Kassi, Gargalionis, & Papavassiliou, 2015). This can gradually thicken the blood vessels reducing the blood flow and oxygen supply to the organs. Impairment of structural and functional properties of vascular structure may lead to progression of various diseases including kidney dysfunction, hypertension and hepatic failure (Otsuka et al., 2016; Stapleton, Goodwill, James, Brock, & Frisbee, 2010).

Additionally, dysfunction in the endothelial lining of the arteries due to high level of circulating lipid initiates inflammatory response in coronary vascular system. Enhanced inflammatory response, consequently, promotes accumulation of atherosclerotic plaques in arteries leading to heart failure, heart attack and ischemic stroke (Holven, Ulven, & Bogsrud, 2017; Linton et al., 2019). However, current knowledge of hyperlipidemia associated risk factors is limited due to its complex and systemic effect throughout the body. Thus, establishment of experimental models are of great importance to understand the nature of disease as well as to define therapeutic interventions.

1.1.3. Animal Models

Development of hyperlipidemic animal models provide a key research tool in order to conduct a systemic research and to understand the underlying mechanisms of the disease. Diet supplementation and genetic manipulations are widely used techniques for inducing hyperlipidemia in animals. These animals provide a great insight for hyperlipidemia studies since they display many aspects of human hyperlipidemia (Chan, Karere, Cox, & Vandeberg, 2015; Madariaga et al., 2015).

First approach is diet-induced hyperlipidemia. Feeding wild type mice with commercially available lipid supplementations such as triglyceride and/or cholesterol for 8 or 12 weeks has been shown to almost double the blood cholesterol in the animal compared to standard diet fed control group (Madariaga et al., 2015). Second approach is genetic manipulations. Apolipoprotein E (ApoE) is a component of plasma

lipoprotein particles and facilitates lipid transport from plasma to tissues through LDL receptor binding (Huang & Mahley, 2014). *ApoE* knock out (*ApoE*^{-/-}) animals develop severe hypercholesterolemia even with the standard chow diet and their cholesterol level increases three or four-times compared to wild type (WT) animals. High fat diet (HFD) exacerbates this increase to around twenty fold and makes mice susceptible to atherosclerosis (Zhang, Reddick, Piedrahita, & Maeda, 1992). Second most common genetic manipulation used in hyperlipidemic studies is *ldl* knock out in order to diminish LDL receptor mediated transportation of plasma lipoprotein particles and to decrease plasma cholesterol clearance. Chow diet increases plasma cholesterol around three fold and high cholesterol diet increases cholesterol level around five fold in *ldl*^{-/-} mice compared to standard diet fed WT ones (Ishibashi et al., 1993). Hence, the effect is more moderate in *ldl*^{-/-} mice compared to *ApoE*^{-/-} ones. Many studies have employed one or the other model in order to explore hyperlipidemia progression as well as its underlying reasons yielding valuable insights into the mechanisms of the disease (Getz & Reardon, 2016).

1.2. Hyperlipidemia and Brain

Brain is the most cholesterol rich organ which constitutes almost 25% of total body cholesterol (Maria Giudetti, Romano, Michele Lavecchia, & Gaetani, 2016). Cholesterol is important for myelination, dendrite formation and synaptogenesis, therefore, allowing more efficient synaptic transmission to take place in the brain. Cholesterol synthesis mainly occurs in oligodendrocytes and astrocytes in the brain. Under normal conditions, Blood Brain Barrier (BBB) restricts systemic cholesterol to enter the brain. Even though the brain operates its own cholesterol metabolism, studies show that high lipid level in the circulation has a negative impact on white matter integrity (Cohen, Cazes, & Convit, 2011) and it is associated with increased possibility of cognitive impairment in humans (Davidson et al., 2012). Additionally, longitudinal studies show that elevated serum cholesterol can be a risk factor for mild

cognitive impairment in humans later in life (Solomon et al., 2007). Furthermore, it has been shown that risk of brain infarction in subjects with familial hyperlipidemia is almost twenty times higher compared to general population (Kaste & Koivisto, 1988). Even though several studies aimed to understand the link between hyperlipidemia and cognitive function in the last few decades, the mechanisms of hyperlipidemia-induced cognitive decline is still not well-understood.

Back then, it has been repeatedly shown that lipoprotein bound cholesterol does not cross BBB. Studies found no evidence that lipoprotein cholesterol (HDL-C or LDL-C) that originates in the plasma crosses BBB and is transported into CNS (Turley, Burns, Rosenfeld, & Dietschy, 1996). Additionally, it has been shown that some lipoproteins in the circulation are excluded from the CNS by the BBB because of their sizes (M. Liu, Kuhel, Shen, Hui, & Woods, 2012). Taken together, studies were in agreement with the view that since circulating plasma lipoproteins do not cross BBB, plasma cholesterol is not transported to the brain. This raises the question, then how hyperlipidemia affects the brain performance severely? There are now some emerging hypotheses to explain that transporter proteins involved in the movement of cholesterol in the body are also found in BBB which may facilitate the net movement of cholesterol across BBB (Panzenboeck et al., 2002). Also, it is possible that there may be a small amount of plasma lipoprotein movement across BBB via endocytosis (Quan, Xie, Dietschy, & Turley, 2003). Conclusively, it has been demonstrated that oxygenated product of cholesterol may passively diffuse across BBB (Björkhem, 2006). Nonetheless, further research is necessary to clarify the communication between circulating cholesterol and the brain. In that manner, understanding the cellular and molecular mechanisms of hyperlipidemia-induced cognitive decline holds a great importance for any therapeutic interventions.

1.2.1. Hyperlipidemia Associated Neurodegeneration

Even though the exact mechanism is still not well characterized, hyperlipidemia has been shown to change BBB integrity in addition to its effects on peripheral and coronary vascular system (Kanoski & Davidson, 2011). Since neuronal survival partially depends on the integrity of the microvasculature through regulating oxygen and nutrients delivery, elucidating the mechanisms of hyperlipidemia-induced BBB disruption is important to understand the possible link between hyperlipidemia and neurodegeneration (Hermann & ElAli, 2012).

Physiological functions of the BBB as well as the regulation of lipid metabolism in the brain are managed by astrocytes. Therefore, any form of insult to the Central Nervous System (CNS) initiates a respond in astrocytes through reactive astrogliosis which is often associated with increased level of various cytokines in the brain (Sofroniew & Vinters, 2010a). In rodents, hyperlipidemia downregulates the tight junction proteins in cerebral microvessels leading to increased BBB permeability. As a result, leaky nature of BBB facilitates infiltration of the circulating immune cells into the brain (ElAli, Doeppner, Zechariah, & Hermann, 2011; Stapleton et al., 2010). Studies show that hyperlipidemia-induced cerebral BBB impairment is accompanied by elevated cerebral cytokine level and enhanced astrogliosis which in turn may damage the neurons (Yang et al., 2017). In addition to its global effect on the brain, HFD has been shown to decrease expression of hippocampal capillary tight junction proteins and increase BBB permeability which is often followed by astrogliosis and elevated inflammatory response in the hippocampus (Kanoski, Zhang, Zheng, & Davidson, 2010; Pekny & Pekna, 2016). However, it is not entirely clear what regions of the brain confer greater vulnerability to hyperlipidemia-induced inflammation and neuronal degeneration. Therefore, understanding the region-specific effects of hyperlipidemia in the brain may contribute to a better understanding of hyperlipidemia-associated neurodegeneration and consequent cognitive impairment.

1.2.1.1. Hippocampus

Hippocampus is important for memory consolidation and it brings multiple inputs together to store long-term memory in the cortical regions of the brain (Wible, 2013). The hippocampus is a well-defined structure and it consists of two principle regions; Dentate Gyrus (DG) and Cornu Ammonis (CA). CA is further subdivided into CA1, CA2 and CA3 regions (Figure 1.1.). Hippocampus has been a region of interest in recent hyperlipidemia studies for several reasons. First, it displays some of the earliest signs of neurodegenerative diseases because of its role in memory consolidation. (de Flores, La Joie, & Chételat, 2015). Second, DG is the site of the hippocampus where *de novo* production of neurons occurs and any impairment in neurogenesis due to high level of circulating cholesterol may underlie hyperlipidemia-induced neurodegeneration (Mu & Gage, 2011). Last, animal and human studies suggest that hippocampus may be important for food intake regulation through various interconnected pathways in the brain (Stevenson & Francis, 2017). Thus, understanding hyperlipidemia-induced cellular and molecular alterations in the hippocampus will shed light on why hyperlipidemia may be a risk factor for progression of cognitive decline.

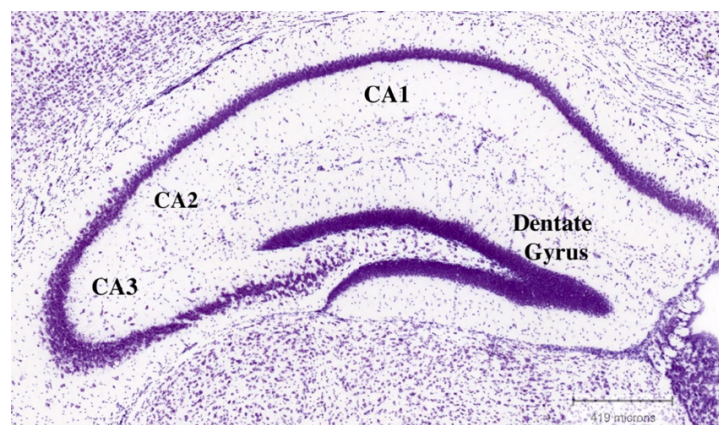


Figure 1.1. Image of Nissl-stained mouse brain section showing the principle areas of hippocampus. Hippocampus is embedded into temporal lobe and can be distinguished by layers of densely packed neurons. Based on its histology, hippocampus is divided into four major areas, namely Dentate Gyrus, CA1, CA2 and CA3 (Lein et al., 2007).

Hyperlipidemia has been shown to contribute to hippocampal-dependent memory impairment in rodents which is usually accompanied by enhanced inflammatory response and neuronal damage in hippocampus (Kosari, Badoer, Nguyen, Killcross, & Jenkins, 2012; Thirumangalakudi et al., 2008) Additionally, hyperlipidemia has shown to increase lipid accumulation in hippocampus indicating a possible BBB leakage. It also leads to degenerative changes in neuron morphology and apoptosis in hippocampal areas (Zhao et al., 2017). Dendritic spine density and pre-synaptic proteins are significantly decreased in the hippocampus of hyperlipidemic animals (Calvo-Ochoa, Hernández-Ortega, Ferrera, Morimoto, & Arias, 2014) Nonetheless, how hyperlipidemia causes these alterations in hippocampal neurons has not been completely elucidated.

Studies show that synaptic damage and consequent synaptic and neuronal loss in hippocampus is the best correlate to the cognitive decline (Wilde, Overk, Sijben, & Masliah, 2016). The loss of synapses begins with modifications in the synaptic vesicle machinery which is usually accompanied by organelle dysfunction, loss of neurotrophic support and reduced synaptic transmission (Overk & Masliah, 2014). These alterations could be reversible in some circumstances. Nonetheless, alterations can become irreversible as the process advances which permanently damages synapses and spines leading to synaptic impairment and neuronal loss. Together, such alterations may be responsible for cognitive decline seen in various neurodegenerative diseases as well as hyperlipidemia-induced neurodegeneration (Knobloch & Mansuy, 2008). Hence, understanding how hyperlipidemia changes organelle function and synaptic machinery would provide a great insight to better understand the mechanism of hyperlipidemia-induced neurodegeneration.

1.3. Endoplasmic Reticulum (ER) Stress

ER is an intracellular organelle important for lipid synthesis, protein folding and processing. Around 30% of the cell's proteome is produced in the ER, therefore, it is critical to maintain ER homeostasis for proper cell function and survival (Navid & Colbert, 2017). Some physiological and pathological conditions require high demand of protein folding which exceeds ER folding capacity, leading to accumulation of unfolded or misfolded proteins in the ER lumen, thereby causing ER stress. Consequently, a collection of signaling pathways relay signals from the ER lumen to the other compartments of the cell to set some responses against the excess protein load. These responses are, together, termed as Unfolded Protein Response (UPR) (J. H. Lin et al., 2007). First, as a transient adaptation, protein load to ER is reduced by lowering protein synthesis. Second, as a long-term adaptation, ER folding capacity is increased via transcriptional activation of protein folding machinery components such as chaperons and if the stress is still persistent, cell death mechanisms can be triggered which usually results in apoptosis (Ron & Walter, 2007).

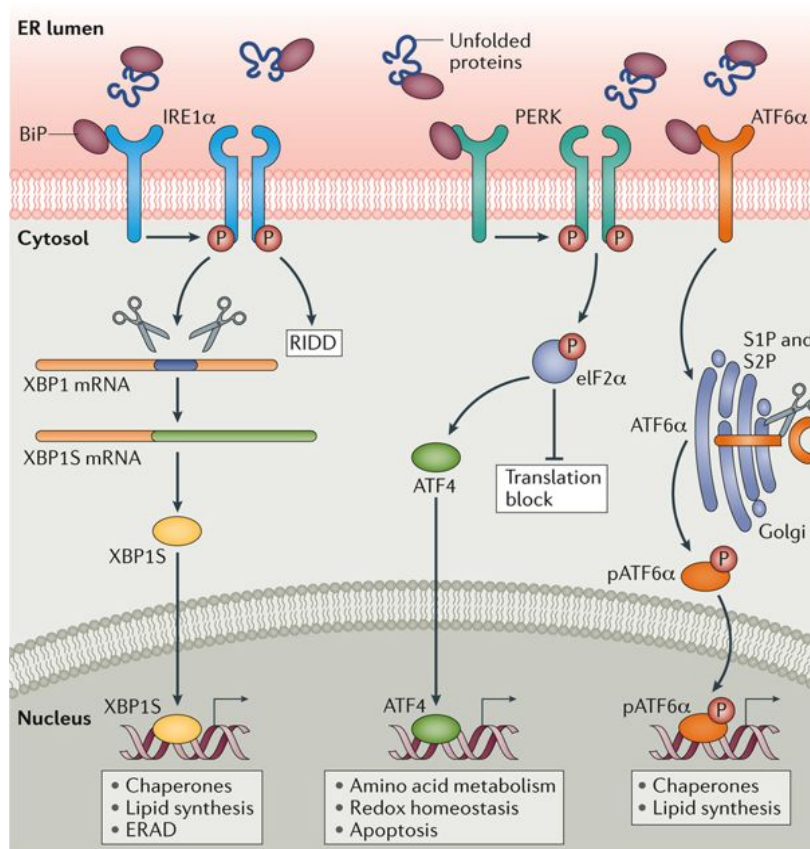
1.3.1. Unfolded Protein Response (UPR)

UPR has many regulatory components involved in maintaining cellular and protein homeostasis. There are three branches of UPR which consists of ER-resident transmembrane proteins, known as inositol-requiring protein 1 (IRE1), PKR-like endoplasmic reticulum kinase (PERK), and activating transcription factor 6 (ATF6) (Jonathan H Lin, Walter, & Yen, 2008). Each transmembrane protein has ER lumen domain which binds to 78 kDa glucose regulated chaperone protein (GRP78), also referred as immunoglobulin heavy chain binding protein (BiP). BiP detaches from these transmembrane sensors in response to misfolded protein accumulation in the ER lumen. Then, IRE1, PERK and ATF6 orchestrate in a coordinated manner and constitute the UPR system to restore ER homeostasis (Navid & Colbert, 2017).

IRE1 is the most conserved branch of the UPR (Patil & Walter, 2001). In its cytosolic domain, it has both serine/threonine protein kinase and endoribonuclease (RNase) activity. Dissociation of BiP from IRE1 due to unfolded and misfolded protein accumulation in ER lumen causes oligomerization and autophosphorylation of IRE1 and activates its RNase activity in the cytosolic domain. Then, activated IRE1 removes 26-base fragment from X box-binding protein 1 (XBP1) encoding mRNA. Spliced mRNA, then, can be translated into a transcription factor and translocated into the nucleus. As a result, it upregulates expression of genes involved in ER associated protein degradation, protein folding and phospholipid synthesis for the expansion of ER membrane under ER stress (Ron & Hubbard, 2008). Therefore, this branch is important to increase the folding capacity of ER in some physiological and pathological conditions that require high demand of protein folding.

PERK is the second branch of the UPR. PERK has a kinase activity on its cytosolic domain, and it resembles IRE1 in that manner. PERK activity is controlled by BiP like IRE1. Removal of BiP triggers homodimerization and autophosphorylation of PERK (p-PERK). It, in return, phosphorylates the α subunit of eukaryotic translation initiation factor-2 (eIF2 α). Phosphorylated eIF2 α (p-eIF2 α) inhibits conversion of guanosine diphosphate (GDP) to guanosine triphosphate (GTP) and inhibits translation initiation complex assembly. Consequently, translation of capped mRNAs is inhibited (Heather P Harding, Zhang, Bertolotti, Zeng, & Ron, 2000). Attenuation of global protein synthesis via PERK mediated eIF2 α phosphorylation is vital because it decreases protein influx to the already stressed ER lumen and copes with the cytotoxic effects of misfolded and unfolded proteins (Navid & Colbert, 2017). On the other hand, p-eIF2 α favors preferential translation of certain mRNAs that have short upstream regulatory elements such as activating transcription factor 4 (ATF4). PERK regulates amino acid metabolism, protein folding and autophagy via ATF4. If the ER stress is persistent, pro-apoptotic factor, C/EBP-homologous protein (CHOP) is upregulated via ATF4. CHOP is another transcription factor which upregulates the expression of genes that involve in apoptosis under severe ER stress (Hetz, 2012).

The last branch of UPR, ATF6, involves leucine zipper motif and can work as a transcription factor. It has Golgi localization sequence in the ER lumen domain masked by BiP. Release of BiP from ATF6 due to misfolded or unfolded protein accumulation unmasks the Golgi localization sequence. Consequently, ATF6 is transported to Golgi through small vesicles. In Golgi, ATF6 is phosphorylated and cleaved by Golgi resident proteases which results in release of leucine zipper transcription factor domain from Golgi membrane. The released fragment of ATF6 is translocated into nucleus and activates transcription UPR target genes to increase ER folding capacity (Schönthal, 2012). ATF6 and IRE1 share common UPR target genes. However, studies show that global inhibition of IRE1 can be embryonically lethal unlike ATF6 (Reimold et al., 2000; Wu et al., 2007). Therefore, ATF6 provides a support to the other UPR branches to handle ER stress.



Nature Reviews | Rheumatology

Figure 1.2. Overview of UPR signaling pathways. Association of BiP with IRE1, PERK and ATF6 blocks their activation in the absence of ER stress. Accumulation of unfolded proteins in the ER lumen releases BiP and activates the transmembrane proteins. Dimerization and autophosphorylation of IRE1 activates its endonuclease activity that splices XBP1 mRNA. Spliced mRNA encodes for a transcription factor regulating synthesis of chaperones, lipids and protein degradation. Dimerization and autophosphorylation of PERK lead to eIF2 α phosphorylation which inhibits global protein translation while enabling preferential translation of ATF4. Upon activation of ATF6, it is transported into Golgi. After phosphorylation and cleavage of the luminal domain, phosphorylated ATF6 releases and acts as a transcription factor in the nucleus contributing upregulation of ER resident chaperon transcription and lipid synthesis (Navid & Colbert, 2017).

These three arms of UPR provide a coordinated response against ER stress by increasing ER folding capacity, degrading unfolded and misfolded proteins and by inhibiting global protein synthesis (Figure 1.2.). However, if ER stress become persistent and these pro-survival responses are not enough to restore the cellular homeostasis, UPR system initiates pro-apoptotic mechanisms eventually leading to cell death (Schönthal, 2012).

1.3.1.1. PERK - eIF2 α Regulated Stress Response

PERK arm of the UPR is important for both global translation inhibition and preferential translation of stress induced genes under severe stress conditions. This paradoxical regulation is achieved through a well-tuned mechanism in which eIF2 α acts as the core component by creating a network between these responses. Hence, eIF2 α has a vital role in determining the cell fate under stress conditions (B'chir et al., 2013).

Unphosphorylated form of eIF2 α is required for proper assembly of translation initiation complex, thereby global protein synthesis can take place (Reid et al., 2016). Dephosphorylation of p-eIF2 α is a tightly regulated process controlled by two different phosphatases, namely stress induced and constitutive phosphatases. They both act through recruiting a catalytic subunit of protein phosphatase 1 (PP1c) in order to remove the phosphate group from p-eIF2 α (Jousse et al., 2003).

In a stressed cell, activated PERK phosphorylates eIF2 α and it starts preferential translation of transcription factor ATF4. ATF4 upregulates CHOP translation, another transcription factor that controls translation of stress induced phosphatase, growth arrest and DNA damage-inducible protein, GADD34, (*Ppp1r15a*). Thus, GADD34 mediated dephosphorylation p-eIF2 α allows protein synthesis to occur at the later stages of stress response and activates other eIF2 α kinases. (Novoa, Zeng, Harding, & Ron, 2001). In other words, stress induced GADD34 activation provides a negative feedback by promoting p-eIF2 α dephosphorylation. Consequently, GADD34 mediated p-eIF2 α dephosphorylation leads to translation of other eIF2 α kinases, namely translational recovery, allowing stress response and apoptotic transcripts to be expressed at the later stages of severe stress (Ryoo & Vasudevan, 2017). Second, constitutive dephosphorylation of p-eIF2 α is governed by phosphatase CReP (*Ppp1r15b*) whose expression does not change in stressed cells, unlike GADD34. Constitutive dephosphorylation of p-eIF2 α through CReP is shown to keep p-eIF2 α level low in unstressed cells (Jousse et al., 2003).

CReP mediated constitutive dephosphorylation is thought to prevent persistent phosphorylation of eIF2 α which would be lethal otherwise (Scheuner et al., 2006).

Activation of PERK-eIF2 α -ATF4-CHOP signaling pathway under severe stress conditions has been implicated in many diseases such as metabolic disease, ischemia diseases and neurodegenerative disorders (Li, Guo, Tang, Jiang, & Chen, 2014). There is now emerging evidence that this pathway may also be involved in hyperlipidemia-induced changes in the brain (Kim, Haque, Goo, & Moon, 2018). Therefore, understanding the role of this pathway in hyperlipidemia-induced neurodegeneration would enable researchers to modulate the pathway and find a therapeutic approach to diminish or prevent the negative effects of hyperlipidemia on the brain.

1.4. Hyperlipidemia-Induced ER Stress in Brain

Dietary lipids are essential for providing energy for the body. Nonetheless, excess intake of dietary lipids increases plasma lipid level and starts to accumulate in various cells and tissues. Consequently, cells cannot handle lipid accumulation due to the lack of adequate machinery for their utilization and storage, and impairment in cellular machineries eventually may lead to cell damage. Elevated plasma lipids exert their cytotoxic effects through their action on organelles, specifically ER (Han & Kaufman, 2016). Chronic ER stress coupled with elevated inflammation due to high plasma lipid levels has been shown to contribute to the pathogenesis of many diseases such as diabetes, cardiovascular diseases and fatty liver diseases (Fu, Watkins, & Hotamisligil, 2012).

In addition to its effects on peripheral organs, hyperlipidemia has been shown to affect the brain metabolism and induce inflammation and apoptosis in the brain leading to neurodegeneration and cognitive impairment (Rutkowsky et al., 2018). Even though the exact underlying molecular mechanisms are not well-established, there is an emerging evidence that organelle dysfunction, particularly ER may be involved in hyperlipidemia-induced neurodegeneration.

It has been demonstrated that cholesterol accumulation in hippocampal neurons changes ER morphology *in vivo*. Electron micrographs shows that ER is swollen and dilated in cholesterol accumulated neurons. Additionally, levels of phosphorylated form of PERK and CHOP are elevated in cholesterol accumulated hippocampal neurons which is the indicator of PERK arm activation of UPR. Cholesterol accumulation also upregulates expression of stress response genes and increases major components of apoptosis such as cleaved caspase 3 and caspase 9. Apoptosis of hippocampal neurons contributes to the progression of hippocampal atrophy and cognitive impairment (Djelti et al., 2015). Studies also show that spliced form XBP1 mRNA expression is higher in the cortex and hippocampus of hyperlipidemic mice compared to control group. This indicates that IRE1 arm of the UPR is activated as well as PERK pathway in the brains of hyperlipidemic animals (Park, Ko, Jeon, & Kwon, 2016). The upregulation of ER stress responsive genes such as *Bip*, *xbp-1*, *chop* and *atf4* in response to hyperlipidemia is correlated with down regulation of synaptic proteins in hippocampus. Thus, ER stress may be associated with altered synaptic structure and function and underlies hyperlipidemia-induced neurodegeneration (Kim et al., 2018).

Several lines of evidence suggest that ER stress may be linked to hyperlipidemia-induced synaptic dysfunction, neurodegeneration and subsequent cognitive impairment. Both *in vitro* and *in vivo* studies show that high cholesterol induces cascade of events that result in BBB leakage, cholesterol accumulation in neurons, inflammation, ER stress and consequent synaptic dysfunction and apoptosis in hippocampus as well as other parts of the brain. Hence, attenuation of UPR activation would provide a neuroprotective effect against negative effects of hyperlipidemia. Modulation of UPR arms with current applications, therefore, would be beneficial to prevent stress induced synaptic impairment and neuronal loss seen in hyperlipidemia.

1.5. PERK Pathway as a Potential Therapeutic Target

While PERK mediated eIF2 α phosphorylation attenuates protein translation, it also causes stress induced gene expression through different mechanisms. ATF4 dependent stress response is heavily studied mostly due to its role in cell fate determination (McQuiston & Diehl, 2017). p-eIF2 α mediated ATF4 translation consequently facilitates expression of pro-apoptotic signals such as CHOP under persistent and unresolvable ER stress. Thus, amount of p-eIF2 α mediated CHOP translation serves as a measure of sustained ER stress (H P Harding et al., 2000). Studies show that upregulation of CHOP is correlated with increased level of stress induced phosphatase GADD34 during severe stress. These findings implicate that expression of stress genes requires translation recovery through GADD34 mediated p-eIF2 α dephosphorylation (Jousse et al., 2003).

PERK signaling has been the interest of many research due to its role in cell fate. Studies show that modulating PERK pathway at different levels can be beneficial for cells and organisms to handle persistent stress and its adverse effects (Pérez-Arancibia, Rivas, & Hetz, 2017). Among them, first identified inhibitor of PERK pathway was Guanabenz (GBZ) that was initially used in hypertension treatment since it acts as an adrenergic receptor agonist (Holmes, Brogden, Heel, Speight, & Avery, 1983). Recently, it has been shown that GBZ inhibits p-eIF2 α dephosphorylation and prolongs p-eIF2 α signal duration. As a result, it protects cells against detrimental effects of misfolded protein accumulation since p-eIF2 α inhibits assembly of translation initiation complex. Consequently, it increases chaperone/substrate ratio and favors protein folding in stressed cells providing an adaptive response. Since stress induced genes requires translation recovery, sustained eIF2 α phosphorylation with GBZ decreases pro-apoptotic protein level during persistent stress (Balch, Morimoto, Dillin, & Kelly, 2008). However, it has been later shown that GBZ cannot be used *in vivo* to selectively target eIF2 α phosphorylation due to its affinity to adrenergic receptor and its consequent side effects such as hypotension, drowsiness, dry mouth and fatigue (Hall, Smolinske, Kulig, & Rumack, 1985).

1.5.1. Selective Inhibition of Stress Induced Phosphatase

Due to its adrenergic receptor affinity and subsequent severe side effects *in vivo*, GBZ is no longer used as a therapeutic approach for progressive diseases. Thus, researchers have started to search for stress induced phosphatase inhibitors devoid of adrenergic activity. Wrabetz et al. 2015, synthesized GBZ derivative, Sephin1, to selectively inhibit stress induced phosphatase GADD34 without any adrenergic receptor activity. Sephin1 specifically disrupts GADD34/PPc1 complex but not constitutive CReP/PPc1. Hence, it prolongs eIF2 α phosphorylation and delays translational recovery. As a consequence, stress induced gene expression and pro-apoptotic markers show no difference between stressed and unstressed cells after Sephin1 treatment, hence, it protects cells from the cytotoxic effect of ER stress. They also show that Sephin1 does not exert any adrenergic receptor activity confirming its specificity to stress induced phosphatase, GADD34/PPc1. Additionally, Sephin1 can reach the brain while exhibiting no adverse effects on general health and memory *in vivo* (Wrabetz et al., 2015). Furthermore, a very recent study showed that Sephin1 administration to multiple sclerosis mouse model protects the CNS against inflammation, asserting a neuroprotective effect (Chen et al., 2019). Thus, Sephin1 may serve as an important potential therapeutic target for wide array of neurodegenerative diseases.

1.6. Aim of the Study

Several studies have shown that hyperlipidemia initiates stress induced signaling cascades and activates transcription of stress response genes in the brain, specifically in hippocampus. Therefore, PERK-eIF2 α mediated upregulation of apoptotic signals as well as elevated inflammatory response may be involved in hyperlipidemia-induced synaptic impairment and neuronal loss. Hyperlipidemia-induced synaptic and neuronal changes, consequently, may lead to progression of cognitive impairment.

Therefore, the first aim of the study was to comprehend the role of PERK-eIF2 α pathway in hyperlipidemia-induced inflammatory and synaptic changes in cortex and hippocampus due to its role in memory and learning. The second aim of the study was to modulate the PERK pathway using a small molecule, Sephin1, *in vivo* in order to reduce or suppress hyperlipidemia-induced synaptic impairment in hippocampus.

CHAPTER 2

MATERIALS AND METHODS

2.1. Ethics Statement

All animal studies were conducted in Bilkent University, Institute of Materials Science and Nanotechnology (UNAM) in collaboration with Prof.Dr.Michelle Adams, Department of Psychology, Bilkent University, Ankara, Turkey and Prof.Dr.Ebru Erbay, Department of Molecular Biology and Genetics, Bilkent University, Ankara, Turkey and the experimental animal ethical care committees of Bilkent University approved all animal experiment protocols used in this study (protocol no: 2018/2).

2.2. Animal Studies

For non-Sephin1 group, *ApoE*^{-/-} mice were used in order to obtain hyperlipidemic phenotype, and they were received from Jackson Laboratory, Bar Harbor, Maine created by Nobuyo Maeda, University of North Carolina. C57BL6/J WT animals were included to the experimental design as a control group, which were purchased from Charles River Wiga GmbH, Sulzfeld, Germany.

2.3. Non-Sephin1 Groups

Experiments were initiated with male *ApoE*^{-/-} mice at 9 weeks of age. Animals were placed on Western diet that consists of 0.21% cholesterol, 21% fat by weight (Ssniff-Spezialdiäten, Soest, Germany, TD.88137/E15721) for 16 weeks or maintained on standard chow diet, 5.2% fat by weight, as a control group ($n=7$ per diet).

In addition to *Apoe*^{-/-} group, 9 weeks of WT animals were placed on both Western and chow diet for the same duration (*n*=7 per diet) (Figure 2.1.). Animals were housed in separate cages and they were kept in a room maintained on a 12hours light/12 hours dark cycle at a temperature of 21–23°C. Animals were randomly assigned into one of two diet groups, Western diet or chow diet, and were allowed to eat their designated diet having free access to water throughout the experiment.



Figure 2.1. Experimental design for non-Sephin1 animal groups. Animals were assigned into either Western diet or chow diet. There were 7 male mice in each diet group for both *ApoE*^{-/-} and WT mice at the age of 9 weeks. Mice had free access to their designated diet ad libitum for 16 weeks. At the end of 16 weeks of diet duration, animals were sacrificed.

At the end of 16-week duration of diet, mice were subjected to fasting for 12 hours and were anesthetized by intraperitoneal injection of ketamine (100 mg/kg) and xylazine (10 mg/kg) solution (Flecknell, 1993). Ketaset (100 mg/mL) and Xylaject (20 mg/mL) solutions were prepared from sterile PBS and they were protected from light. After a period of 3-5 minutes following intraperitoneal injection, mice were examined by a pinch to the paw in order to check that they were under the anesthesia.

With this method, deep anesthesia of the mice lasts 1-2 hours. While the mice were under anesthesia, the abdominal and thoracic cages were opened and around 1 mL of blood was taken from the apex of the heart to measure the metabolic parameters. Then, 10-20 mL ice cold PBS was injected to the apex of the heart and a small incision was made to the right atrium of the heart, allowing PBS and blood to drain from there. The purpose of PBS injection was to wash out the remaining blood in the vascular system and prevent a possible clot formation (Maganto-Garcia, Tarrío, & Lichtman, 2012).

2.3.1. Brain Dissection

After cleaning the vascular system with PBS, animals were euthanized via the cervical dislocation procedure. Then, decapitation was performed in order to dissect the brain tissue. After decapitation, head was fixed in position with forceps and a midline incision was made from posterior to anterior with fine scissors in order to remove the skin. Then, the scissors was placed in foramen magnum and cranium was carefully cut towards the nose. At this step, one should be very careful in order not to perturb the brain. Later, lateral cuts were performed in the direction of eyes and ears and two halves of the skull were separated to reveal the brain. Next, optic nerves were cut, and intact brain was removed using a small spatula. Then, whole brain was placed in a petri dish placed on ice. Brain was washed with ice cold PBS two or three times in order to remove surface contaminants (Carvalho & I. Moreira, 2017). In order to obtain total RNA and protein with desired quality, dissection of the brain should be as fast as possible.

Dissection of hippocampus was started with removal of olfactory bulb and cerebellum using a clean razor blade. Then, in order to isolate the intact hippocampi from each hemisphere, the brain was divided into two halves through the midline. Left and right hemispheres were placed in a petri dish in which the medial surfaces were facing upwards. Left hemisphere was hold in position using forceps and both anterior and posterior portion of the hippocampi were cut in order to free the tissue.

Hippocampi was then peeled off from the cortex by gently sliding of the microspatula from posterior to anterior. The same procedure was applied to the right hemisphere as well (Figure 2.2.) (Sultan, 2013). Once both hippocampi were removed from left and right hemispheres, they were weighed and put into the same 1.5 mL microcentrifuge tube. The remaining parts of each hemisphere containing different regions of the brain were also weighed separately and stored as left and right cortex in different 1.5 mL microcentrifuge tubes. Brain tissues were snap frozen in liquid nitrogen and stored at -80°C until the experiment day.

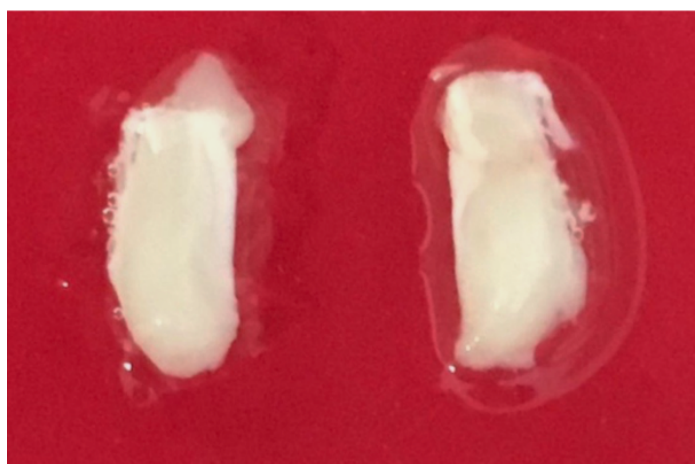


Figure 2.2. Dissected hippocampi from left and right hemispheres of the mouse brain. After removal of olfactory bulb and cerebellum, whole brain was divided into two halves through the midline. Both hemispheres were placed in a petri dish in which the medial surfaces were facing upwards. One hemisphere was hold in position using forceps and both anterior and posterior portion of the hippocampi were cut in order to free the tissue. Hippocampi was then peeled off from the cortex by gently sliding of the microspatula from posterior to anterior.

2.3.2. Brain Tissue Homogenization

Brain tissues were homogenized in ice cold homogenization buffer with protease inhibitors (Appendix B) at around 700 μL buffer per 100 mg tissue (Graham, 2002; Wirths, 2017). Homogenization procedure was done for bilateral hippocampi collected in the same centrifuge tube and for right hemisphere of the cortex. Left hemispheres were stored in -80°C . Samples were homogenized in dounce glass homogenizer and then passed six or eight times through 1 mL of 26 gauge needle (Morse, Shaw, & Larner, 2006). One should be careful that no visible particles remain in the homogenate that should have a milky appearance. Then, the homogenate was divided into two different 1.5 mL centrifuge tubes, one for the RNA isolation (Appendix C) and one for the protein isolation.

2.3.3. Total Protein Isolation

Homogenates of the cortex and hippocampus were centrifuged at 8.000 X g, and the supernatant was discarded in order to remove excess homogenization buffer. Pellets of the cortex and hippocampus were resuspended in 1000 μL and 400 μL , respectively, ice cold RIPA buffer (Appendix D) with protease inhibitors. Samples were sonicated on ice at 50 amp for 0.5-1 cycle for 5-6 times and incubated on ice for 30 minutes. Centrifuge tubes were mixed gently by inversion for every 10 minutes. After 30 minutes of incubation, samples were centrifuged at 11.000 X g for 10 minutes at 4°C . Supernatant containing soluble proteins was carefully transferred into a new centrifuge tube and aliquoted as 100 μL protein samples. The pellet that contained cell debris was discarded.

2.3.4. Protein Concentration Measurement

Coomassie Plus (Bradford) Assay was used according to the manufacturer's instructions. For construction of a standard curve, 1 mg/mL BSA was used according to Table E.1. in Appendix E. Also, protein samples were used in given amount in Table E.2. in Appendix E. Protein measurements were replicated twice for each sample.

After all components were added in the order of ddH₂O, the protein sample and Bradford reagent to 96 well plate, it was incubated at room temperature for 10 minutes. After the incubation, absorbance values were measured at 595A in Spectrophotometer (SpectraMax M5, Molecular Devices, Sunnyvale, CA, USA) in UNAM, Bilkent University. Protein concentrations were then calculated using obtained standard curve equation.

2.3.5. Western Blot

Western blot protocol was followed in order to separate and detect proteins according to their sizes (Eslami & Lujan, 2010).

2.3.5.1. Sample Preparation

After protein concentration was calculated, samples were diluted to 40 µg concentration with ddH₂O and mixed with 2X loading dye (Appendix E) at 1:1 ratio. Then, they were boiled at 95°C for 5 minutes.

2.3.5.2. Preparation of Resolving and Stacking Gel

One and half mm glass and a thin glass were placed on glass holder and placed in a gel casting apparatus without any leakage. Ten percent resolving gel was prepared

according to Table E.4. in Appendix E in a given order and poured between two glasses. Isopropanol was gently added on top of ten percent gel. After polymerization of resolving gel, isopropanol was removed. Five percent stacking gel, prepared according to Table E.4. in Appendix E, was poured onto ten percent resolving gel. One and half mm, fifteen well comb was carefully inserted in five percent resolving gel without any bubble formation. After polymerization, glasses were placed on cassette and placed inside the tank. The tank was loaded with the running buffer (Appendix E) and the comb was removed very carefully in order not to damage the gel. Each well was cleaned with Pasteur pipette in order to remove gel contaminants.

2.3.5.3. Loading and Running the Samples

40 μ g samples were loaded into each well and 2 μ L pre-stained protein ladder (10-250 kDa) was used as a marker. Samples were run at 80 V for thirty minutes until the loading dye reached the middle of the gel, then, the voltage was increased to 100 V and samples were run for about two hours until the loading dye reached the bottom of the gel.

2.3.5.4. Transfer of Proteins to PVDF Membrane

PVDF membrane was incubated in 100% methanol for fifteen seconds and transferred into cold transfer buffer (Appendix E) for ten minutes to equilibrate it. Sponges, filter papers and transfer cassette were soaked into the cold transfer buffer prior to the construction of transfer sandwich. When running of the samples was completed, gels were taken out from the cassette. Glasses were separated from each other and thin glass was removed with the help of spatula, so the gel remained on the thick glass. Stacking gel was discarded with the spatula. Transfer stack was prepared by sandwiching PVDF membrane and gel between two filter papers and two sponges. The membrane should be placed towards positive electrode and the gel should be

placed towards negative electrode. Then, transfer sandwich was placed in tank filled with cold transfer buffer (Appendix E). To keep the system cool, transfer procedure was performed either at 4°C or on ice at 100 V for ninety minutes.

2.3.5.5. Blocking and Antibody Incubation

After transfer was finished, the membrane was taken carefully and washed with cold 0.1% TBS-Triton X (TBS-T) for five minutes. Membrane was horizontally cut according to size of the protein of interest taking protein ladder as a reference. Then, membrane was blocked with either in 5% BSA-TBS-T or 5% milk-TBS-T depending on the antibody for one hour at room temperature. After blocking, the membrane was incubated with primary antibody for overnight at 4°C. For antibodies work properly, best working dilution and dilution reagent (BSA or milk) was determined after different dilution trials, Appendix F. After overnight primary incubation, membrane was washed in cold TBS-T for three times, ten minutes each. Membrane was incubated in suitable HRP conjugated secondary antibody diluted in the blocking solution, Appendix F. Secondary antibody incubation was performed at room temperature for one hour. After secondary antibody incubation, membrane was again washed in cold TBS-T for three times, ten minutes each.

2.3.5.6. Chemiluminescent Detection

After washing steps, the membrane was placed on a flat and clean surface and it was covered with chemiluminescent reagent and incubated for five minutes at room temperature in the dark. Next, excess of chemiluminescent reagent was drained off and placed on transparent plastic file, visualized by Biorad-Chemidoc™ MP imaging system (Bio-Rad, Hercules, CA, USA) in UNAM, Bilkent University. Exposure duration is determined based on the signal intensity.

2.3.5.7. Band Intensity Quantification

ImageJ program (NIH, Bethesda, MD, USA) was used for the band intensity measurements. Each band was selected with rectangular frame, and frame size must be the same for all the other bands across the same row. Band intensities were measured, and intensity of each band was normalized by the average of the total intensity in the same row. Normalized band intensities were then re-normalized by the intensity of internal control, tubulin (Karoglu et al., 2017). Quantification was performed blindly and in an unbiased manner.

2.3.5.8. Statistical Analysis

For each antibody, samples from seven different animal were used individually as a biological replicate ($n=7$) and samples were run at least two times as technical replicates in order to minimize variations which may occur during sample preparation or Western blot. Quantified data was first tested for normality and homogeneity using SPSS program in order to check the assumptions for parametric tests (IBM Corp. Released 2017, n.d.). Then, two-way ANOVAs with the factors of genotype (*ApoE*^{-/-} and WT) and diet (Western and chow diet) was performed with %5 significance level (* $p<0.05$, ** $p<0.01$ and *** $p<0.0005$).

2.4. Sephin1 Groups

The second part of the study aimed at studying the effects of Sephin1 injection on hyperlipidemia-induced synaptic impairment. Eight weeks of *Apo^e-/-* males were fed Western diet ($n=6$). After ten weeks of Western diet, Sephin1, a gift from Anne Bertolotti, MRC, UK, were intraperitoneally (I.P.) injected to half of the animals (5 mg/kg/day) (Wrabetz et al., 2015). The other half was injected with Dimethyl sulfoxide (DMSO) as a control group.

Both Sephin1 and DMSO were daily injected to the animals in 16% (vol/vol) Cremophor EL saline solution and injections were continued for four weeks along with the Western diet (Figure 2.3.).

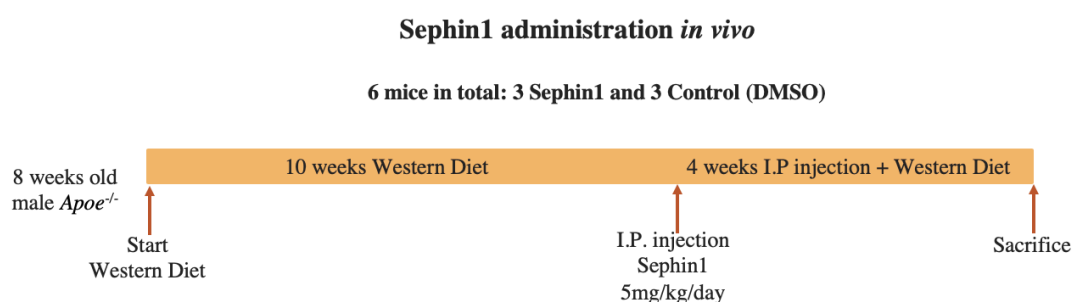


Figure 2.3. Experimental design for Sephin1 animal groups. *Apo^e-/-* male mice were assigned into either Sephin1 injection group or DMSO control group ($n=3$ per group). Diet started at the age of 9-week and after 10 weeks of Western diet, intraperitoneal injection of Sephin1 (5 mg/kg/day) and DMSO was started. Injections were continued for the last 4 weeks with Western diet. After 14 weeks of diet, animals were sacrificed.

At the end of 14-week duration of diet, same anesthesia procedure was applied as in the Non-Sephin1 group (Section 2.3. Non-Sephin1 Groups). After washing out the vascular system with ice cold PBS, animals were transcardially perfused with approximately twenty mL of fresh ten percent formalin solution in PBS, pH 7.4 until the animal became stiff and the tissues were sufficiently fixed.

2.4.1. Whole Brain Cryopreservation

After perfusion of the fixative to the animal, brains were dissected as explained elsewhere (Section 2.3.1. Brain Dissection). Animal information and orientation of the brain is labeled on 15 mm x15 mm x 5mm disposable cryomolds. One or two drops of Optimum Cutting Temperature (O.C.T.) embedding compound were put inside the cryomold in order to hold the brain in position.

Then, the brain was placed inside the O.C.T. filled mold using forceps with proper orientation in which midline of the brain should be vertical (Figure 2.4.). The brain was, then, covered with enough O.C.T. and bubble formation was avoided at this step. O.C.T. covered brain was incubated at room temperature for ten minutes and cryomold was slowly/carefully put inside the cold isopentane which was placed on dry ice. As O.C.T. freezes, its color turns into white from the bottom up (Figure 2.4). The top of the cryomold should not be in contact with isopentane until it completely turns into white, otherwise it may lead to crack formations and tissue damage. When the O.C.T. was fully white and solid, mold was dipped into the isopentane for around ten minutes. Frozen cryomold was wrapped with aluminum foil and stored at -80°C until the cryosectioning of the tissue (Dewan/Loomis-Protocol, 2016).

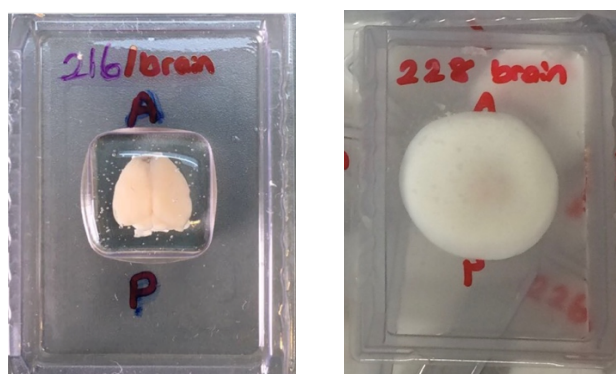


Figure 2.4. Cryopreservation of whole brain. The brain was placed inside the labeled cryomold in a proper orientation in which midline should be vertical (Left). Orientation of the tissue should be labeled on cryomold, A stands for anterior and P stands for Posterior. After freezing step, O.C.T. was solidified. Color of O.C.T. changes from transparent to white as it freezes and there shouldn't be any crack formation (Right).

2.4.2. Cryosectioning

Cryosectioning of the O.C.T. embedded brain was performed in a Leica CM1850 cryostat (Leica Microsystems GmbH, Wetzlar, Germany) in UNAM, Bilkent University. Cryomold was taken and allowed to equilibrate at $-23 \pm 2^{\circ}\text{C}$ inside the cryostat chamber for half an hour prior to sectioning (Ferry, 2014). Equilibrated cryomold was attached to the specimen holder with O.C.T. and oriented relative to the blade. Anterior part of the brain should face toward the blade so that brain sectioning coronally starts from the front (Figure 2.5.). When O.C.T block was ready for sectioning, it was trimmed at 20 or 30 μm until the brain tissue is visible. After reaching the tissue, it was trimmed further at 10 μm in a controlled manner until the first indication of hippocampus was visible according to Allen Mouse Brain Atlas (Lein et al., 2007). Then, 10 μm thick hippocampus sections were serially collected on pre-labelled positively charged adhesive microscope slides. Sectioning continued until the end of the hippocampus, estimated between -0.94 mm / -2.92 mm from the bregma according to mouse brain atlas (Figure 2.6.) (Paxinos & Franklin, 2001). Determination of section thickness was based on different thickness trials and literature (Kayakabe et al., 2014).

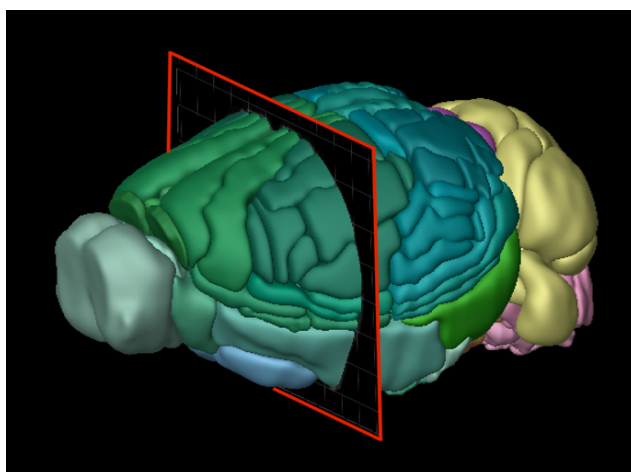


Figure 2.5. Coronal plane within the volumetric mouse brain atlas, developed by Allen Institute for Brain Research. The coronal plane, represented by a red frame in the figure, divides the brain into an anterior (left side of the image) and posterior (right side of the image) portion parallel to the long axis.



Figure 2.6. Schematic illustration of serial hippocampal sectioning. Hippocampus slice collection started when the hippocampal tissue became visible. 10 μm thick sections coronally and sequentially collected onto the microscope slides until the end of the hippocampus. Estimated stereological coordinates of the sliced hippocampus were between -0.94 mm / -2.92 mm from the bregma. White structures represent hippocampus in the figure and images were acquired from Allen Mouse Brain Atlas for construction of the illustration (Lein et al., 2007).

Whole hippocampus was sectioned at 10 μm which gave approximately 120 sections from beginning to the end of the hippocampus. Three sections were placed onto one microscope slide next to each other. Therefore, 40 microscope slides, three sections on each, were obtained from one animal's hippocampus. Prior to sectioning, slides were labelled with slide numbers (1st slide, 2nd slide, 3rd slide...) and hippocampus section numbers (s1, s2, s3...). The sections were collected such that the first set of hippocampus sections, from s1 to s40, were serially placed onto left side of the microscope slides. Second set of hippocampus sections, from s41 to s80, were taken onto the middle. Finally, the last set of hippocampus sections, from s81 to s120 were collected onto the right side of the microscope slides (Figure 2.7.). As a result of this sampling arrangement, one microscope slide provided three sections of hippocampus; one from early, one from middle and one from late regions of the hippocampus (A. Liu, Aoki, & Wickens, 2017; Olesen, Needham, & Pakkenberg, 2017).

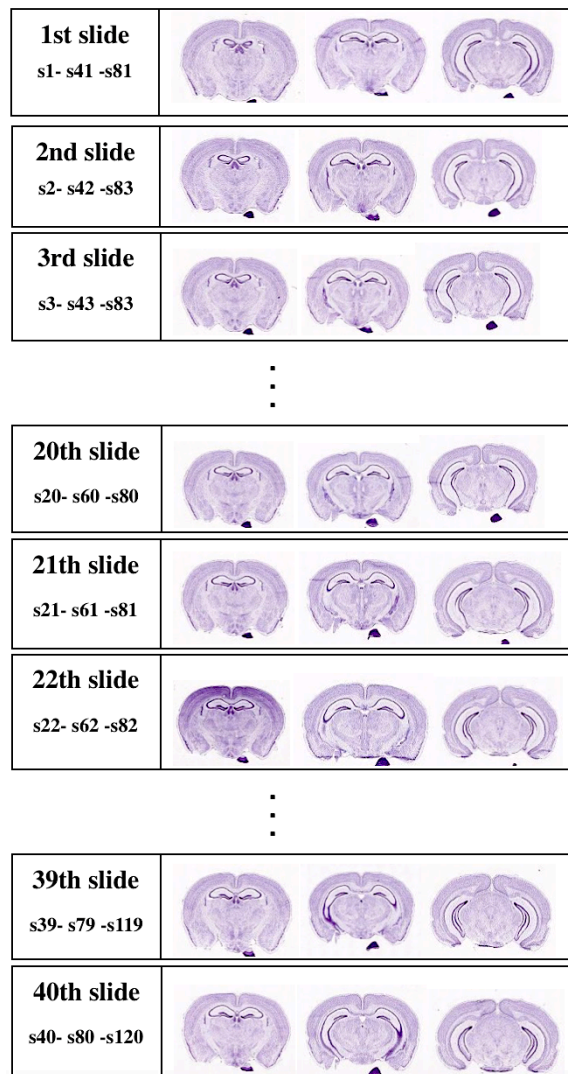


Figure 2.7. Schematic illustration of serial slice collection from whole hippocampus. Rectangles represent microscope slides, which were labelled with slide number and sections numbers. Sections were collected sequentially in labelled microscope slides. 10 μm thick hippocampal section sets, s1 to s40, s41 to s80, and s81 to s120, were serially placed onto left side, middle and right side of the microscope slides, respectively. Whole hippocampus was sectioned in 40 slides x 3 sections/slide. In total, 120 coronal sections were obtained from a single mouse. Nissl stained mouse brain images were taken from Allen Mouse Brain Atlas for construction of the illustration (Lein et al., 2007).

At the end of the sectioning procedure, slides were incubated at room temperature for 15 minutes. After the incubation, slides were placed in a slide box and stored at -80°C until the immunostaining procedure.

2.4.3. Immunostaining

Three equally spaced series of slides, every 10th one, were used per animal for immunostaining procedure. Beginning of the slides had a random starting point for each animal in order to prevent sampling bias (Smith, Adams, Gallagher, Morrison, & Rapp, 2000a). With this method, nine hippocampal sections were included for immunostaining/animal and the space between the sections was fixed to 100 μ m for every animal.

Slides were incubated on ice for thirty minutes. Then, they were boiled in citrate solution (Appendix G) for antigen retrieval for thirty minutes. Next, slides were incubated in citrate solution until they cooled down to room temperature, approximately twenty minutes. After the antigen retrieval step, slides were washed in 0.025% TBS-TritonX two times, ten minutes each with gentle agitation in order to remove the excess citrate buffer. After the washing step, brain sections were surrounded with hydrophobic pen. Eighty μ L blocking solution (five percent BSA in TBS-TritonX (Appendix G)) were added onto each section and incubated at room temperature for one hour in order to prevent unspecific binding of antibodies. When the incubation was done, excess blocking solution was drained off from the section and eighty μ L rabbit anti-Gephyrin primary antibody (Abcam, Cambridge, MA, USA, #ab83765), diluted in blocking solution to 1:750, was added onto the sections. No primary and no secondary stainings were included as controls. Slides were put in a plastic petri dish and incubated overnight at 4°C. Petri dishes were cover with wet tissue paper in order to prevent vaporization of the antibody solution. The next day, excess primary antibody was removed, and slides were washed three times, fifteen minutes each in 0.025% TBS-TritonX with gentle agitation. Secondary antibody incubation was performed with Alexa Fluor® 555 Conjugate anti-rabbit (Cell Signaling Technology, Beverley, MA, USA, #4413) (1:1000) for 1 hour at room temperature. Then, slides were washed three times, fifteen minutes each, in TBS with gentle agitation. Finally, excess TBS was drained off from the sections and slides were mounted with mounting media with DAPI.

Sections were covered with 24 mm x 50 mm cover glass without any bubble formation and edges were sealed with nail polish. After nail polish was completely dry, immunostained slides were put in a slide box and stored at 4°C in the dark until the microscopy imaging.

2.4.4. Microscopy Imaging

Images of immunostained hippocampal sections were acquired using Zeiss fluorescent microscope (AxioVision AX10, Zeiss, Oberkochen, Germany) in UNAM, Bilkent University. Acquisition parameters were kept constant for every section from each experimental group. The specificity of immunofluorescence staining as well as fluorescence crosstalk were checked by acquiring images in separate wavelength channels. An entire hippocampal section was manually screened side by side with 10 X objective. Open source Hugin software (<http://www.hugin.sourceforge.net>) was used for computerized alignment and reconstruction of a whole hippocampal structure from multiple tile images (Figure 2.8.) (Replogle et al., 2018). Thereby, it facilitated signal quantification of whole hippocampus at once (Chappelow, Tomaszewski, Feldman, Shih, & Madabhushi, 2011).

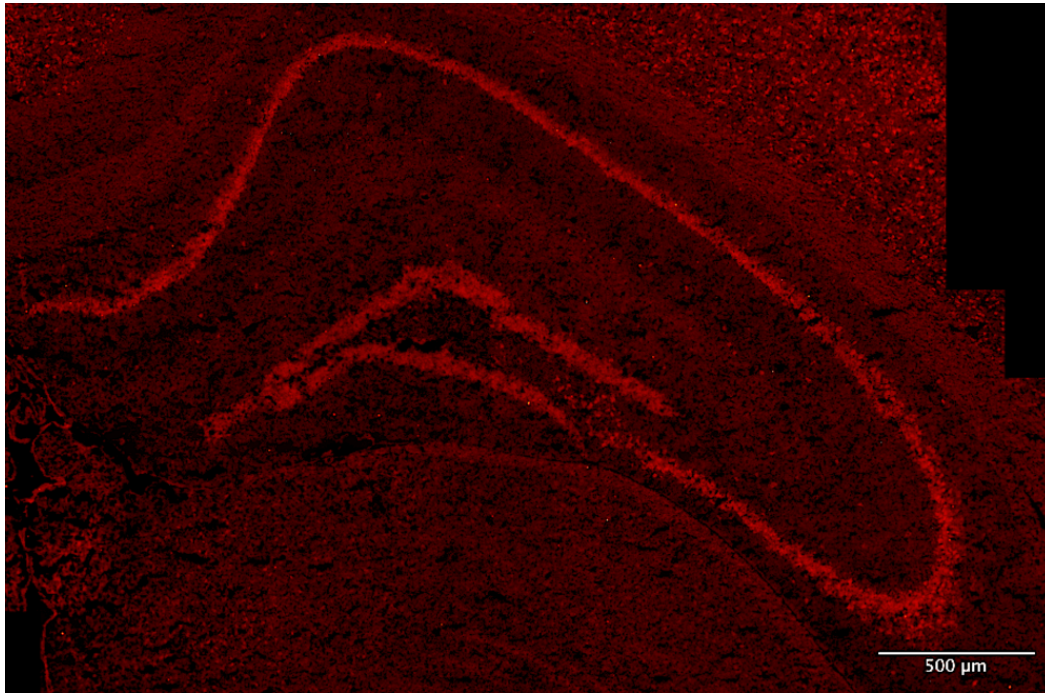


Figure 2.8. Representative fluorescence image of the entire right hippocampi stained with anti-Gephyrin. 24 tile images, which were obtained from manual and side by side scanning of the entire hippocampal section, were aligned, stitched and reconstructed by Hugin software. Images were acquired with Zeiss fluorescent microscopy, AxioVision AX10 with 10X objective.

2.4.5. Stereological Analysis

Systematic stereological sampling method was applied to quantify mean fluorescence intensity of gephyrin staining throughout the entire hippocampal tissue using ImageJ software (NIH, Bethesda, MD, USA). Systematic sampling includes sampling of the whole region of interest with defined intervals at a random starting point. Therefore, it provides a defined periodicity. Additionally, all segments of the tissue can be sampled with equal probability with this method (Gundersen, Jensen, Kiêu, & Nielsen J, 1999). After conversion of stitched images into 8-bit gray scale, threshold was set for every image in order to distinguish background fluorescence from gephyrin signal. For systematic sampling, 212 μm x 212 μm sampling grids were generated with a random starting point throughout one hippocampi (Alexander et al., 2016).

Left and right hippocampi were sampled at every 212 μm through X and Y axis and mean intensity measurements were done separately for CA1, CA3 and DG (Figure 2.9) (Kneynsberg & Kanaan, 2017). With this design, CA1 region was sampled an average of ~ 75 , CA3 and DG regions were sampled an average of ~ 60 sites in every hippocampal region of each animal (Smith, Adams, Gallagher, Morrison, & Rapp, 2000b). Fluorescence intensity was obtained by averaging the mean intensities of sampling frames for each region and each animal. All image analyses were performed blindly by randomized labelling of the images.

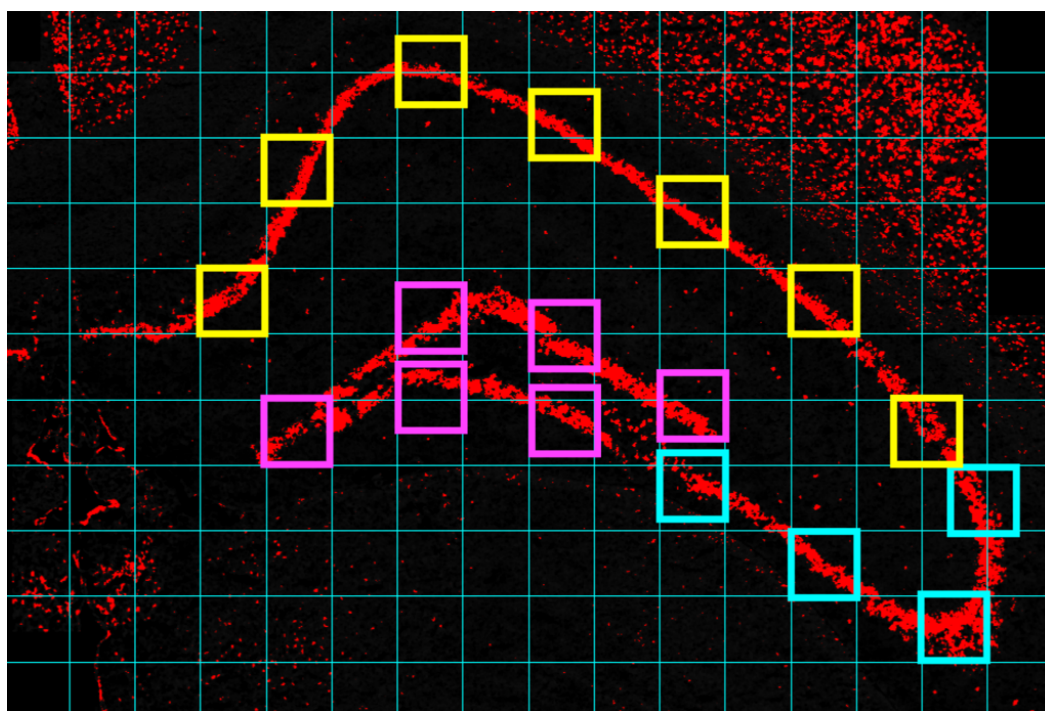


Figure 2.9. Schematic illustration of systematic stereological sampling method. After conversion of stitched image into a gray scale, threshold was adjusted in order to differentiate background fluorescence from gephyrin signal. 212 μm x 212 μm sampling grids were randomly generated across whole image. CA1, CA3 and DG regions in left and right hippocampi were sampled with sampling frame at every 212 μm in X and Y level. Yellow frames were located at CA1, blue frames were located at CA3 and purple frames were located at DG. For each animal, mean fluorescence intensity was calculated by averaging values obtained from sampling frames of each subfield ($n=3$).

2.4.6. Statistical Analysis

In order to identify significant differences in mean fluorescence intensity between Sephin1 and DMSO group for each subfields of hippocampus, independent sample t-test was applied using SPSS program (IBM Corp. Released 2017, n.d.).

CHAPTER 3

RESULTS

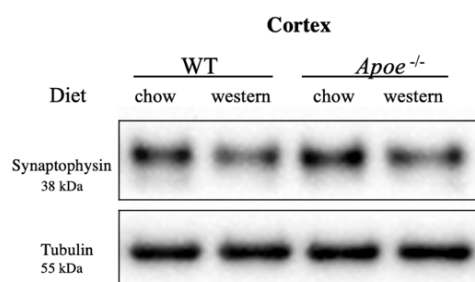
3.1. Hyperlipidemia Status of Experimental Groups

When WT mice with C57BL6/J background fed a HFD, they develop mild to moderate hypercholesterolemia phenotype which exhibits only minor changes in their lipid profile (Heydemann, 2016; Unruh et al., 2015). Nevertheless, the effect of HFD was exacerbated in *ApoE*^{-/-} animals, and their cholesterol level increases two or three times as compared with *ApoE*^{-/-} mice fed a chow diet (Kolbus et al., 2010). Therefore, *ApoE*^{-/-} mice fed a Western diet were expected to exhibit severe hyperlipidemia compared to other animal groups in the experimental design (Figure 2.3.). Assessment of lipid profile in severe hyperlipidemic group was done by Dr.Umut İnci Onat and , in agreement with the earlier findings, Onat et al. 2019 showed that *ApoE*^{-/-} mice fed Western diet exhibited significantly elevated total cholesterol levels in their circulation (~ 500 mg/dl).

3.2. Effects of Hyperlipidemia on Synaptic Protein Levels

Western blot analysis of synaptophysin and gephyrin was performed in order to investigate the effects of hyperlipidemia on pre-synaptic and post-synaptic protein levels in the cortex and hippocampus. Normalized data implicated that, pre-synaptic protein synaptophysin level significantly decreased after Western diet in the cortex of WT mice, * $p=0.022$ and similarly, Western diet markedly lowered synaptophysin levels in the cortex of *ApoE*^{-/-} animals, * $p=0.015$ (Figure 3.1).

A.



B.

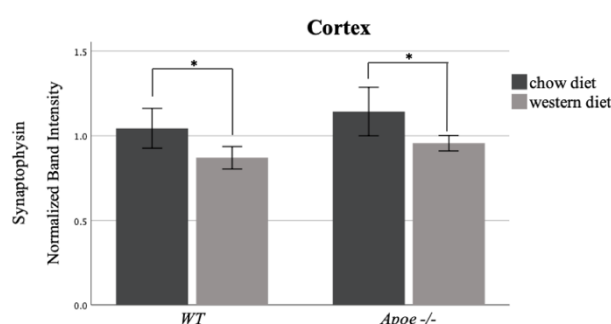
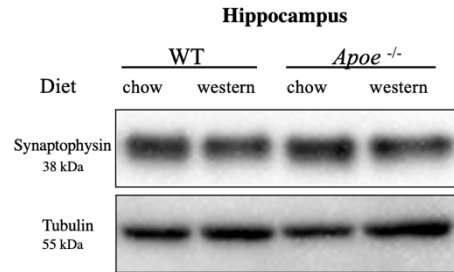


Figure 3.1. Effects of hyperlipidemia on pre-synaptic protein level in cortex. After 16 weeks of diet duration, animals were sacrificed, and brain dissection was carried out. After protein isolation, relative synaptophysin protein levels were analyzed with Western blot in the cortex of WT and *Apoe*^{-/-} mice fed on either chow or Western diet, ($n=7$ per group). For the detection of protein of interest, 40 μ g protein sample were loaded. (A.) Protein bands corresponding to the synaptophysin were detected at 38 kDa. Tubulin was used as a loading control (55 kDa). (B.) At least 2 technical replicates were used for synaptophysin level comparison between the animal groups. Synaptophysin level in the cortex was calculated relative to tubulin. Significance was determined using two-way ANOVA. Each bar represents the mean \pm SEM, $*p < 0.05$.

In contrast to the cortex, Western diet did not substantially affect the synaptophysin levels in the hippocampus of WT and *Apoe*^{-/-} mice. Although synaptophysin level was not statistically different between WT and *Apoe*^{-/-} groups, normalized data implicated that synaptophysin tended to be decreased with Western diet in the hippocampus. (Figure 3.2.). Additionally, effect of western diet on synaptophysin level was more pronounced in *Apoe*^{-/-} animals ($p=0.088$) compared to WT groups ($p=0.540$). Besides, severe hypercholesteremic group displayed the lowest synaptophysin level in the hippocampus compared to the rest of the animals.

A.



B.

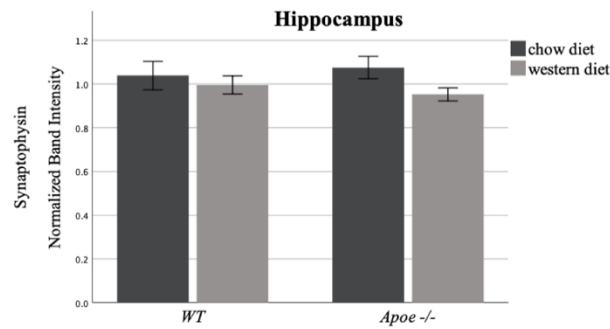
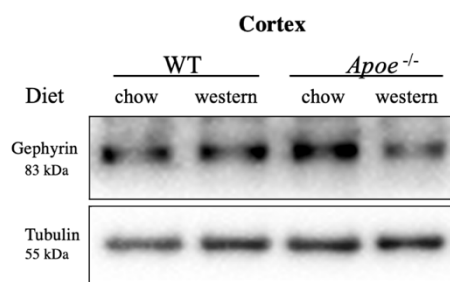


Figure 3.2. Effects of hyperlipidemia on pre-synaptic protein level in hippocampus. After 16 weeks of diet duration, animals were sacrificed, and brain dissection was carried out. Hippocampi was isolated from left and right hemisphere. Relative synaptophysin protein levels were analyzed with Western blot in the hippocampus of WT and *ApoE*^{-/-} mice fed on either chow or western diet, ($n=7$ per group). (A.) Representative image shows corresponding synaptophysin (38 kDa) and tubulin (55 kDa) bands (B.) 3 technical replicates were used for synaptophysin level comparison between the animal groups. Synaptophysin level in the hippocampus was calculated relative to tubulin. Statistical significance was determined using two-way ANOVA. Each bar represents the mean \pm SEM.

Further, Western blot analysis showed that Western diet not only affected pre-synaptic protein level but also affected post-synaptic protein gephyrin levels in the same manner. In particular, gephyrin level was markedly reduced in the cortex of *Apoe*^{-/-} mice fed Western diet (***p*=0.009) compared to chow diet fed *Apoe*^{-/-} mice (Figure 3.3). Additionally, WT animals showed a tendency for reduced gephyrin level in their cortex when they were fed on Western diet. Furthermore, pairwise comparisons of diet, chow vs Western, implicated that Western diet notably reduces gephyrin levels in cortex regardless of the genotype (**p*=0.016).

A.



B.

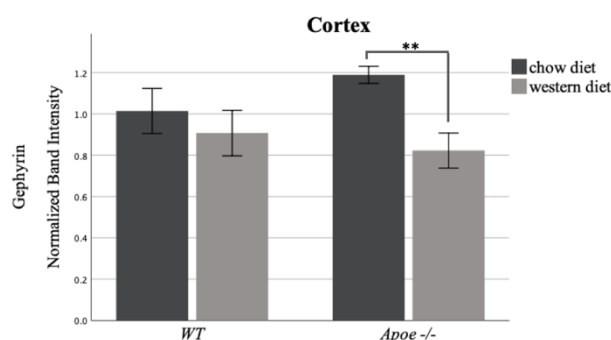
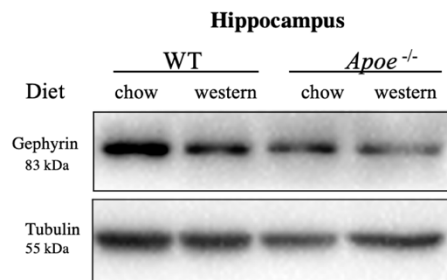


Figure 3.3. Effects of hyperlipidemia on gephyrin protein level in cortex. Relative gephyrin protein levels were analyzed with Western blot in the cortex of WT and *ApoE*^{-/-} mice fed on either chow or Western diet, (*n*=7 per group). (A.) Protein bands corresponding to the gephyrin were detected at 83 kDa. Tubulin was used as a loading control (55 kDa). (B.) At least 2 technical replicates were used for gephyrin level comparison between the animal groups. Gephyrin level in the cortex was calculated relative to tubulin. Statistical significance was determined using two-way ANOVA. Each bar represents the mean ± SEM, ***p* < 0.01.

Similar to the cortex, gephyrin levels were significantly decreased in the hippocampus of the severe hyperlipidemic group compared to chow diet fed *Apoe*^{-/-} mice (***p*=0.009). Additionally, hippocampal gephyrin levels tended to be reduced in the mild hyperlipidemic mice group, WT mice fed a Western diet, compared to chow diet fed control group (Figure 3.4.). The effect of Western diet on gephyrin levels in *Apoe*^{-/-} animals was more pronounced in the hippocampus (**p*=0.004) compared to the cortex (**p*=0.016).

A.



B.

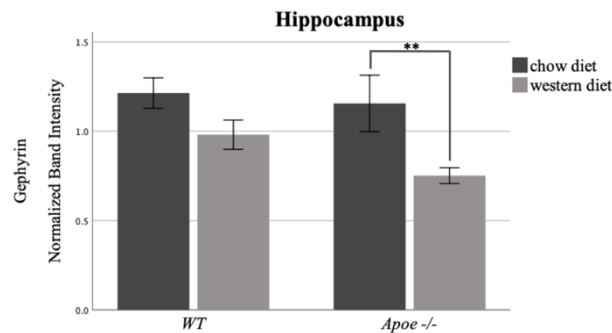


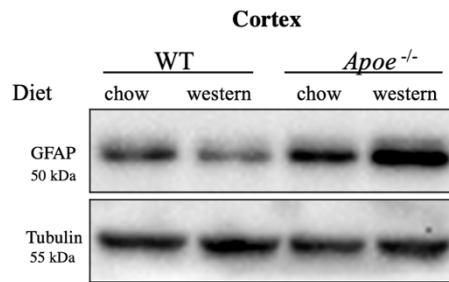
Figure 3.4. Effects of hyperlipidemia on gephyrin protein level in hippocampus. Relative gephyrin protein levels were analyzed with Western blot in the hippocampus of WT and *ApoE*^{-/-} mice fed a chow vs Western diet (*n*=7 per group). (A.) Protein bands corresponding to the gephyrin were detected at 83 kDa. Tubulin was used as a loading control (55 kDa). (B.) Each experiment was repeated 3 times for comparison of gephyrin levels between the animal groups. Gephyrin level in the hippocampus was calculated relative to tubulin. Statistical significance was determined using two-way ANOVA. Each bar represents the mean \pm SEM, ***p* < 0.01.

3.3. Effects of Hyperlipidemia on Astrogliosis

Astrocytes play a vital role in maintaining brain homeostasis. They regulate maintenance of BBB, neuronal signaling and synaptic integrity (Sofroniew & Vinters, 2010a). In response to acute or chronic insult to the brain, astrocytes become reactive astrogliosis. Increased levels of glial fibrillary acidic protein (GFAP) is an indicator of astroglial activation and gliosis i.e. proliferation of astrocytes (Brahmachari, Fung, & Pahan, 2006). In order to examine astroglial activation in response to hyperlipidemia and to assess relationship between decreased synaptic proteins and astrocyte activation in hyperlipidemic animals, GFAP levels were analyzed in the cortex and hippocampus with Western blot.

Western blot analysis showed that Western diet markedly increased GFAP levels in the cortex of *ApoE*^{-/-} animals compared to WT ones (**p*=0.035). This result indicated that severe hyperlipidemic mice showed elevated cortical astrogliosis in contrast to mild hyperlipidemic WT mice. Interestingly, astrogliosis levels in *ApoE*^{-/-} mice were not changed with Western diet (Figure 3.5.). Pair-wise comparisons of genotype indicated that astrogliosis was considerably elevated in the cortex of *ApoE*^{-/-} mice compared to WT regardless of diet (**p*=0.018).

A.



B.

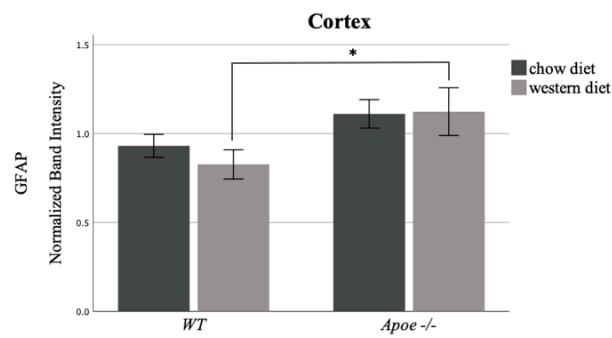
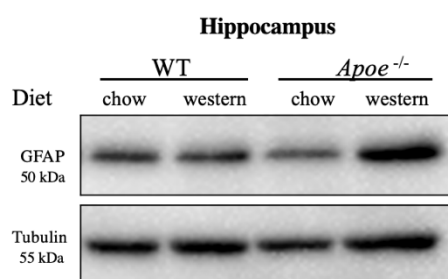


Figure 3.5. Effects of hyperlipidemia on GFAP protein level in cortex. Relative GFAP protein levels were analyzed with Western blot in the cortical tissue of WT and *Apo^e-/-* mice fed a chow vs Western diet ($n=7$ per group). (A.) Protein bands corresponding to the GFAP were detected at 50 kDa. Tubulin was used as a loading control (55 kDa). (B.) Each experiment was repeated at least 2 times for comparison of GFAP levels between the animal groups. GFAP level in the cortex was calculated relative to tubulin. Statistical significance was determined using two-way ANOVA. Each bar represents the mean \pm SEM, $*p < 0.05$.

In the hippocampus, Western diet significantly increased astrogliosis in contrast to chow diet in *ApoE*^{-/-} mice (***p*=0.003) and GFAP level was the highest in the severe hyperlipidemic group compared to the others. Overall, the data showed that decrease in post-synaptic protein gephyrin level was accompanied by markedly increased astrogliosis in the hippocampal tissue of the severe hyperlipidemic group (Figure 3.4 and Figure 3.6).

A.



B.

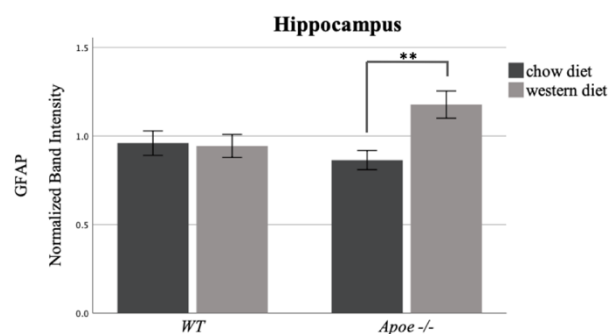


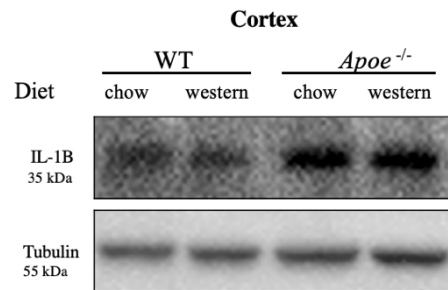
Figure 3.6. Effects of hyperlipidemia on GFAP protein level in hippocampus. Relative GFAP protein levels were analyzed with Western blot in the hippocampus of WT and *ApoE*^{-/-} mice fed a chow vs Western diet (*n*=7 per group). (A.) Protein bands corresponding to the GFAP were detected at 50 kDa. Tubulin was used as a loading control (55 kDa). (B.) Each experiment was repeated at least 2 times for comparison of GFAP levels between the animal groups. Hippocampal GFAP level was calculated relative to tubulin. Statistical significance was determined using two-way ANOVA. Each bar represents the mean \pm SEM, ***p* < 0.01.

3.4. Effects of Hyperlipidemia on Cytokine Level

In the brain, number of astrocytes increases in response to an injury or neurodegenerative processes. Therefore, astrogliosis is often an indicator of pathology in CNS. Many mediators have been shown to involve in astrocyte activation in the brain. Pro-inflammatory cytokines are one of the regulators of astrogliosis, specifically IL1-B has been shown to upregulate astrogliosis in response to a CNS insult. (Pekny & Pekna, 2014). (Herx & Yong, 2001). Therefore, IL-1 β protein levels were analyzed with Western blot in cortex (Mengi, 2019) and hippocampus in order to examine the effects of hyperlipidemia on pro-inflammatory cytokine level as well as its relationship between GFAP levels.

The data showed that IL-1 β levels were not changed with diet in the cortex of WT and *Apo^e^{-/-}* mice. However, pair-wise analysis showed that IL-1 β levels were markedly increased in the cortex of transgenic mice (* $p=0.047$) compared to WT mice.

A.



B.

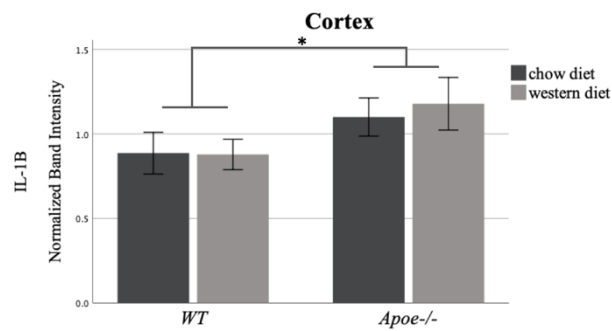
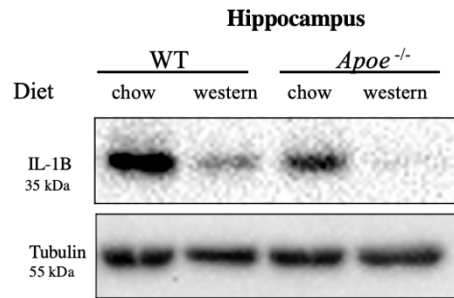


Figure 3.7. Effects of hyperlipidemia on IL-1 β protein level in cortex. Relative IL-1 β protein levels were analyzed with Western blot in the cortical tissue of WT and *ApoE*^{-/-} mice fed a chow vs Western diet ($n=7$ per group). (A.) Protein bands corresponding to the IL-1 β were detected at 35 kDa. Tubulin was used as a loading control (55 kDa). (B.) Each experiment was repeated at least 2 times for comparison of IL-1 β levels between the animal groups. IL-1 β level in cortex was calculated relative to tubulin. Statistical significance was determined using two-way ANOVA. Each bar represents the mean \pm SEM.

In the hippocampus, IL-1 β levels significantly reduced in mice on Western diet. In WT mice Western diet significantly decreased IL-1 β levels (** $p=0.001$) and same decreasing pattern with Western diet was observed in *ApoE*^{-/-} mice as well ($*p=0.025$).

A.



B.

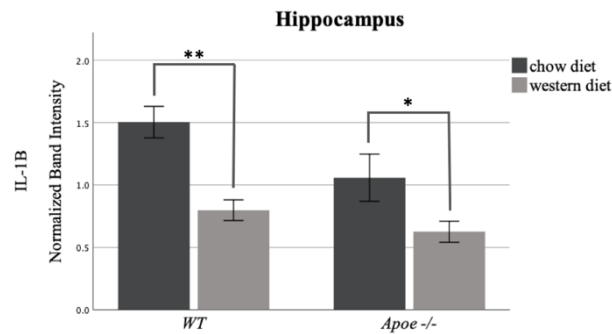


Figure 3.8. Effects of hyperlipidemia on IL-1 β protein level in hippocampus. Relative IL-1 β protein levels were analyzed with Western blot in the hippocampal tissue of WT and *ApoE*^{-/-} mice fed a chow vs Western diet (n=7 per group). (A.) Protein bands corresponding to the IL-1 β were detected at 35 kDa. Tubulin was used as a loading control (55 kDa). (B.) Each experiment was repeated at least 2 times for comparison of IL-1 β levels between the animal groups. Hippocampal IL-1 β level was calculated relative to tubulin. Statistical significance was determined using two-way ANOVA. Each bar represents the mean \pm SEM, $*p < 0.05$ and $**p < 0.01$.

3.5. Effects of Hyperlipidemia on PERK pathway Activation

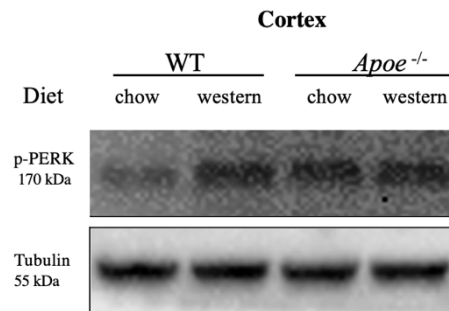
Thus far, results suggested that hyperlipidemia may affect synaptic protein and pro-inflammatory cytokine levels as well as astrogliosis in the cortex and hippocampus. In order to comprehend the relationship between hyperlipidemia-induced changes and UPR activation in the brain, levels of PERK arm components were analyzed with Western blot analysis in experimental animals.

3.5.1. p-PERK

The first step in PERK mediated signal transduction is oligomerization and autophosphorylation of PERK. Therefore, p-PERK is often used as a measure of PERK arm activation in ER stress (Scheper & Hoozemans, 2015).

In the cortex, Western diet significantly increased p-PERK level in WT mice ($*p=0.023$). However, p-PERK level were not changed with diet in *ApoE*^{-/-} mice (Figure 3.9.). Even though p-PERK level did not change with Western and chow diet in *ApoE*^{-/-} animals, p-PERK level was dramatically higher than WT ones regardless of the diet choice ($***p=0.000365$) implicating that basal levels of p-PERK was increased in transgenic animals regardless of the diet type .

A.



B.

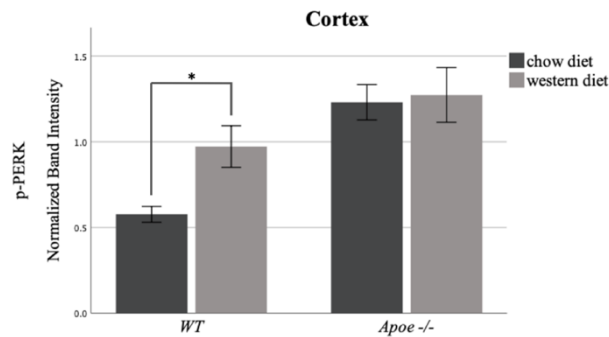
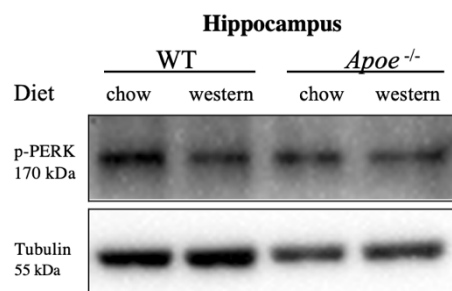


Figure 3.9. Effects of hyperlipidemia on p-PERK level in cortex. Relative p-PERK protein levels were analyzed with Western blot in the cortical tissue of WT and *ApoE*^{-/-} mice fed a chow vs western diet ($n=7$ per group). (A.) Protein bands corresponding to the p-PERK were detected at 170 kDa. Tubulin was used as a loading control (55 kDa). (B.) Each experiment was repeated at least 2 times for comparison of p-PERK levels between the animal groups. p-PERK level in cortex was calculated relative to tubulin. Statistical significance was determined using two-way ANOVA. Each bar represents the mean \pm SEM, * $p < 0.05$.

In contrast to the cortex, neither diet nor genotype markedly affected p-PERK levels in the hippocampus (Figure 3.10.), nevertheless, there was a tendency towards decreased p-PERK level with Western diet in both mice strain.

A.



B.

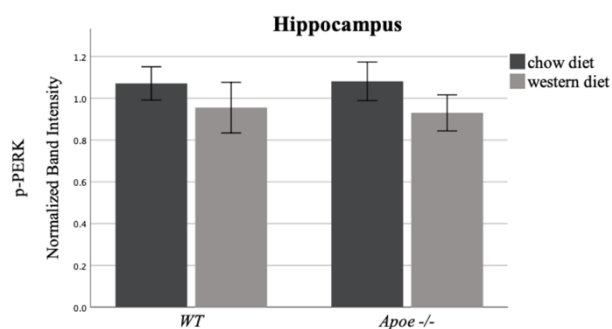


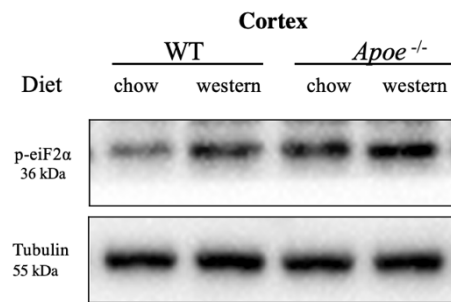
Figure 3.10. Effects of hyperlipidemia on p-PERK level in hippocampus. Relative p-PERK protein levels were analyzed with Western blot in the hippocampal tissue of WT and *Apoe*^{-/-} mice fed a chow vs Western diet ($n=7$ per group). (A.) Protein bands corresponding to the p-PERK were detected at 170 kDa. Tubulin was used as a loading control (55 kDa). (B.) Each experiment was repeated at least 2 times for comparison of p-PERK levels between the animal groups. p-PERK level was calculated relative to tubulin. Statistical significance was determined using two-way ANOVA. Each bar represents the mean \pm SEM.

3.5.2. p-eiF2 α

In order to examine the PERK arm activation further, levels of PERK pathway downstream components were assessed in the cortical and hippocampal tissues with Western blot analysis. Upon PERK activation through its phosphorylation, p-eiF2 α is phosphorylated in order to attenuate global protein synthesis and activate transcription of stress induced genes. Thus, elevated p-eiF2 α level is often an indirect indicator of PERK activation in ER stress (Leitman et al., 2014).

Western blot analysis results for p-eiF2 α were obtained from N. Mengi, 2019. Our results showed that Western diet increased p-eiF2 α levels significantly in the cortex of WT mice (* $p=0.021$). In that manner, increase in p-eiF2 α with Western diet followed the same pattern as p-PERK confirming that PERK pathway was activated in the cortex of WT animals upon Western diet (Figure 3.9. and Figure 3.11.). Furthermore, p-eiF2 α level was markedly increased in the cortex of *ApoE*^{-/-} mice despite the fact that they were fed on different diets confirming that PERK pathway was activated in the cortical tissues of *ApoE*^{-/-} animals even when they fed on a chow diet (Figure 3.9. and Figure 3.11.).

A.



B.

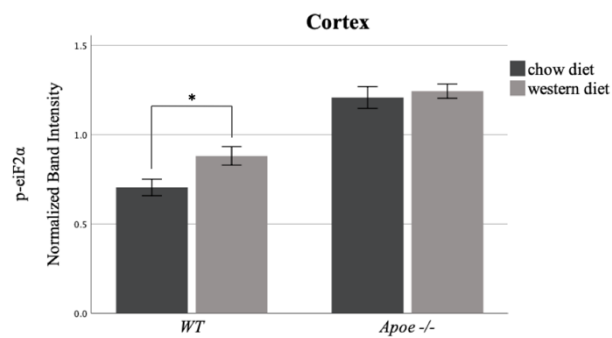
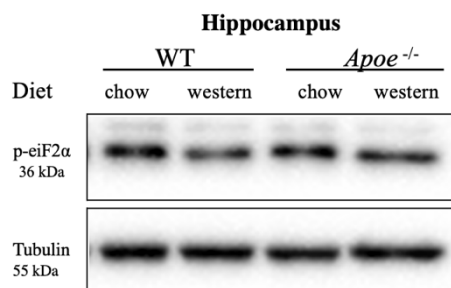


Figure 3.11. Effects of hyperlipidemia on p-eIF2 α level in cortex. Relative p-eIF2 α protein levels were analyzed with Western blot in the cortical tissue of WT and *Apoe*^{-/-} mice fed a chow vs Western diet ($n=7$ per group). (A.) Protein bands corresponding to the p-eIF2 α were detected at 36 kDa. Tubulin was used as a loading control (55 kDa). (B.) Each experiment was repeated at least 2 times for comparison of p-eIF2 α levels between the animal groups. p-eIF2 α level in cortex was calculated relative to tubulin. Statistical significance was determined using two-way ANOVA. Each bar represents the mean \pm SEM, * $p < 0.05$.

Unlike cortex, neither genotype nor diet altered p-eiF2 α level in the hippocampus (Figure 3.12). However, similar to p-PERK, Western diet fed animals exhibited a tendency towards decreased p-eiF2 α level (Figure 3.10. and Figure 3.12.).

A.



B.

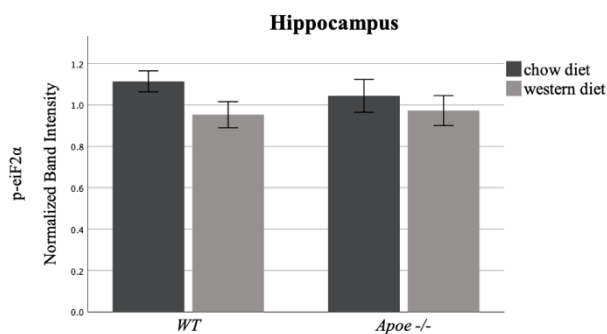
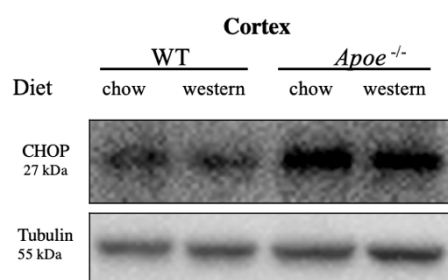


Figure 3.12. Effects of hyperlipidemia on p-eiF2 α level in hippocampus. Relative p-eiF2 α protein levels were analyzed with Western blot in the cortical tissue of WT and *Apoe*^{-/-} mice fed a chow vs Western diet ($n=7$ per group). (A.) Protein bands corresponding to the p-eiF2 α were detected at 36 kDa. Tubulin was used as a loading control (55 kDa). (B.) Each experiment was repeated at least 2 times for comparison of p-eiF2 α levels between the animal groups. p-eiF2 α level in hippocampus was normalized to tubulin and statistical significance was determined using two-way ANOVA. Each bar represents the mean \pm SEM.

3.5.3. CHOP

In order to examine the severity of the stress, level of ER stress apoptotic factor, CHOP, was assessed in the cortex (Mengi, 2019) and hippocampus of experimental groups. Western blot analysis showed that diet did not change CHOP level in WT group well as *ApoE*^{-/-} group. However, cortical CHOP level was considerably higher in *ApoE*^{-/-} mice regardless of diet compared to WT ones (***p*=0.003). Consistent with the previously shown data, increase in CHOP level was correlated with increase in other PERK pathway components; p-PERK and p-eif2 α in the cortex of *ApoE*^{-/-} animals compared to WT ones regardless of the diet type (Figure 3.13).

A.



B.

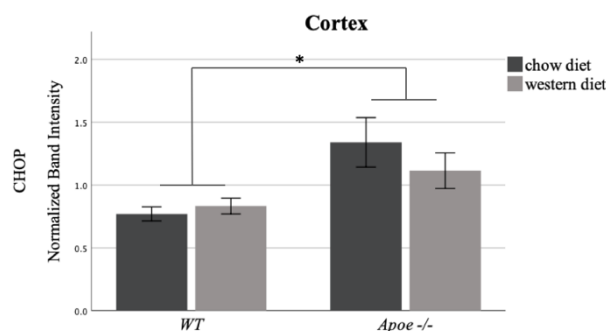
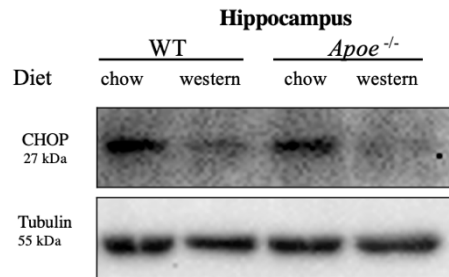


Figure 3.13. Effects of hyperlipidemia on CHOP level in cortex. Relative CHOP protein levels were analyzed with Western blot in the cortical tissue of WT and *ApoE*^{-/-} mice fed a chow vs Western diet (*n*=7 per group). (A.) Protein bands corresponding to the CHOP were detected at 27 kDa. Tubulin was used as a loading control (55 kDa). (B.) Each experiment was repeated at least 2 times for comparison of CHOP levels between the animal groups. p-eif2 α level in cortex was normalized to tubulin and statistical significance was determined using two-way ANOVA. Each bar represents the mean \pm SEM.

In the hippocampus, on the other hand, Western diet markedly decreases CHOP level in both WT and *ApoE*^{-/-} animals, ****p*=0.00010 and **p*=0.013 respectively. Additionally, *ApoE*^{-/-} mice displayed lower level of CHOP in their hippocampus than WT ones, **p*=0.018, regardless of diet (Figure 3.14).

A.



B.

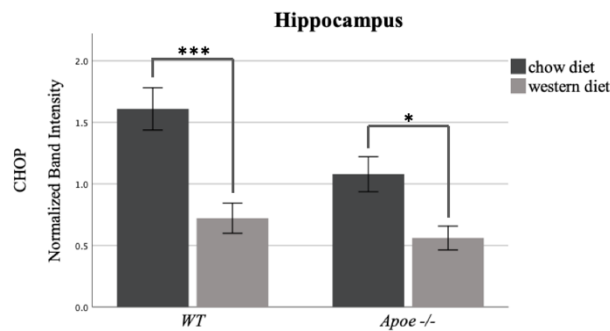


Figure 3.14. Effects of hyperlipidemia on CHOP level in hippocampus. Relative CHOP protein levels were analyzed with Western blot in the hippocampal tissue of WT and *ApoE*^{-/-} mice fed a chow vs Western diet (*n*=7 per group). (A.) Protein bands corresponding to the CHOP were detected at 27 kDa. Tubulin was used as a loading control (55 kDa). (B.) Each experiment was repeated at least 2 times for comparison of CHOP levels between the animal groups. CHOP level in hippocampus was normalized to tubulin. Statistical significance was determined using two-way ANOVA. Each bar represents the mean ± SEM. **p* < 0.05, ****p* < 0.0005.

3.6. Effects of Sephin1 Injection on Hippocampal Gephyrin Level

Even though levels of PERK components did not show a significant increase, the severe hyperlipidemic group, *ApoE*^{-/-} mice fed with Western diet, exhibited markedly decreased post-synaptic protein, gephyrin, level compared to control groups. In order to investigate the effects of intercepting PERK pathway with Sephin1 on hyperlipidemia-induced post-synaptic protein loss, gephyrin immunoreactivity was analyzed with immunohistochemistry in the subfields of hippocampus, and the intensity was compared between Sephin1 and DMSO groups (Figure 3.15.).

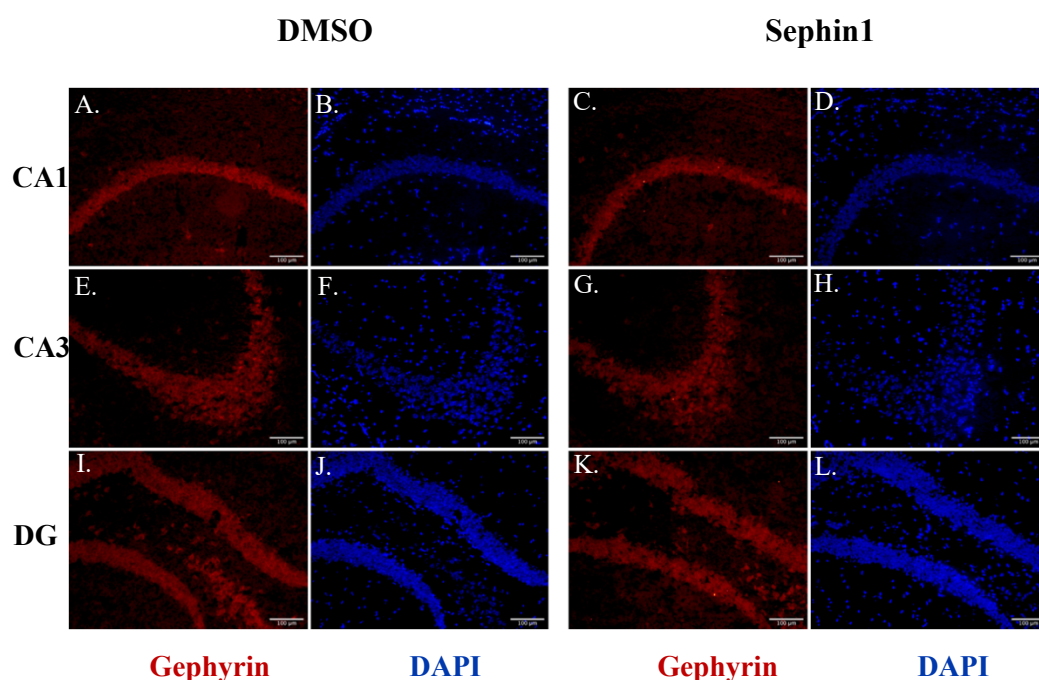


Figure 3.15. Representative immunofluorescence images for gephyrin and DAPI staining in hippocampus. *ApoE*^{-/-} male mice were started to be fed Western diet at the age of 9-week. After 10 weeks of Western diet, half of the animals were intraperitoneally injected with Sephin1(5mg/kg/day) and the rest of the animals were injected with DMSO (*n*=3), injection continued for the last 4 weeks along with the diet. After 14 weeks of diet duration, animals were perfused with 10% formalin and brain tissue was dissected. After cryopreservation of the brain tissue, hippocampal tissue was serially sectioned at 10 μ m and immunofluorescence of gephyrin was performed. Images were acquired with Zeiss fluorescent microscopy, AxioVision AX10. Image A, E and I show gephyrin staining of CA1, CA3 and DG subfields of hippocampus in DMSO group, respectively. B, F and J show DAPI staining of CA1, CA3 and DG subfields of hippocampus in DMSO group, respectively. C, G and K show Gephyrin staining of CA1, CA3 and in Sephin1 group, respectively. D, H and L show Gephyrin staining of CA1, CA3 and in Sephin1 group, respectively. Scale bars, 100 μ m.

In *ApoE*^{-/-} mice fed a Western diet, Sephin1 injection did not change gephyrin intensity in the subfields of hippocampus as no significant change in gephyrin intensity was noted between DMSO and Sephin1 groups (Figure 3.16).

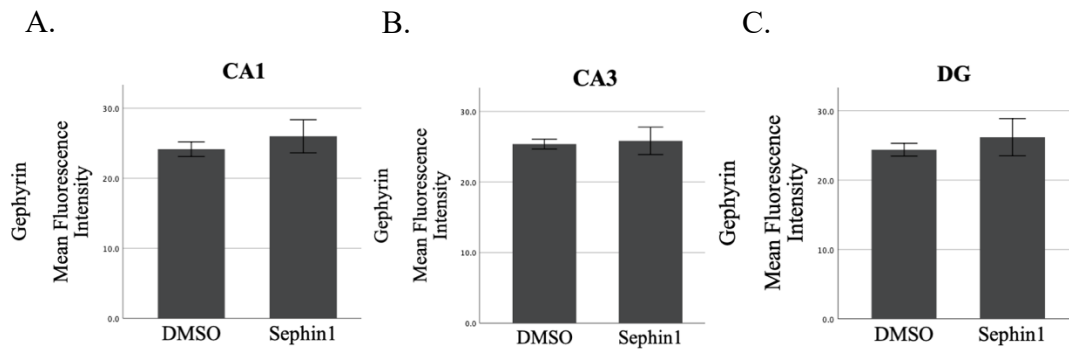


Figure 3.16. Changes in gephyrin immunoreactivity in CA1, CA3 and DG regions between DMSO and Sephin1 groups. Mean intensity quantification of gephyrin was performed with systematic sampling method at every 212 μm through X and Y axis through left and right hippocampi. Intensity measurements were done separately in CA1, CA3 and DG regions. CA1, CA3 and DG were sampled an average of ~ 75 , ~ 60 and ~ 60 sites for each animal, respectively ($n=3$). Measurements were obtained by averaging the mean intensities of total sampling frames for each region and each animal. Statistical differences were determined with independent sample t-test between DMSO and Sephin1 group for each subfields of hippocampus. Each bar represents the mean \pm SEM.

CHAPTER 4

DISCUSSION

Animal and longitudinal studies have shown that chronic exposure to diets high in saturated fats and elevated blood lipids are associated with increased risk of neurodegeneration and consequent cognitive impairment (Morris & Tangney, 2014). Hyperlipidemia increases BBB permeability allowing plasma lipids and peripheral pro-inflammatory cytokines to take advantage of leaky BBB and exert their cytotoxic effects on astrocytes and neurons in brain. Upon chronic exposure to elevated serum cholesterol, astrocytes start to proliferate which is usually characterized by increased expression of GFAP and they are converted to an activated pro-inflammatory phenotype, namely reactive astrogliosis (Götz et al., 2018). Increased BBB permeability, accumulation of reactive astrocytes and elevated inflammatory status in brain has been thought to induce synaptic impairment and neuronal degeneration (Kanoski et al., 2010; Yang et al., 2017). Despite the fact that many studies aimed to understand the possible link between hyperlipidemia and neurodegeneration, the underlying molecular mechanisms of this connection remains to be elucidated. Nevertheless, there is an emerging evidence that ER stress may play a role in hyperlipidemia-induced neurodegeneration and subsequent cognitive decline (Rutkowsky et al., 2018). Therefore, the first half of the study was aimed to investigate the role of ER stress, specifically the PERK pathway due to its role in protein translation and cell fate determination, in hyperlipidemia-induced astrogliosis and synaptic impairment in the cortex and hippocampus. The second half of the study, on the other hand, was aimed to examine the effects of stress-induced phosphatase inhibition via a small molecule, Sephin1, against negative effects of hyperlipidemia on hippocampal post-synaptic protein gephyrin level.

To study the assessment of the integrity of pre-synaptic regions, synaptophysin levels were examined since it is widely used as a synaptic marker for the assessment of the integrity of pre-synaptic regions and it is well-documented that reduction in synaptophysin protein is often the indication of decreased neurotransmission due to lower neurotransmitter release from axon terminals (Reddy et al., 2005). It is ubiquitously found in brain and it is synthesized in almost all neurons together with the other synaptic proteins. It is the major component of the pre-synaptic vesicle membranes at axon terminals (Tarsa & Goda, 2002). Hence, synaptophysin is believed to be important for the release of vesicle content, thereby, it facilitates neurotransmission (Sarnat, 2013). Additionally, diminished pre-synaptic protein level has been shown to be a strong evidence for various neurodegenerative diseases (Bae & Kim, 2017). In this study, the results showed that severe hyperlipidemic group, *ApoE*^{-/-} fed a Western diet, exhibited decreased synaptophysin levels in their cortex. Diminished synaptophysin levels in the cortex of severe hyperlipidemic group indicated a possible synaptic impairment since synaptic transmission requires an accurate matching of pre-synaptic site, neurotransmitter release machinery and post-synaptic site (Petzoldt & Sigrist, 2014).

For long term stability of the neuronal network, maintaining a balance between excitatory and inhibitory synaptic transmission is quite essential, therefore, for further understanding of neurotransmission at the post-synaptic sites, gephyrin was used as a marker which is a cytoplasmic protein and important for clustering of inhibitory neurotransmitter, glycine and GABA, receptors at post-synaptic sites (Fritschy, Harvey, & Schwarz, 2008). It contributes to the formation of inhibitory post-synaptic sites and inhibitory neurotransmission in brain (Tyagarajan & Fritschy, 2010). Studies show that high fat consumption disrupts the inhibition process in different parts of the brain and impairs the inhibitory control of food intake (Sandoval-Salazar, Ramírez-Emiliano, Trejo-Bahena, Oviedo-Solís, & Solís-Ortiz, 2016).

In agreement with the earlier findings, the gephyrin level was the lowest in the cortex of severe hyperlipidemic group in our study. Data suggested that inhibitory control of feeding motivation as well as appetite was impaired with hyperlipidemia due to low levels of gephyrin and probably due to the subsequent diminished inhibitory signals in the cortex.

Astrocytes provide a metabolic and structural support to neurons and contribute to the maintenance of synaptic integrity and synaptic transmission. Aberrant astrogliosis has been shown to be the hallmark of various CNS diseases. CNS injury or diseases alter astrocyte activity which consequently influences synapse integrity and survival of the surrounding neurons (Dossi, Vasile, & Rouach, 2018). Studies show that severe astrocyte activation may lead to faulty clearance of neurotoxic molecules and abnormal expression of growth factors which may eventually impair synaptic plasticity and synaptic transmission (C.-Y. Liu, Yang, Ju, Wang, & Zhang, 2018). Pro-inflammatory cytokines have been shown to trigger astrogliosis in brain. Upon their activation, astrocytes can in return express various pro-inflammatory cytokines and their receptors contributing to the neuroinflammatory process in brain (Lee et al., 2013). Therefore, it was hypothesized that astrocyte activation would increase in response to hyperlipidemia and increased astrogliosis would coincide with increased pro-inflammatory cytokine, IL-1 β , in the cortex of hyperlipidemic animals. Indeed, our data showed that Western diet exposure markedly increased the cortical GFAP level in *ApoE*^{-/-} mice which was coupled with the increased IL-1 β level. However, Western and chow diet fed *ApoE*^{-/-} animals exhibited similar levels of GFAP indicating that *ApoE*^{-/-} animals displayed elevated cortical GFAP levels regardless of the diet choice. There may be a number of explanations that one is well-documented that ApoE is synthesized in neurons, oligodendrocytes, but primarily in microglia and astrocytes in CNS. Allelic variants of *ApoE* gene in astrocytes impair lipid and glucose metabolism and consequently weaken astrocyte's ability to support neurons which confers an increase in pro-inflammatory cytokine production in brain. (Fernandez, Hamby, McReynolds, & Ray, 2019).

In agreement, Liu et al. (2015) showed that in the brains of *ApoE*^{-/-} mice, fed on standard laboratory chow diet, astrocyte-mediated inflammatory response was elevated compared to C57BL/6, therefore, it is likely that *ApoE*^{-/-} mice used in our study displayed higher basal levels of cortical GFAP and IL-1 β than WT mice regardless of diet type due to the fact that ApoE contributes to the modulation of astrocyte function and the CNS inflammatory response. Second explanation would be that when they were fed on chow diet, serum cholesterol level in *ApoE*^{-/-} mice increases but to a lesser extent compared to Western diet fed *ApoE*^{-/-} mice. Elevated serum cholesterol induces moderately increased peripheral inflammation in these animals which may also affect CNS and lead to development of astrogliosis (Ouyang et al., 2015). Therefore, it is conceivable that astrocytes were already maximally activated with chow diet in *ApoE*^{-/-} mice which hindered further activation in response to Western diet.

Astrocyte activation, elevated inflammation and disruption to proteostasis are well-documented features of the hyperlipidemia-induced neurodegeneration. Recent evidences propose that the PERK pathway and its downstream effectors may be involved in the disease-specific features. Our data showed that p-PERK and p-eIF2 α levels were increased with Western diet in the cortex of WT animals but CHOP levels, in contrast, had not changed. The reason for unchanged CHOP levels may be due to the fact that under mild ER stress, PERK mediated expressions of pro-apoptotic components are highly unstable at mRNA and protein levels. This was because moderate ER stress provides an adaptive feedback mechanism against further unfolded or misfolded protein load into ER lumen via temporary attenuation of global protein synthesis (Matus, Castillo, & Hetz, 2012). Therefore, it may be concluded that Western diet did not affect cholesterol metabolism in WT mice as markedly as in *ApoE*^{-/-} mice, nevertheless it was enough to induce a mild ER stress in WT mice.

In *ApoE*^{-/-} animals, on the other hand, p-PERK, p-eIF2 α and CHOP levels were significantly higher regardless of the diet type. Increased GFAP and IL-1 β levels together with elevated stress status in transgenic animals supported the notion that ApoE protein may be important against hyperlipidemia-induced stress in the cortex. Studies show that *ApoE*^{-/-} mice are prone to neuronal damage induced by cerebral ischemia and lack of ApoE lead to ischemic neuronal death via severe ER stress (Osada, Kosuge, Kihara, Ishige, & Ito, 2009). The proposed mechanism in which ApoE provides a protection in brain was that it delivers lipids for neuronal repairing and remodeling in response to an injury (Laskowitz et al., 1997). In agreement with the earlier findings, increase in astrogliosis as well as the activation of the PERK pathway in the cortex of transgenic animals in this study implicated that ApoE may indeed provide a protection against hyperlipidemia-induced persistent ER stress. Therefore, lack of *ApoE* gene induced severe ER stress via upregulating the PERK pathway components in the cortex of hyperlipidemic animals and this regulation was not affected by diet choice.

In this study, levels of synaptic proteins and the PERK pathway mediators had also been examined in the hippocampus since it is the earliest and most severely affected region in brain in many neurodegenerative diseases due to its crucial role in learning and memory (Anand & Dhikav, 2012). Our results showed that 16-weeks of Western diet did not markedly affect synaptophysin levels in WT and *ApoE*^{-/-} mice even though Western diet fed WT and *ApoE*^{-/-} mice exhibited a tendency towards decreased synaptophysin levels. On the contrary, the gephyrin level significantly decreased in the hippocampus of *ApoE*^{-/-} mice when they were fed on Western diet. Involvement of hippocampus in learning and memory functions is well-established, however, its potential involvement in feeding behavior and energy homeostasis has received increasing attention lately (Stevenson & Francis, 2017). Inhibitory neurotransmission is significantly reduced with high fat diet through disruption of GABA metabolism in hippocampus (Sickmann, Waagepetersen, Schousboe, Benie, & Bouman, 2010; Valladolid-Acebes et al., 2012).

Therefore, the decrease in hippocampal gephyrin levels in severe hyperlipidemic group was consistent with the previous findings. It is likely that diminished inhibitory signals in hippocampus impaired animal's ability to elicit a memory for food by contextual cues and subsequently impaired their control of appetite behavior (Sandoval-Salazar et al., 2016). As a consequence of this impairment, inhibitory control of food intake was probably diminished in *ApoE*^{-/-} mice fed on Western diet.

Consistent with the cortex, GFAP levels increased in the hippocampus of severe hyperlipidemic animals. Interestingly, p-PERK and p-eIF2 α levels did not change while IL-1 β and CHOP levels markedly decreased with Western diet in both WT and *ApoE*^{-/-} mice. These findings were in contrast with several rodent and human studies in which hyperlipidemia has been repeatedly shown to have negative effects on hippocampus induced by ER stress. Contrary to general consensus, one recent study showed that hippocampal volume was increased and hippocampal dependent memory was not affected by high-caloric diet, rich in saturated fatty acids even though mice exhibited a strong metabolic syndrome-like phenotype (Sack et al., 2017). Why synaptophysin, and ER stress markers did not change in Western diet and more importantly why IL-1 β and CHOP levels were markedly decreased in Western diet? A potential explanation would be that some compensatory mechanisms may be activated in hippocampus to protect it against the early effects of Western diet. It may be deduced from 16-weeks of Western diet data that the duration of the diet was not enough to induce a potential adverse effect on hippocampus. Additionally, mice were in the adult stage when they were sacrificed, therefore, the harmful effects of hyperlipidemia may be exacerbated as the mice age. These findings then raise the following questions: why was the hippocampus protected against the negative effects of hyperlipidemia but cortex was not and how this protection was achieved?

In CNS, neural progenitor cells are multipotent that generate neurons, astrocytes and oligodendrocytes. Neural progenitor cells appear to be ubiquitously present within the adult mammalian CNS.

However, hippocampus is a privileged structure in this regard in which newborn neurons have been consistently found and the hippocampal microenvironment, namely neurogenic niche, has specific factors permitting differentiation and integration of new neurons (Stangl & Thuret, 2009). Hence, maintenance of this microenvironment is of great importance for well-functioning of the hippocampal network. That is why a compensatory or a protective mechanism may be activated in hippocampus but not in the cortex in order to protect it against the early effects of hyperlipidemia. Upon observing an increase in the hippocampal GFAP levels in hyperlipidemic animals, it was also tempting to speculate that astrogliosis may have provided a neuroprotective mechanism in hippocampus. Under severe pathological conditions, hyperreactive astrocytes contribute to cell cytotoxicity leading to neuronal dysfunction and cell death. Therefore, astrogliosis may become detrimental when the damage was too severe for homeostasis to be restored (Sofroniew & Vinters, 2010b). On the other hand, it has been repeatedly reported that reactive astrogliosis may also be neuroprotective by providing neurotrophic factors that promote cell survival under neurodegenerative conditions. Nevertheless, the circumstances in which it triggers cytotoxicity or provides a neuroprotective activity still remain obscure. There is an accumulating evidence that dual role of astrocytes in brain homeostasis pretty much depends on intercellular communication (Becerra-Calixto & Cardona-Gómez, 2017). Astrocytes can be potentially neuroprotective by releasing wide range of neuroprotective trophic factors such as nerve growth factor (NGF), ciliary neurotrophic factor (CNTF), glial cell-line derived neurotrophic factor (GDNF), fibroblast growth factor (FGF) and mesencephalic astrocyte-derived neurotrophic factor (MANF) (Bélanger & Magistretti, 2009). In rats, ischemia can induce expression of stress inducible neurotrophic factor, MANF, in astrocytes as well as in neurons (Shen et al., 2012). MANF facilitates cysteine bridge formation and protein folding in ER, resulting in a possible reduction in ER stress due to decreased accumulation of misfolded or unfolded proteins (Lindholm & Saarna, 2010).

Therefore, a possible explanation for unchanged PERK mediators and decreased IL-1 β and CHOP levels with Western diet would be that astrocytes may have a region-specific neuroprotective feature in brain in response to hyperlipidemia. They may gain this feature through the secretion of neurotrophic factors and attenuation of pro-inflammatory and pro-apoptotic mediators. Therefore, astrocytes may preserve hippocampal neurogenic niche to a certain extent. However, extending the diet duration may induce hyperreactive astrocytes in hippocampus which probably would shift astrocyte phenotype from neuroprotective to neurotoxic.

Even though ER stress was not induced in the hippocampus of hyperlipidemic animals, the decrease in gephyrin levels in hippocampus was more pronounced compared to the decrease in cortex. In order to examine the effects of PERK pathway modulation with Sephin1, immunoreactivity of gephyrin was assessed in the subfields of hippocampus of severe hyperlipidemic mice. Our data showed that Sephin1 injection did not change gephyrin levels in hippocampus indicating that it has not exerted any beneficial effects against hyperlipidemia-induced gephyrin loss. Under severe ER stress, PERK activation attenuates global protein synthesis through phosphorylation of eIF2 α . p-eIF2 α in return promotes expression of stress response genes as well as stress inducible phosphatase, GADD34. Therefore, GADD34 promotes eIF2 α dephosphorylation providing a translational recovery so that expression of stress-induced mRNAs may take place in stressed cells (H P Harding et al., 2000). Sephin1 particularly inhibits stress inducible GADD34 and attenuates global protein translation by prolonging phosphorylation of eIF2 α in stressed cells. Thus, it allows ER to refold or degrade abnormally folded proteins and attenuate expression of stress responsive genes such as CHOP (Wrabetz et al., 2015). Even though Sephin1 has been shown to be a promising therapeutic for various neurodegenerative disease (Chen et al., 2019), it has not showed any beneficial effects on hyperlipidemia-induced low gephyrin levels in hippocampus. Ineffective Sephin1 injection in these animals would be that stress was not yet induced in the hippocampus.

Therefore, it was probable that stress-induced GADD34 was expressed at very low levels in hippocampus in the absence of stress in which Sephin1 had no measurable effects on GADD34 inhibition. In conclusion, other factors apart from the ER stress may likely to involved in hyperlipidemia-induced gephyrin loss in hippocampus and the further molecular and cellular mechanisms still remain to be elucidated.

CHAPTER 5

CONCLUSION AND FUTURE ASPECTS

Overall, this study has advanced our knowledge of the region-specific effects of hyperlipidemia on brain. Our data supported that hyperlipidemia increases the stress status of the cortex and possibly impairs synaptic integrity. In contrast to the cortex, hippocampus appeared to be protected against the early effects of hyperlipidemia, presumably due to its privileged involvement in neurogenesis. Since the stress was not yet generated in hippocampus, Sephin1 was not an effective therapeutic approach to prevent gephyrin loss detected in the hippocampus of severe hyperlipidemic mice.

In this study, even though it was observed that hyperlipidemia-induced ER stress, inflammation and synaptic impairment in the cortex, further region-specific studies were required to assess hyperlipidemia-induced changes in the cortex. For instance, hypothalamus is vulnerable to diet-induced changes due to its involvement in caloric intake and energy expenditure (Cai, 2013). Therefore, the cortex areas would be split further to evaluate the effects of hyperlipidemia on the particular brain regions in future studies. As a therapeutic approach, available other potent and selective PERK inhibitors may be employed for hyperlipidemia-induced neurodegeneration due to their high therapeutic potential for a variety of diseases. In the future studies, diet content and diet duration may be modulated since the 16-week diet duration was not enough to induce ER stress in hippocampus. The choice of transgenic animal models also possess a great importance for prospective studies since the lack of *ApoE* seem to be hindering the effects of hyperlipidemia in the cortex.

REFERENCES

- Alexander, G. M., Farris, S., Pirone, J. R., Zheng, C., Colgin, L. L., & Dudek, S. M. (2016). Social and novel contexts modify hippocampal CA2 representations of space. *Nature Communications*, 7(1), 10300. <https://doi.org/10.1038/ncomms10300>
- Anand, K. S., & Dhikav, V. (2012). Hippocampus in health and disease: An overview. *Annals of Indian Academy of Neurology*, 15(4), 239–246. <https://doi.org/10.4103/0972-2327.104323>
- B'chir, W., Maurin, A.-C., Carraro, V., Averous, J., Jousse, C., Muranishi, Y., ... Bruhat, A. (2013). The eIF2 α /ATF4 pathway is essential for stress-induced autophagy gene expression. *Nucleic Acids Research*, 41(16), 7683–7699. <https://doi.org/10.1093/nar/gkt563>
- Bae, J. R., & Kim, S. H. (2017). Synapses in neurodegenerative diseases. *BMB Reports*, 50(5), 237–246. <https://doi.org/10.5483/bmbrep.2017.50.5.038>
- Balch, W. E., Morimoto, R. I., Dillin, A., & Kelly, J. W. (2008). Adapting proteostasis for disease intervention. *Science (New York, N.Y.)*, 319(5865), 916–919. <https://doi.org/10.1126/science.1141448>
- Becerra-Calixto, A., & Cardona-Gómez, G. P. (2017). The Role of Astrocytes in Neuroprotection after Brain Stroke: Potential in Cell Therapy. *Frontiers in Molecular Neuroscience*, 10, 88. <https://doi.org/10.3389/FNMOL.2017.00088>
- Bélanger, M., & Magistretti, P. J. (2009). The role of astroglia in neuroprotection. *Dialogues in Clinical Neuroscience*, 11(3), 281. Retrieved from <https://www.ncbi.nlm.nih.gov/pmc/articles/PMC3181926/>
- Björkhem, I. (2006, December). Crossing the barrier: Oxysterols as cholesterol transporters and metabolic modulators in the brain. *Journal of Internal Medicine*. <https://doi.org/10.1111/j.1365-2796.2006.01725.x>
- Brahmachari, S., Fung, Y. K., & Pahan, K. (2006). Induction of glial fibrillary acidic protein expression in astrocytes by nitric oxide. *The Journal of Neuroscience : The Official Journal of the Society for Neuroscience*, 26(18), 4930–4939. <https://doi.org/10.1523/JNEUROSCI.5480-05.2006>
- Cai, D. (2013). Neuroinflammation and neurodegeneration in overnutrition-induced diseases. *Trends in Endocrinology & Metabolism*, 24, 40–47. <https://doi.org/10.1016/j.tem.2012.11.003>
- Calvo-Ochoa, E., Hernández-Ortega, K., Ferrera, P., Morimoto, S., & Arias, C. (2014). Short-Term High-Fat-and-Fructose Feeding Produces Insulin Signaling Alterations Accompanied by Neurite and Synaptic Reduction and Astroglial Activation in the Rat Hippocampus. *Journal of Cerebral Blood Flow &*

- Metabolism*, 34(6), 1001–1008. <https://doi.org/10.1038/jcbfm.2014.48>
- Carvalho, C., & I. Moreira, P. (2017). Isolation of Rodent Brain Vessels. *BIO-PROTOCOL*, 7(17). <https://doi.org/10.21769/BioProtoc.2535>
- Chan, J., Karere, G. M., Cox, L. A., & Vandeberg, J. L. (2015). Animal Models of Diet-induced Hypercholesterolemia, 3–32.
- Chappelow, J., Tomaszewski, J. E., Feldman, M., Shih, N., & Madabhushi, A. (2011). HistoStitcher(©): an interactive program for accurate and rapid reconstruction of digitized whole histological sections from tissue fragments. *Computerized Medical Imaging and Graphics: The Official Journal of the Computerized Medical Imaging Society*, 35(7–8), 557–567. <https://doi.org/10.1016/j.compmedimag.2011.01.010>
- Chen, Y., Podojil, J. R., Kunjamma, R. B., Jones, J., Weiner, M., Lin, W., ... Popko, B. (2019). Sepsin1, which prolongs the integrated stress response, is a promising therapeutic for multiple sclerosis. *Brain*, 142(2), 344–361. <https://doi.org/10.1093/brain/awy322>
- Chomczynski, P., & Sacchi, N. (2006). The single-step method of RNA isolation by acid guanidinium thiocyanate–phenol–chloroform extraction: twenty-something years on. *Nature Protocols*, 1(2), 581–585. <https://doi.org/10.1038/nprot.2006.83>
- Cohen, J. I., Cazettes, F., & Convit, A. (2011). Abnormal cholesterol is associated with prefrontal white matter abnormalities among obese adults: A diffusion tensor imaging study. *Neuroradiology Journal*, 24(6), 854–861. <https://doi.org/10.1177/197140091102400604>
- Cuchel, M., Bruckert, E., Ginsberg, H. N., Raal, F. J., Santos, R. D., Hegele, R. A., ... Wiklund, O. (2014). Homozygous familial hypercholesterolaemia: new insights and guidance for clinicians to improve detection and clinical management. A position paper from the Consensus Panel on Familial Hypercholesterolaemia of the European Atherosclerosis Society. *European Heart Journal*, 35(32), 2146–2157. <https://doi.org/10.1093/eurheartj/ehu274>
- Davidson, T. L., Monnot, A., Neal, A. U., Martin, A. A., Horton, J. J., & Zheng, W. (2012). The effects of a high-energy diet on hippocampal-dependent discrimination performance and blood–brain barrier integrity differ for diet-induced obese and diet-resistant rats. *Physiology & Behavior*, 107(1), 26–33. <https://doi.org/10.1016/j.physbeh.2012.05.015>
- de Flores, R., La Joie, R., & Chételat, G. (2015, November). Structural imaging of hippocampal subfields in healthy aging and Alzheimer’s disease. *Neuroscience*. <https://doi.org/10.1016/j.neuroscience.2015.08.033>
- Dewan/Loomis-Protocol. (2016). *Freezing tissues for histology: Embedding protocol*

for Frozen Samples. Retrieved from <http://www.bdbiosciences.com/us/resources/s/frozentissue>

- DiNicolantonio, J. J., & O’Keefe, J. H. (2018). Effects of dietary fats on blood lipids: a review of direct comparison trials. *Open Heart*, 5(2), e000871. <https://doi.org/10.1136/openhrt-2018-000871>
- Djelti, F., Braudeau, J., Hudry, E., Dhenain, M., Varin, J., Bièche, I., ... Cartier, N. (2015). CYP46A1 inhibition, brain cholesterol accumulation and neurodegeneration pave the way for Alzheimer’s disease. *Brain*, 138(8), 2383–2398. <https://doi.org/10.1093/brain/awv166>
- Dossi, E., Vasile, F., & Rouach, N. (2018). Human astrocytes in the diseased brain. *Brain Research Bulletin*, 136, 139–156. <https://doi.org/10.1016/J.BRAINRESBULL.2017.02.001>
- ElAli, A., Doeppner, T. R., Zechariah, A., & Hermann, D. M. (2011). Increased Blood–Brain Barrier Permeability and Brain Edema After Focal Cerebral Ischemia Induced by Hyperlipidemia. *Stroke*, 42(11), 3238–3244. <https://doi.org/10.1161/strokeaha.111.615559>
- Eslami, A., & Lujan, J. (2010). Western Blotting: Sample Preparation to Detection. *Journal of Visualized Experiments*, (44). <https://doi.org/10.3791/2359>
- Fernandez, C. G., Hamby, M. E., McReynolds, M. L., & Ray, W. J. (2019). The Role of APOE4 in Disrupting the Homeostatic Functions of Astrocytes and Microglia in Aging and Alzheimer’s Disease. *Frontiers in Aging Neuroscience*, 11, 14. <https://doi.org/10.3389/fnagi.2019.00014>
- Ferry, B. (2014). *Stereotaxic neurosurgery in laboratory rodent*. Springer. Retrieved from <https://books.google.com.tr/books?id=JGC4BAAAQBAJ&pg=PA159&lpg=PA159&dq=cryostat+sectioning+of+the+brain+temperature+-20&source=bl&ots=neaxygiMK&sig=ACfU3U3YhqwuAv1H9MehXgQSed5yftvAkA&hl=tr&sa=X&ved=2ahUKEwjmlJzG1LjiAhWj5aYKHRB1D9MQ6AEwC3oECAkQAQ#v=onepa>
- Flecknell, P. A. (1993). ANAESTHESIA OF ANIMALS FOR BIOMEDICAL RESEARCH. *British Journal of Anaesthesia*, 71(6), 885–894. <https://doi.org/10.1093/BJA/71.6.885>
- Fritschy, J.-M., Harvey, R. J., & Schwarz, G. (2008). Gephyrin: where do we stand, where do we go? *Trends in Neurosciences*, 31(5), 257–264. <https://doi.org/10.1016/J.TINS.2008.02.006>
- Fu, S., Watkins, S. M., & Hotamisligil, G. S. (2012). The Role of Endoplasmic Reticulum in Hepatic Lipid Homeostasis and Stress Signaling. *Cell Metabolism*, 15(5), 623–634. <https://doi.org/10.1016/j.cmet.2012.03.007>

- Getz, G. S., & Reardon, C. A. (2016). Do the Apoe^{-/-} and Ldlr^{-/-} Mice Yield the Same Insight on Atherogenesis? *Arteriosclerosis, Thrombosis, and Vascular Biology*, 36(9), 1734–1741. <https://doi.org/10.1161/ATVBAHA.116.306874>
- Götz, A., Lehti, M., Donelan, E., Striese, C., Cucuruz, S., Sachs, S., ... Hofmann, S. M. (2018). Circulating HDL levels control hypothalamic astrogliosis via apoA-I. *Journal of Lipid Research*, 59(9), 1649–1659. <https://doi.org/10.1194/jlr.M085456>
- Graham, J. M. (2002). Homogenization of Mammalian tissues. *TheScientificWorldJournal*, 2, 1626–1629. <https://doi.org/10.1100/tsw.2002.849>
- Gundersen, H. J., Jensen, E. B., Kiêu, K., & Nielsen J. (1999). The efficiency of systematic sampling in stereology--reconsidered. *Journal of Microscopy*, 193(Pt 3), 199–211. Retrieved from <http://www.ncbi.nlm.nih.gov/pubmed/10348656>
- Hall, A. H., Smolinske, S. C., Kulig, K. W., & Rumack, B. H. (1985). Guanabenz overdose. *Annals of Internal Medicine*, 102(6), 787–788. Retrieved from <http://www.ncbi.nlm.nih.gov/pubmed/3994191>
- Han, J., & Kaufman, R. J. (2016). The role of ER stress in lipid metabolism and lipotoxicity. *Journal of Lipid Research*, 57(8), 1329–1338. <https://doi.org/10.1194/jlr.R067595>
- Harding, H P, Novoa, I., Zhang, Y., Zeng, H., Wek, R., Schapira, M., & Ron, D. (2000). Regulated translation initiation controls stress-induced gene expression in mammalian cells. *Molecular Cell*, 6(5), 1099–1108. Retrieved from <http://www.ncbi.nlm.nih.gov/pubmed/11106749>
- Harding, Heather P, Zhang, Y., Bertolotti, A., Zeng, H., & Ron, D. (2000). Perk Is Essential for Translational Regulation and Cell Survival during the Unfolded Protein Response. *Molecular Cell*, 5(5), 897–904. [https://doi.org/10.1016/S1097-2765\(00\)80330-5](https://doi.org/10.1016/S1097-2765(00)80330-5)
- Hermann, D. M., & ElAli, A. (2012). The Abluminal Endothelial Membrane in Neurovascular Remodeling in Health and Disease. *Science Signaling*, 5(236), re4–re4. <https://doi.org/10.1126/scisignal.2002886>
- Herx, L. M., & Yong, V. W. (2001). Interleukin-1 β is Required for the Early Evolution of Reactive Astrogliosis Following CNS Lesion. *Journal of Neuropathology & Experimental Neurology*, 60(10), 961–971. <https://doi.org/10.1093/jnen/60.10.961>
- Hetz, C. (2012). The unfolded protein response: controlling cell fate decisions under ER stress and beyond. *Nature Reviews Molecular Cell Biology*, 13(2), 89–102. <https://doi.org/10.1038/nrm3270>
- Heydemann, A. (2016). An Overview of Murine High Fat Diet as a Model for Type 2 Diabetes Mellitus. *Journal of Diabetes Research*, 2016, 2902351.

<https://doi.org/10.1155/2016/2902351>

- Holmes, B., Brogden, R. N., Heel, R. C., Speight, T. M., & Avery, G. S. (1983). Guanabenz A Review of its Pharmacodynamic Properties and Therapeutic Efficacy in Hypertension. *Drugs*, 26(3), 212–229. <https://doi.org/10.2165/00003495-198326030-00003>
- Holven, K. B., Ulven, S. M., & Bogsrud, M. P. (2017). Hyperlipidemia and cardiovascular disease with focus on familial hypercholesterolemia. *Current Opinion in Lipidology*, 28(5), 445–447. <https://doi.org/10.1097/MOL.0000000000000449>
- Huang, Y., & Mahley, R. W. (2014). Apolipoprotein E: Structure and Function in Lipid Metabolism, Neurobiology, and Alzheimer's Diseases. *Neurobiology of Disease*, 72PA, 3. <https://doi.org/10.1016/J.NBD.2014.08.025>
- IBM Corp. Released 2017. (n.d.). IBM How to cite IBM SPSS Statistics or earlier versions of SPSS.
- Ishibashi, S., Brown, M. S., Goldstein, J. L., Gerard, R. D., Hammer, R. E., & Herz, J. (1993). Hypercholesterolemia in low density lipoprotein receptor knockout mice and its reversal by adenovirus-mediated gene delivery. *Journal of Clinical Investigation*, 92(2), 883–893. <https://doi.org/10.1172/JCI116663>
- Jousse, C., Oyadomari, S., Novoa, I., Lu, P., Zhang, Y., Harding, H. P., & Ron, D. (2003). Inhibition of a constitutive translation initiation factor 2alpha phosphatase, CReP, promotes survival of stressed cells. *The Journal of Cell Biology*, 163(4), 767–775. <https://doi.org/10.1083/jcb.200308075>
- Kanoski, S. E., & Davidson, T. L. (2011). Western diet consumption and cognitive impairment: Links to hippocampal dysfunction and obesity. *Physiology and Behavior*, 103(1), 59–68. <https://doi.org/10.1016/j.physbeh.2010.12.003>
- Kanoski, S. E., Zhang, Y., Zheng, W., & Davidson, T. L. (2010). The Effects of a High-Energy Diet on Hippocampal Function and Blood-Brain Barrier Integrity in the Rat. *Journal of Alzheimer's Disease*, 21(1), 207–219. <https://doi.org/10.3233/JAD-2010-091414>
- Karoglu, E. T., Halim, D. O., Erkaya, B., Altaytas, F., Arslan-Ergul, A., Konu, O., & Adams, M. M. (2017). Aging alters the molecular dynamics of synapses in a sexually dimorphic pattern in zebrafish (*Danio rerio*). *Neurobiology of Aging*, 54, 10–21. <https://doi.org/10.1016/J.NEUROBIOLAGING.2017.02.007>
- Karr, S. (2017a). Epidemiology and management of hyperlipidemia. *The American Journal of Managed Care*, 23(9 Suppl), S139–S148. Retrieved from <http://www.ncbi.nlm.nih.gov/pubmed/28978219>
- Karr, S. (2017b). Epidemiology and management of hyperlipidemia. *The American Journal of Managed Care*, 23(9 Suppl), S139–S148. Retrieved from

<http://www.ncbi.nlm.nih.gov/pubmed/28978219>

- Kaste, M., & Koivisto, P. (1988). Risk of brain infarction in familial hypercholesterolemia. *Stroke*, *19*(9), 1097–1100. <https://doi.org/10.1161/01.STR.19.9.1097>
- Kayakabe, M., Kakizaki, T., Kaneko, R., Sasaki, A., Nakazato, Y., Shibasaki, K., ... Yanagawa, Y. (2014). Motor dysfunction in cerebellar Purkinje cell-specific vesicular GABA transporter knockout mice. *Frontiers in Cellular Neuroscience*, *7*, 286. <https://doi.org/10.3389/fncel.2013.00286>
- Kim, J., Haque, M. N., Goo, T.-W., & Moon, I. S. (2018). Alleviation of Hippocampal Endoplasmic Reticulum Stress by *Allomyrina dichotoma* Larvae Extract. *The American Journal of Chinese Medicine*, *46*(03), 633–650. <https://doi.org/10.1142/s0192415x18500337>
- Kneysberg, A., & Kanaan, N. M. (2017). Aging Does Not Affect Axon Initial Segment Structure and Somatic Localization of Tau Protein in Hippocampal Neurons of Fischer 344 Rats. *ENeuro*, *4*(4), ENEURO.0043-17.2017. <https://doi.org/10.1523/ENeuro.0043-17.2017>
- Knobloch, M., & Mansuy, I. M. (2008). Dendritic Spine Loss and Synaptic Alterations in Alzheimer's Disease. *Molecular Neurobiology*, *37*(1), 73–82. <https://doi.org/10.1007/s12035-008-8018-z>
- Kolbus, D., Ramos, O. H., Berg, K. E., Persson, J., Wigren, M., Björkbacka, H., ... Nilsson, J. (2010). CD8+T cell activation predominate early immune responses to hypercholesterolemia in *ApoE*^{-/-} mice. *BMC Immunology*, *11*(1), 58. <https://doi.org/10.1186/1471-2172-11-58>
- Kosari, S., Badoer, E., Nguyen, J. C. D., Killcross, A. S., & Jenkins, T. A. (2012). Effect of western and high fat diets on memory and cholinergic measures in the rat. *Behavioural Brain Research*, *235*(1), 98–103. <https://doi.org/10.1016/j.bbr.2012.07.017>
- Laskowitz, D. T., Sheng, H., Bart, R. D., Joyner, K. A., Roses, A. D., & Warner, D. S. (1997). Apolipoprotein E-Deficient Mice Have Increased Susceptibility To Focal Cerebral Ischemia. *Journal of Cerebral Blood Flow & Metabolism*, *17*(7), 753–758. <https://doi.org/10.1097/00004647-199707000-00005>
- Lee, W.-H., Suk Jung-Wan Seo, K., Jin, M., Lee, M.-G., Eunha Jang, I.-S., Kim, J.-H., ... Kim, J.-H. (2013). Astrocytes in the Classical Inflammatory Activation of Astrocytes: The Critical Role of Lipocalin-2 Phenotypic Polarization of Activated. <https://doi.org/10.4049/jimmunol.1301637>
- Lein, E. S., Hawrylycz, M. J., Ao, N., Ayres, M., Bensinger, A., Bernard, A., ... Jones, A. R. (2007). Genome-wide atlas of gene expression in the adult mouse brain. *Nature*, *445*(7124), 168–176. <https://doi.org/10.1038/nature05453>

- Leitman, J., Barak, B., Benyair, R., Shenkman, M., Ashery, U., Hartl, F. U., & Lederkremer, G. Z. (2014). ER stress-induced eIF2-alpha phosphorylation underlies sensitivity of striatal neurons to pathogenic huntingtin. *PloS One*, *9*(3), e90803. <https://doi.org/10.1371/journal.pone.0090803>
- Li, Y., Guo, Y., Tang, J., Jiang, J., & Chen, Z. (2014). New insights into the roles of CHOP-induced apoptosis in ER stress. *Acta Biochimica et Biophysica Sinica*, *46*(8), 629–640. <https://doi.org/10.1093/abbs/gmu048>
- Lin, C.-J., Lai, C.-K., Kao, M.-C., Wu, L.-T., Lo, U.-G., Lin, L.-C., ... Lin, C.-D. (2015). Impact of cholesterol on disease progression. *BioMedicine*, *5*(2), 7. <https://doi.org/10.7603/s40681-015-0007-8>
- Lin, J. H., Li, H., Yasumura, D., Cohen, H. R., Zhang, C., Panning, B., ... Walter, P. (2007). IRE1 Signaling Affects Cell Fate During the Unfolded Protein Response. *Science*, *318*(5852), 944–949. <https://doi.org/10.1126/science.1146361>
- Lin, Jonathan H, Walter, P., & Yen, T. S. B. (2008). Endoplasmic reticulum stress in disease pathogenesis. *Annual Review of Pathology*, *3*, 399–425. <https://doi.org/10.1146/annurev.pathmechdis.3.121806.151434>
- Lindholm, P., & Saarma, M. (2010). Novel CDNF/MANF family of neurotrophic factors. *Developmental Neurobiology*, *70*(5), NA-NA. <https://doi.org/10.1002/dneu.20760>
- Linton, M. F., Yancey, P. G., Davies, S. S., Jerome, W. G., Linton, E. F., Song, W. L., ... Vickers, K. C. (2019). The Role of Lipids and Lipoproteins in Atherosclerosis. Retrieved from <https://www.ncbi.nlm.nih.gov/books/NBK343489/>
- Liu, A., Aoki, S., & Wickens, J. (2017). A Streamlined Method for the Preparation of Gelatin Embedded Brains and Simplified Organization of Sections for Serial Reconstructions. *BIO-PROTOCOL*, *7*(22). <https://doi.org/10.21769/BioProtoc.2610>
- Liu, C.-Y., Yang, Y., Ju, W.-N., Wang, X., & Zhang, H.-L. (2018). Emerging Roles of Astrocytes in Neuro-Vascular Unit and the Tripartite Synapse With Emphasis on Reactive Gliosis in the Context of Alzheimer's Disease. *Frontiers in Cellular Neuroscience*, *12*, 193. <https://doi.org/10.3389/fncel.2018.00193>
- Liu, M., Kuhel, D. G., Shen, L., Hui, D. Y., & Woods, S. C. (2012). Apolipoprotein E does not cross the blood-cerebrospinal fluid barrier, as revealed by an improved technique for sampling CSF from mice. *American Journal of Physiology. Regulatory, Integrative and Comparative Physiology*, *303*(9), R903-8. <https://doi.org/10.1152/ajpregu.00219.2012>
- Lowden, J. A. (2002). *insm 34_103 Mp_26 File # 03em New Guidelines from the National Cholesterol Education Program: What is the Impact on Risk Assessment? Journal of Insurance Medicine J Insur Med* (Vol. 34). Retrieved

from <http://www.nhlbi.nih.gov/index.htm>

- Madariaga, Y. G., Cárdenas, M. B., Irsula, M. T., Alfonso, O. C., Cáceres, B. A., & Morgado, E. B. (2015). Assessment of four experimental models of hyperlipidemia. *Lab Animal*, *44*(4), 135–140. <https://doi.org/10.1038/labam.710>
- Maganto-Garcia, E., Tarrío, M., & Lichtman, A. H. (2012). Mouse Models of Atherosclerosis. In *Current Protocols in Immunology* (Vol. Chapter 15, p. Unit 15.24.1-23). Hoboken, NJ, USA: John Wiley & Sons, Inc. <https://doi.org/10.1002/0471142735.im1524s96>
- Manning, S., & Oakeshott, P. (2009). Familial hypercholesterolaemia. *British Journal of General Practice*, *59*(569), 944.2-945. <https://doi.org/10.3399/bjgp09x473213>
- Maria Giudetti, A., Romano, A., Michele Lavecchia, A., & Gaetani, S. (2016). The Role of Brain Cholesterol and its Oxidized Products in Alzheimer's Disease. *Current Alzheimer Research*, *13*(2), 198–205. <https://doi.org/10.2174/1567205012666150921103426>
- Matus, S., Castillo, K., & Hetz, C. (2012). Hormesis: Protecting neurons against cellular stress in Parkinson disease. *Autophagy*, *8*(6), 997–1001. <https://doi.org/10.4161/auto.20748>
- McQuiston, A., & Diehl, J. A. (2017). Recent insights into PERK-dependent signaling from the stressed endoplasmic reticulum. *F1000Research*, *6*, 1897. <https://doi.org/10.12688/f1000research.12138.1>
- Mengi, N. (2019). *The Effects of High Cholesterol/High Fat Diet on Endoplasmic Reticulum Stress and Neuronal Dysfunction in the Hippocampus and the Cerebral Cortex of Apoe^{-/-} Mice*. Middle East Technical University.
- Morris, M. C., & Tangney, C. C. (2014). Dietary fat composition and dementia risk. *Neurobiology of Aging*, *35*, S59–S64. <https://doi.org/10.1016/J.NEUROBIOLAGING.2014.03.038>
- Morse, S. M. J., Shaw, G., & Larner, S. F. (2006). Concurrent mRNA and protein extraction from the same experimental sample using a commercially available column-based RNA preparation kit. *BioTechniques*, *40*(1), 54–58. <https://doi.org/10.2144/000112100>
- Mu, Y., & Gage, F. H. (2011). Adult hippocampal neurogenesis and its role in Alzheimer's disease. *Molecular Neurodegeneration*, *6*(1), 85. <https://doi.org/10.1186/1750-1326-6-85>
- Navid, F., & Colbert, R. A. (2017). Causes and consequences of endoplasmic reticulum stress in rheumatic disease. *Nature Reviews Rheumatology*, *13*(1), 25–40. <https://doi.org/10.1038/nrrheum.2016.192>
- Neki, N. S. (2002). Lipid Profile in Chronic Smokers – A Clinical Study Key words.

- Clinical Medicine*, 3(1), 51–54. Retrieved from <http://medind.nic.in/jac/t02/i1/jact02i1p51.pdf>
- Nelson, R. H. (2013). Hyperlipidemia as a risk factor for cardiovascular disease. *Primary Care*, 40(1), 195–211. <https://doi.org/10.1016/j.pop.2012.11.003>
- Novoa, I., Zeng, H., Harding, H. P., & Ron, D. (2001). Feedback inhibition of the unfolded protein response by GADD34-mediated dephosphorylation of eIF2alpha. *The Journal of Cell Biology*, 153(5), 1011–1022. <https://doi.org/10.1083/jcb.153.5.1011>
- Olesen, M. V., Needham, E. K., & Pakkenberg, B. (2017). The Optical Fractionator Technique to Estimate Cell Numbers in a Rat Model of Electroconvulsive Therapy. *Journal of Visualized Experiments*, (125), e55737. <https://doi.org/10.3791/55737>
- Onat, U. I., Yildirim, A. D., Tufanlı, Ö., Çimen, I., Kocatürk, B., Veli, Z., ... Erbay, E. (2019). Intercepting the Lipid-Induced Integrated Stress Response Reduces Atherosclerosis. *Journal of the American College of Cardiology*, 73(10), 1149–1169. <https://doi.org/10.1016/j.jacc.2018.12.055>
- Ooi, E. M. M., Watts, G. F., Ng, T. W. K., & Barrett, P. H. R. (2015). Effect of dietary Fatty acids on human lipoprotein metabolism: a comprehensive update. *Nutrients*, 7(6), 4416–4425. <https://doi.org/10.3390/nu7064416>
- Osada, N., Kosuge, Y., Kihara, T., Ishige, K., & Ito, Y. (2009). Apolipoprotein E-deficient mice are more vulnerable to ER stress after transient forebrain ischemia. *Neurochemistry International*, 54(7), 403–409. <https://doi.org/10.1016/j.neuint.2009.01.010>
- Otsuka, T., Takada, H., Nishiyama, Y., Kodani, E., Saiki, Y., Kato, K., & Kawada, T. (2016). Dyslipidemia and the Risk of Developing Hypertension in a Working-Age Male Population. *Journal of the American Heart Association*, 5(3), e003053. <https://doi.org/10.1161/JAHA.115.003053>
- Ouyang, Q., Huang, Z., Lin, H., Ni, J., Lu, H., Chen, X., ... Lin, L. (2015). Apolipoprotein E deficiency and high-fat diet cooperate to trigger lipodosis and inflammation in the lung via the toll-like receptor 4 pathway. *Molecular Medicine Reports*, 12(2), 2589–2597. <https://doi.org/10.3892/mmr.2015.3774>
- Overk, C. R., & Masliah, E. (2014). Pathogenesis of synaptic degeneration in Alzheimer's disease and Lewy body disease. *Biochemical Pharmacology*, 88(4), 508–516. <https://doi.org/10.1016/j.bcp.2014.01.015>
- Panzenboeck, U., Balazs, Z., Sovic, A., Hrzenjak, A., Levak-Frank, S., Wintersperger, A., ... Sattler, W. (2002). ABCA1 and scavenger receptor class B, type I, are modulators of reverse sterol transport at an in vitro blood-brain barrier constituted of porcine brain capillary endothelial cells. *Journal of Biological*

- Chemistry*, 277(45), 42781–42789. <https://doi.org/10.1074/jbc.M207601200>
- Papapanagiotou, A., Siasos, G., Kassi, E., Gargalionis, A. N., & Papavassiliou, A. G. (2015). Novel Inflammatory Markers in Hyperlipidemia: Clinical Implications. *Current Medicinal Chemistry*, 22(23), 2727–2743. Retrieved from <http://www.ncbi.nlm.nih.gov/pubmed/25989910>
- Park, Y.-J., Ko, J., Jeon, S., & Kwon, Y. (2016). Protective Effect of Genistein against Neuronal Degeneration in ApoE^{-/-} Mice Fed a High-Fat Diet. *Nutrients*, 8(11), 692. <https://doi.org/10.3390/nu8110692>
- Patil, C., & Walter, P. (2001). Intracellular signaling from the endoplasmic reticulum to the nucleus: the unfolded protein response in yeast and mammals. *Current Opinion in Cell Biology*, 13(3), 349–355. Retrieved from <http://www.ncbi.nlm.nih.gov/pubmed/11343907>
- Paxinos, G., & Franklin, K. (2001). *The Mouse Brain in Stereotaxic Coordinates* (Second edi). San Diego, CA: Elsevier Academic Press.
- Pekny, M., & Pekna, M. (2014). Astrocyte Reactivity and Reactive Astrogliosis: Costs and Benefits. *Physiological Reviews*, 94(4), 1077–1098. <https://doi.org/10.1152/physrev.00041.2013>
- Pekny, M., & Pekna, M. (2016). Reactive gliosis in the pathogenesis of CNS diseases. *Biochimica et Biophysica Acta (BBA) - Molecular Basis of Disease*, 1862(3), 483–491. <https://doi.org/10.1016/J.BBADIS.2015.11.014>
- Pérez-Arancibia, R., Rivas, A., & Hetz, C. (2017). Expert Opinion on Therapeutic Targets (off)Targeting UPR signaling: the race toward intervening ER proteostasis. <https://doi.org/10.1080/14728222.2018.1420169>
- Petzoldt, A. G., & Sigrist, S. J. (2014). Synaptogenesis. *Current Biology*, 24(22), R1076–R1080. <https://doi.org/10.1016/J.CUB.2014.10.024>
- Quan, G., Xie, C., Dietschy, J. M., & Turley, S. D. (2003). Ontogenesis and regulation of cholesterol metabolism in the central nervous system of the mouse. *Brain Research. Developmental Brain Research*, 146(1–2), 87–98. Retrieved from <http://www.ncbi.nlm.nih.gov/pubmed/14643015>
- Reddy, P. H., Mani, G., Park, B. S., Jacques, J., Murdoch, G., Whetsell, W., ... Manczak, M. (2005). Differential loss of synaptic proteins in Alzheimer's disease: Implications for synaptic dysfunction. *Journal of Alzheimer's Disease*, 7(2), 103–117. <https://doi.org/10.3233/JAD-2005-7203>
- Reid, D. W., Tay, A. S. L., Sundaram, J. R., Lee, I. C. J., Chen, Q., George, S. E., ... Shenolikar, S. (2016). Complementary Roles of GADD34-and CReP-Containing Eukaryotic Initiation Factor 2 Phosphatases during the Unfolded Protein Response. <https://doi.org/10.1128/MCB.00190-16>

- Reimold, A. M., Etkin, A., Clauss, I., Perkins, A., Friend, D. S., Zhang, J., ... Glimcher, L. H. (2000). An essential role in liver development for transcription factor XBP-1. *Genes & Development*, *14*(2), 152–157. Retrieved from <http://www.ncbi.nlm.nih.gov/pubmed/10652269>
- Replogle, M. R., Sreevidya, V. S., Lee, V. M., Laiosa, M. D., Svoboda, K. R., & Udvadia, A. J. (2018). Establishment of a murine culture system for modeling the temporal progression of cranial and trunk neural crest cell differentiation. *Disease Models & Mechanisms*, *11*(12). <https://doi.org/10.1242/dmm.035097>
- Ron, D., & Hubbard, S. R. (2008). How IRE1 Reacts to ER Stress. *Cell*, *132*(1), 24–26. <https://doi.org/10.1016/J.CELL.2007.12.017>
- Ron, D., & Walter, P. (2007). Signal integration in the endoplasmic reticulum unfolded protein response. *Nature Reviews Molecular Cell Biology*, *8*(7), 519–529. <https://doi.org/10.1038/nrm2199>
- Rutkowsky, J. M., Lee, L. L., Puchowicz, M., Golub, M. S., Befroy, D. E., Wilson, D. W., ... Group, on behalf of the M. M. P. C. I. W. (2018). Reduced cognitive function, increased blood-brain-barrier transport and inflammatory responses, and altered brain metabolites in LDLr ^{-/-} and C57BL/6 mice fed a western diet. *PLOS ONE*, *13*(2), e0191909. <https://doi.org/10.1371/journal.pone.0191909>
- Ryoo, H. D., & Vasudevan, D. (2017). Two distinct nodes of translational inhibition in the Integrated Stress Response. *BMB Reports*, *50*(11), 539–545. <https://doi.org/10.5483/BMBREP.2017.50.11.157>
- S. Mannu, G., J.S. Zaman, M., Gupta, A., U. Rehman, H., & K. Myint, P. (2013). Evidence of Lifestyle Modification in the Management of Hypercholesterolemia. *Current Cardiology Reviews*. <https://doi.org/10.2174/157340313805076313>
- Sack, M., Lenz, J. N., Jakovcevski, M., Biedermann, S. V., Falfán-Melgoza, C., Deussing, J., ... Auer, M. K. (2017). Early effects of a high-caloric diet and physical exercise on brain volumetry and behavior: a combined MRI and histology study in mice. *Brain Imaging and Behavior*, *11*(5), 1385–1396. <https://doi.org/10.1007/s11682-016-9638-y>
- Sacks, F. M., Lichtenstein, A. H., Wu, J. H. Y., Appel, L. J., Creager, M. A., Kris-Etherton, P. M., ... Van Horn, L. V. (2017, July 18). Dietary fats and cardiovascular disease: A presidential advisory from the American Heart Association. *Circulation*. Lippincott Williams & Wilkins Hagerstown, MD. <https://doi.org/10.1161/CIR.0000000000000510>
- Sandoval-Salazar, C., Ramírez-Emiliano, J., Trejo-Bahena, A., Oviedo-Solís, C. I., & Solís-Ortiz, M. S. (2016). A high-fat diet decreases GABA concentration in the frontal cortex and hippocampus of rats. *Biological Research*, *49*(1), 15. <https://doi.org/10.1186/s40659-016-0075-6>

- Sarnat, H. B. (2013). Clinical neuropathology practice guide 5-2013: markers of neuronal maturation. *Clinical Neuropathology*, 32(5), 340–369. <https://doi.org/10.5414/NP300638>
- Scheper, W., & Hoozemans, J. J. M. (2015). The unfolded protein response in neurodegenerative diseases: a neuropathological perspective. *Acta Neuropathologica*, 130(3), 315–331. <https://doi.org/10.1007/s00401-015-1462-8>
- Scheuner, D., Patel, R., Wang, F., Lee, K., Kumar, K., Wu, J., ... Kaufman, R. J. (2006). Double-stranded RNA-dependent protein kinase phosphorylation of the alpha-subunit of eukaryotic translation initiation factor 2 mediates apoptosis. *The Journal of Biological Chemistry*, 281(30), 21458–21468. <https://doi.org/10.1074/jbc.M603784200>
- Schönthal, A. H. (2012). Endoplasmic reticulum stress: its role in disease and novel prospects for therapy. *Scientifica*, 2012, 857516. <https://doi.org/10.6064/2012/857516>
- Shen, Y., Sun, A., Wang, Y., Cha, D., Wang, H., Wang, F., ... Shen, Y. (2012). *Upregulation of mesencephalic astrocyte-derived neurotrophic factor in glial cells is associated with ischemia-induced glial activation*. <https://doi.org/10.1186/1742-2094-9-254>
- Sickmann, H. M., Waagepetersen, H. S., Schousboe, A., Benie, A. J., & Bouman, S. D. (2010). Obesity and type 2 diabetes in rats are associated with altered brain glycogen and amino-acid homeostasis. *Journal of Cerebral Blood Flow and Metabolism*, 30(8), 1527–1537. <https://doi.org/10.1038/jcbfm.2010.61>
- Smith, T. D., Adams, M. M., Gallagher, M., Morrison, J. H., & Rapp, P. R. (2000a). Circuit-specific alterations in hippocampal synaptophysin immunoreactivity predict spatial learning impairment in aged rats. *The Journal of Neuroscience : The Official Journal of the Society for Neuroscience*, 20(17), 6587–6593. <https://doi.org/10.1523/JNEUROSCI.20-17-06587.2000>
- Smith, T. D., Adams, M. M., Gallagher, M., Morrison, J. H., & Rapp, P. R. (2000b). Circuit-specific alterations in hippocampal synaptophysin immunoreactivity predict spatial learning impairment in aged rats. *The Journal of Neuroscience : The Official Journal of the Society for Neuroscience*, 20(17), 6587–6593. <https://doi.org/10.1523/JNEUROSCI.20-17-06587.2000>
- Sofroniew, M. V., & Vinters, H. V. (2010a). Astrocytes: biology and pathology. *Acta Neuropathologica*, 119(1), 7–35. <https://doi.org/10.1007/s00401-009-0619-8>
- Sofroniew, M. V., & Vinters, H. V. (2010b). Astrocytes: biology and pathology. *Acta Neuropathologica*, 119(1), 7. <https://doi.org/10.1007/S00401-009-0619-8>
- Solomon, A., Kåreholt, I., Ngandu, T., Winblad, B., Nissinen, A., Tuomilehto, J., ...

- Kivipelto, M. (2007). Serum cholesterol changes after midlife and late-life cognition: twenty-one-year follow-up study. *Neurology*, 68(10), 751–756. <https://doi.org/10.1212/01.wnl.0000256368.57375.b7>
- Stangl, D., & Thuret, S. (2009). Impact of diet on adult hippocampal neurogenesis. *Genes & Nutrition*, 4(4), 271–282. <https://doi.org/10.1007/s12263-009-0134-5>
- Stapleton, P. A., Goodwill, A. G., James, M. E., Brock, R. W., & Frisbee, J. C. (2010, November 18). Hypercholesterolemia and microvascular dysfunction: Interventional strategies. *Journal of Inflammation*. BioMed Central. <https://doi.org/10.1186/1476-9255-7-54>
- Stevenson, R. J., & Francis, H. M. (2017). The hippocampus and the regulation of human food intake. *Psychological Bulletin*, 143(10), 1011–1032. <https://doi.org/10.1037/bul0000109>
- Sultan, F. A. (2013). Dissection of Different Areas from Mouse Hippocampus. *Bio-Protocol*, 3(21). Retrieved from <http://www.ncbi.nlm.nih.gov/pubmed/27390757>
- Tarsa, L., & Goda, Y. (2002). Synaptophysin regulates activity-dependent synapse formation in cultured hippocampal neurons. *Proceedings of the National Academy of Sciences of the United States of America*, 99(2), 1012–1016. <https://doi.org/10.1073/pnas.022575999>
- Thirumangalakudi, L., Prakasam, A., Zhang, R., Bimonte-Nelson, H., Sambamurti, K., Kindy, M. S., & Bhat, N. R. (2008). High cholesterol-induced neuroinflammation and amyloid precursor protein processing correlate with loss of working memory in mice. *Journal of Neurochemistry*, 106(1), 475–485. <https://doi.org/10.1111/j.1471-4159.2008.05415.x>
- Turley, S. D., Burns, D. K., Rosenfeld, C. R., & Dietschy, J. M. (1996). Brain does not utilize low density lipoprotein-cholesterol during fetal and neonatal development in the sheep. *Journal of Lipid Research*, 37(9), 1953–1961. Retrieved from <http://www.ncbi.nlm.nih.gov/pubmed/8895061>
- Tyagarajan, S. K., & Fritschy, J.-M. (2010). GABA(A) receptors, gephyrin and homeostatic synaptic plasticity. *The Journal of Physiology*, 588(Pt 1), 101–106. <https://doi.org/10.1113/jphysiol.2009.178517>
- Unruh, D., Srinivasan, R., Benson, T., Haigh, S., Coyle, D., Batra, N., ... Bogdanov, V. Y. (2015). Red Blood Cell Dysfunction Induced by High-Fat Diet. *Circulation*, 132(20), 1898–1908. <https://doi.org/10.1161/CIRCULATIONAHA.115.017313>
- Valladolid-Acebes, I., Merino, B., Principato, A., Fole, A., Barbas, C., Lorenzo, M. P., ... Cano, V. (2012). High-fat diets induce changes in hippocampal glutamate metabolism and neurotransmission. *American Journal of Physiology-*

- Endocrinology and Metabolism*, 302(4), E396–E402.
<https://doi.org/10.1152/ajpendo.00343.2011>
- WHO. (2008). Global Health Observatory (GHO) data. Retrieved from
https://www.who.int/gho/ncd/risk_factors/cholesterol_text/en/
- Wible, C. G. (2013). Hippocampal Physiology, Structure and Function and the Neuroscience of Schizophrenia: A Unified Account of Declarative Memory Deficits, Working Memory Deficits and Schizophrenic Symptoms. *Behavioral Sciences*, 3(2), 298. <https://doi.org/10.3390/BS3020298>
- Wilde, M. C. de, Overk, C. R., Sijben, J. W., & Masliah, E. (2016). Meta-analysis of synaptic pathology in Alzheimer's disease reveals selective molecular vesicular machinery vulnerability. *Alzheimer's & Dementia: The Journal of the Alzheimer's Association*, 12(6), 633. <https://doi.org/10.1016/J.JALZ.2015.12.005>
- Wirhth, O. (2017). Extraction of Soluble and Insoluble Protein Fractions from Mouse Brains and Spinal Cords. *BIO-PROTOCOL*, 7(15). <https://doi.org/10.21769/BioProtoc.2422>
- Wrabetz, L., D'Antonio, M., Schneider, K., Bertolotti, A., Sigurdardottir, A., Krzyzosiak, A., ... Das, I. (2015). Preventing proteostasis diseases by selective inhibition of a phosphatase regulatory subunit. *Science*, 348(6231), 239–242. <https://doi.org/10.1126/science.aaa4484>
- Wu, J., Rutkowski, D. T., Dubois, M., Swathirajan, J., Saunders, T., Wang, J., ... Kaufman, R. J. (2007). ATF6 α Optimizes Long-Term Endoplasmic Reticulum Function to Protect Cells from Chronic Stress. *Developmental Cell*, 13(3), 351–364. <https://doi.org/10.1016/j.devcel.2007.07.005>
- Yang, W., Shi, H., Zhang, J., Shen, Z., Zhou, G., & Hu, M. (2017). Effects of the duration of hyperlipidemia on cerebral lipids, vessels and neurons in rats. *Lipids in Health and Disease*, 16(1), 26. <https://doi.org/10.1186/s12944-016-0401-6>
- Zhang, S., Reddick, R., Piedrahita, J., & Maeda, N. (1992). Spontaneous hypercholesterolemia and arterial lesions in mice lacking apolipoprotein E. *Science*, 258(5081), 468–471. <https://doi.org/10.1126/science.1411543>
- Zhao, X.-S., Wu, Q., Peng, J., Pan, L.-H., Ren, Z., Liu, H.-T., ... Liu, L.-S. (2017). Hyperlipidemia-induced apoptosis of hippocampal neurons in apoE(-/-) mice may be associated with increased PCSK9 expression. *Molecular Medicine Reports*, 15(2), 712–718. <https://doi.org/10.3892/mmr.2016.6055>
- Zhu, Z., Wu, F., Lu, Y., Wang, Z., Zang, J., Yu, H., ... Ding, G. (2018). The Association of Dietary Cholesterol and Fatty Acids with Dyslipidemia in Chinese Metropolitan Men and Women. *Nutrients*, 10(8). <https://doi.org/10.3390/nu10080961>

APPENDICES

A. General Lab Materials

Table A.1. Company Information and Product Number of Chemicals Used in This Study

Chemical	Company	Product No
2-Mercaptoethanol	Bio-Rad (Hercules, CA, USA)	161-0710
2-Propanol	Sigma-Aldrich (St.Louis, MO, USA)	24137-2.5L-R
Absolute Methanol	Iso lab chemicals (Laborgeräte GmbH, Wertheim, Germany)	947.046.2500-2.5L
Acrylamide	Sigma-Aldrich (St.Louis, MO, USA)	A3553-100G
Ammonium Persulfate (APS)	BioRad (Hercules, CA, USA)	161-0700
Bisacrylamide	AppliedChem (Darmstadt, Germany)	A1096,0050
Bovine Serum Albumin	Sigma-Aldrich (St.Louis, MO, USA)	A6003-25G
Bromophenol Blue	AppliedChem (Darmstadt, Germany)	A2331,0005
Chloroform	Sigma-Aldrich (St.Louis, MO, USA)	24216-2.5L-R
Clarity™ Western ECL Substrate	BioRad (Hercules, CA, USA)	1705060
Coomassie Plus (Bradford) Assay	Fisher Scientific (Loughborough, UK)	1856209

Table A.2. Company Information and Product Number of Chemicals Used in This Study (Continued)

Cover Glass	Paul Marienfeld (GmbH & Co. KG, Lauda-Königshofen, Germany)	0101222
Cryomold	Tissue-Tek (Sakura Finetek, USA Inc.)	27147-2
EDTA	AppliedChem (Darmstadt, Germany)	A5097,0250
Ethanol absolute ≥99.8%	Sigma-Aldrich (St.Louis, MO, USA)	32221-2.5L
Fluoroshield™ Mounting Media with DAPI	Abcam (Cambridge, MA, USA)	F6057
Glycerol	BioShop (Burlington, Ontario, Canada)	CAS#56-81-5
Glycine	Sigma-Aldrich (St.Louis, MO, USA)	33226-250G
HEPES	AppliedChem (Darmstadt, Germany)	A37240100
HistoBond® Microscope Slides	Paul Marienfeld (GmbH & Co. KG, Lauda-Königshofen, Germany)	0810001
ImmEdge™ Hydrophobic Pen	Vector Laboratories (Burlingame, CA, USA)	H-4000
Immun-Blot® PVDF Membrane	Bio-Rad (Hercules, CA, USA)	1620177
Isopentane	Merck (Billerica, MA, USA)	78-78-4
NP-40	Sigma-Aldrich (St.Louis, MO, USA)	127087-87-0

Table A.3. Company Information and Product Number of Chemicals Used in This Study (Continued)

O.C.T. Compund	Tissue-Tek (Sakura Finetek, USA Inc.)	4583
PageRuler™ Plus Prestained Protein Ladder	Thermo Fisher Scientific (Waltham, MA, USA)	26619
Phosphatase Inhibitor Cocktail (PIC)	Sigma-Aldrich (St.Louis, MO, USA)	P0044
Phenylmethylsulfonyl fluoride (PMSF)	Sigma-Aldrich (St.Louis, MO, USA)	329-98-6
Rnase Free Water	Ambion (Ambion, Austin, TX, USA)	AM9937
Sodium chloride (NaCl)	Sigma-Aldrich (St.Louis, MO, USA)	31434-1KG-R
Sodium Deoxycholate	Thermo Fisher Scientific (Waltham, MA, USA)	89904
Sodium Dodecyl Sulfate	Sigma-Aldrich (St.Louis, MO, USA)	L4390-500G
Sodium Orthovanadate (Na ₃ VO ₄)	Sigma-Aldrich (St.Louis, MO, USA)	450243
Sucrose	AppliedChem (Darmstadt, Germany)	A2211,0500
TEMED	AMRESCO (Solon, OH, USA)	0761-100ML

Table A.4. Company Information and Product Number of Chemicals Used in This Study (Continued)

tri-Sodium Citrate	Merck (Billerica, MA, USA)	106448
Tris base	Sigma-Aldrich (St.Louis, MO, USA)	T1503-1KG
Triton™ X-100	Sigma-Aldrich (St.Louis, MO, USA)	T8787-250ML
TRIzol™ reagent	Thermo Fisher Scientific (Waltham, MA, USA)	15596018
Tween 20	BioShop (Burlington, Ontario, Canada)	CAS#56-40-6

B. Homogenization Buffer Preparation

Preparation of Na₃VO₄ stock solution: 3.68 g Na₃VO₄ (200 mM) was dissolved in 100 mL ddH₂O. Its working concentration is 2 mM. Solution was aliquoted and stored at -20 °C.

Preparation of PMSF stock solution: 174 mg of PMSF (100 mM) was dissolved in 100 mL isopropanol and stored at -20 °C as aliquots. Its working concentration is 1 mM.

For 100 mL homogenization buffer; 8.56 g of sucrose (250 mM), 37 mg EDTA (2.0 mM), 238 mg HEPES (10mM) were dissolved in ddH₂O. pH was adjusted to 7.4 and volume was completed to 100 mL with ddH₂O and stored at 4°C. 10 ul PIC (1% (v/v)), 10 ul Na₃VO₄ and 10 ul PMSF were added per 1.0 mL homogenization buffer.

C. Total RNA Isolation

Total RNA isolation was performed by standard acid guanidinium thiocyanate-phenol-chloroform extraction procedure (Chomczynski & Sacchi, 2006). Homogenates of the cortex and hippocampus were centrifuged at 11.000 X g, then supernatant was discarded in order to remove excess homogenization buffer. One thousand μL and 500 μL TRIzol reagent was added to cortex and hippocampus pellets, respectively and pellets were dissolved with pipetting. Centrifuge tubes were incubated at room temperature for 10 minutes. For 1000 μL of TRIzol, 250 μL chloroform was added into the samples and centrifuge tubes were shaken vigorously for 15 seconds. Tubes were incubated at room temperature until the phase separation occurs and they were centrifuged at 12.000 X g for 15 minutes at 4°C. Aqueous phase, the clear supernatant at the top, was carefully removed into a new 1.5 mL centrifuge tube and 500 μL isopropanol was added to the aqueous phase for 1 mL of TRIzol, gently mixed by inversion 3-5 times until RNA clamp became visible. After 10 minutes of incubation at room temperature, samples were centrifuged at 12.000 X g for 30 minutes at 4°C. Supernatant was discarded and 1000 μL 70% ethanol was added for 1000 μL of TRIzol to wash the precipitated RNA. Then, samples were centrifuged at 7.500 X g for 5 minutes at 4°C. Ethanol was discarded and RNA pellet was air dried for 5 or 10 minutes. RNA pellets of cortex and hippocampus were dissolved in 35 μL and 20 μL RNase free water, respectively. 1 μL of RNA sample was used to measure concentration and to check the purity of the sample using NanoDrop 2000 Spectrophotometer (ND2000, Thermo Fisher Scientific, Waltham, MA, USA) in UNAM, Bilkent University. RNA samples were stored at -80°C until the experiment day.

D. RIPA Buffer Preparation

For 100 mL homogenization buffer; 2.5 mL 1M Tris-HCl, pH 8.8 (50mM), 0.876 g NaCl (150 mM), 0.25 g sodium deoxycholate (0.25% (w/v)), 1 mL NP-40 (1% (v/v)) and 0.029 g EDTA (1.0 mM) were added to 50 mL ddH₂O. When all chemicals were dissolved, volume was completed to 100 mL with ddH₂O. Stored at 4°C. 10 ul PIC (1% (v/v)), 10 ul Na₃VO₄ and 10 ul PMSF were added per 1.0 mL RIPA buffer.

E. Western Blot Solutions

1M Tris-HCl, pH 8.8: 48 g Tris base was dissolved in ddH₂O and pH was adjusted to 8.8. Volume was completed to 400 mL and stored at 4°C.

1M Tris-HCl, pH 6.8: 12 g Tris base was dissolved in ddH₂O and pH was adjusted to 6.8. Volume was completed to 100 mL and stored at 4°C.

40 % Acrylamide/Bis (39:1): 77.33g acrylamide and 2.67g Bis-Acrylamide was dissolved in ddH₂O. Volume was completed to 200 mL and stored at 4°C in the dark.

10 % SDS: 5 g SDS was dissolved in ddH₂O, volume was completed to 50 mL and stored at room temperature.

10% APS: 0.5 g APS was dissolved in ddH₂O, volume was completed to 5.0 mL. Solution was aliquoted and stored at -20°C.

1 % Bromophenol Blue: 0.01g Bromophenol blue was dissolved in 1.0 mL water and stored at room temperature.

2X Loading Dye: 1mL 1 M Tris-HCl (pH 6.8), 4 mL 10% SDS, 2mL Glycerol, 500 ul 1 % Bromophenol Blue was mixed. 2-Mercaptoethanol was added freshly prior to the experiment at a 1:3 ratio.

10X Running Buffer Stock: 30 g Tris Base (25 mM), 144 g Glycine (192 mM), 10 g SDS (0.1 %) were dissolved in ddH₂O. Volume was completed to 1 L and stored at 4°C.

10X Transfer Buffer Stock: 30 g Tris Base (25 mM) and 144 g Glycine (192 mM) were dissolved in ddH₂O. Volume was completed to 1 L and stored at 4°C.

1X Transfer Buffer: 100 mL 10X stock buffer, 500 mL ddH₂O, 200 mL methanol were mixed. Volume was completed to 1 L.

10X Tris-Buffered Saline (TBS): 24.2 g Tris base (100mM) and 80 g NaCl (1500mM) were dissolved in ddH₂O. pH is adjusted to 7.6 and stored at room temperature.

0.1% TBS-Tween 20 (TBS-T): 10X TBS was diluted to 1X and 1 mL Tween 20 was added per 1 L of TBS.

5 % Milk-TBST: 2.5 g milk powder was dissolved in TBS-T and volume was completed to 50 mL. It should be freshly prepared prior to the experiment.

5 % BSA- TBST: 2.5 g BSA was dissolved in TBS-T and volume was completed to 50 mL. It should be freshly prepared prior to the experiment.

Table E. 1. Amount of solutions required for construction of a standard curve. 2mg/mL BSA is used and mixture is prepared in 96 well plate.

ul	ddH₂O	BSA	Bradford
0	5	0	250
2	4.5	0.5	250
4	4	1	250
8	3	2	250
12	2	3	250
16	1	4	250
20	0	5	250

Table E. 2. Amount of protein samples and solutions to determine the soluble protein concentration.

ul	ddH₂O	Protein	Bradford
Sample 1	4.5	0.5	250
Sample 2	4.5	0.5	250
Sample 3	4.5	0.5	250

Table E. 3. Recipe of 5% Stacking Gel

Order	Component	Volume
1	ddH ₂ O	3.77 mL
2	1M Tris 6.8	0.625 mL
3	10% SDS	50 uL
4	40% Acrylamide-bis (39:1)	0.5 mL
5	10%APS	50 uL
6	TEMED	5 uL

Table E. 4. Recipe of 10% Resolving Gel

Order	Component	Volume
1	ddH ₂ O	3.54 mL
2	1M Tris 8.8	3.77 mL
3	10% SDS	100 uL
4	40% Acrylamide-bis (39:1)	2.5 mL
5	10%APS	100 uL
6	TEMED	10 L

F. Primary and Secondary Antibody Dilutions

Table F.1. Company and dilution information of both primary and secondary antibodies used in Western blot for this study.

Antibody Name	Company and Catalog #	Dilution
Synaptophysin	Abcam, #ab32594	1:20 000 in 5% Milk TBS-T
Gephyrin	Abcam, #ab83765	1:1000 in 5% Milk TBS-T
GFAP	Abcam, #ab53554	1:2000 in 5% Milk TBS-T
CHOP	Cell Signaling Technology, #5554	1:500 in 5% BSA TBS-T
p-eIF2α	GeneTex, #GTX24837	1:1000 in 5% BSA TBS-T
p-perk	Cell Signaling Technology, #3179	1:1000 in 5% BSA TBS-T
IL-1β	Abcam, #ab9722	1:5000 in 5% BSA TBS-T
β-Tubulin	Cell Signaling Technology, #2146	1:5000 in 5% Milk TBS-T
Rat anti-Rabbit IgG-HRP	Cell Signaling Technology, #7074	1:10 000 in 5% Milk or BSA TBS-T
Rabbit anti- Goat IgG-HRP	Abcam, #ab97100	1:10 000 in 5% Milk TBS-T

G. Immunostaining Solutions

Sodium Citrate Buffer: 2.94 g tri-sodium citrate (10 mM) was dissolved in ddH₂O. pH was adjusted to 6.0. and volume was completed to 1 L. 0.5 mL Tween 20 was added to the solution and mix well and stored at 4°C.

0.025 % TBS-TritonX: 250 ul TritonX was added to 1X TBS and mixed well.

5% BSA- TBS-TritonX: 0.5 g BSA was dissolved in 10 mL 0.025 % TBS-TritonX.